

Evaluation of the Anticancer and Molecular Effects of Green Synthesized Silver Nanoparticles



UNIVERSITY of the
WESTERN CAPE

Sohail Simon
Department of Biotechnology University
of the Western Cape

Supervisor: Prof. Abram Madiehe

Co- supervisor: Dr Nicole Sibuyi

March 2023

Evaluation of the anticancer and molecular effects of green synthesized Silver nanoparticles

Abstract

Sohail Simon, Nicole RS Sibuyi, Abram M Madiehe

*Masters thesis, Nanobiotechnology Research Group, Department of Biotechnology,
University of the Western Cape*

Globally, cancer is considered the second leading cause of death with a staggering tally of 10 million deaths. Breast, lung, colon, rectum and prostate cancers are amongst the most commonly diagnosed cancers. The current cancer treatment strategies such as chemotherapy, radiotherapy, and surgery; are accompanied with a long list of side effects. Nanotechnology has shown potential in improving biocompatibility of the chemotherapeutic drugs, and also provides a novel approach for the development of novel cancer treatment strategies through the application of the widely investigated nano-scaled materials known as nanoparticles (NPs). These NPs have been used as drug delivery systems and have, therefore, made a mark in the fight against cancer. Furthermore, their anti-cancer properties make them prospective anti-cancer agents. Green NPs, in particular have been making waves in the sector as they provide an eco-friendly alternative as opposed to the traditional chemically synthesized metal NPs (MNPs). MNPs such as AuNPs and AgNPs, due to their unique properties have demonstrated a wide range of bioactivities including anti-cancer activity. The aim of this study was to investigate the biocompatibility and anti-cancer activities of plant extract-synthesized (green) AgNPs on several human (cancer and non-cancer) cell lines and evaluate their molecular effects on prostate cancer (PCa) cells. Green AgNPs synthesized from Gum Arabic (GA), *Salvia Africana-lutea* (SAL), *Carpobrotus edulis* (Cefe), *Cotyledon Orbiculata* (CO), and Red Wine (RW) were obtained from the laboratory. The green AgNPs were characterized using Ultraviolet-visible spectroscopy (UVvis) and Dynamic Light Scattering (DLS) methods. Cancer (MCF-7, PC-3, A549, and A375) and non-cancer (KMST-6 and HaCaT) cells were grown under optimal conditions and treated with 0 – 1000 µg/ml of the green AgNPs. The cytotoxicity of the five green AgNPs was evaluated using the MTT assay after 24 h treatment. xCELLigence Real-time Cell Analyser was used to further validate the cytotoxicity effects of GA-AgNPs and SAL-AgNPs at 6.25- 100 µg/ml on PC-3 and MCF-7 cells.

Further studies involving Real Time-quantitative Polymerase Chain Reaction (RT-qPCR) were performed to investigate gene expression in PC-3 cells treated with GA-AgNPs. Following UV-vis analysis, GA-AgNPs had a SPR at 418 nm, SAL-AgNPs at 428 nm, CO-AgNPs at 410 nm, RW-AgNPs at SPR 410 nm and Cefe- AgNPs at SPR 408 nm. GA-AgNPs had a hydrodynamic size of 147.5 d.nm and PDI of 0.375, SAL-AgNPs had a hydrodynamic size of 34.63 d.nm and PDI of 0.63, CO-AgNPs had a hydrodynamic size of 110 d.nm and PDI of 0.15, RW-AgNPs had a hydrodynamic size of 138.3 d.nm and PDI of 0.322, and Cefe-AgNPs had a hydrodynamic size of 66.27 and PDI of 0.210. AgNPs with lower PDI, were the more stable AgNPs. Cytotoxicity of the AgNPs was evaluated by using the MTT assay, and it was found that Cefe- AgNPs, CO-AgNPs, and RW-AgNPs were not cytotoxic to the cancer and normal cells at concentrations 62.5-1000 µg/ml. However, GA-AgNPs and SAL-AgNPs showed non-selective cytotoxicity to both normal and cancer cells at concentration range of 25-1000 µg/ml. At 6.25 µg/ml, little to no effects were observed on the cell viability of the cells. xCELLigence Real-time analysis confirmed the effects of GA-AgNPs and SAL-AgNPs on MCF-7 and PC-3 cells from 6.25-100 µg/ml. RT-qPCR analysis also revealed the cytotoxicity of the GA-AgNPs on PC-3 cells. Seven genes were significantly downregulated by the treatment; TRIB3 was one of the three significantly upregulated genes and reported to play a role in apoptosis. In conclusion, although cytotoxic to normal cells, SAL-AgNPs and GA-AgNPs have potential anticancer properties. Guided by the genes affected by GA-AgNPs in PC-3 cells, these AgNPs might be a prospective tumor suppressor agents that could be used in tandem with traditional strategies in order to induce apoptosis in cancer cells. Further studies are required to explore their application *in vivo*, as well as finding strategies that can prevent or reduce their non-selective toxicity.

Keywords

Nanotechnology

Cancer

Anti-cancer

Silver nanoparticles

Green synthesis



UNIVERSITY *of the*
WESTERN CAPE


Declaration

I declare that *The Evaluation of the anticancer and molecular effects of green synthesized AgNPs* is my work, and that it has not been submitted for any other degree or examination in any other university. All sources I have used or quoted have been indicated and acknowledged by complete reference.

Full name: *Sohail Simon*

Date: March 2023

Signed:



Acknowledgements

I am thankful for the support of my family, my brother Faruk Simon, my sister-in-law Nazleen Simo, my Ma, and close family friends – Godfrey Smith, Aunt Julia Smith, Ravi Moodley, Leon Moodley, Vanessa Moodley, and Maggie Moodley, throughout the project duration. Especially my mom Farieda Simon who has been continuously supportive and kept on pushing me to complete my degree. I would like to give a big Thank You to my supervisor Prof Abram Madiehe and my co-supervisor Dr Nicole Sibuyi for their guidance, patience, encouragement and motivation

throughout the entirety of the project. I have great appreciation for Prof Mervin Meyer and fellow NIC labmates and supervisor

Additionally, I would like to thank my fellow NIC lab mates as they have helped me get through the stressful and off-putting moments during experimental failures (ESPECIALLY when my cells died).

I have gratitude and thanks for all those who have trained me in the methods, and instruments used, especially Dr Bronwyn Kirby, and my fellow NIC lab mates.

I would like to express my thankfulness and gratefulness towards DST/Mintek Nanotechnology Innovation centre for the funding of my project.

Thank you to Mr Thendo Mabuda, Dr Caroline Tyavambiza, Miss Keletso Modise, Miss Miché Meyer, Miss Tswelang Mgijima and Dr Jumoke Aboyewa for training me and helping me with procedures I was not familiar with.

Again, I am so grateful to all my supervisors for giving me the opportunity to be guided and taken under their wings throughout the project, it has been a tough past 2 years and I am extremely thankful for the patience that was exercised.

To all my NIC lab mates, thank you for the laughs, conversations and teambuilding activities, you all have made it a lot easier and always brought a smile to my face through stressful times.

Without the guiding path of Allah, none of this would have been possible. It was a set by Allah and Allah has provided me with the opportunity of meeting people in my lifetime that I admire and look up to.

Table of contents

Abstract	i
Keywords	ii
Declaration	iv
Acknowledgements	v
List of Figures	viii
List of Tables.....	ix
List of Abbreviations.....	x
Chapter 1: Project overview	1
1.1. Introduction	1
1.2. Aims and Objectives of the study.....	3
1.3. Thesis Outline	3
Chapter 2: Literature Review: Biomedical Applications of Plant Extract-Synthesized Silver Nanoparticles (Pages 4 -27)	
Abstract	5
1. Introduction	5
2. Synthesis of AgNPs.....	6
3. Biomedical Applications of Biogenic AgNPs	9
4. Perspectives and Concerns for Clinical Application of AgNPs.....	18
5. Conclusion.....	21
References	21
Chapter 3: Materials and Methods.....	28
3.1. Synthesis and characterization of green AgNPs	28
3.2. Evaluation of the anti-cancer effects of green AgNPs.....	29
3.2.1. Cell culture and maintenance	29
3.2.2. Trypsinization.....	30
3.2.3. Cryo-preservation of cells	30
3.2.4. Cell count	30
3.3. Investigation of the biocompatibility and cytotoxicity of the green AgNPs.....	30
3.3.1. MTT (3-(4,5-Dimethylthiazol-2-yl)-2,5-diphenyltetrazolium bromide) assay.....	30
3.3.2. xCELLigence Real Time Cell Analyzer (RTCA)	31
3.4. Molecular effects of green AgNPs on PC-3 cells.....	32

3.4.1. Cell culture and treatment	32
3.4.2. RNA Extraction using RNeasy Plus Mini Kit	32
3.4.3. RNA quantification using Qubit	33
3.4.4. Agarose gel electrophoresis analysis of the RNA Sample.....	33
3.4.5. cDNA Synthesis and confirmation by PCR.....	33
3.4.6. Analysis of gene expression by RT-qPCR	35
3.3.7. Analysis of the interaction Differentially Expressed Genes	36
3.4. Statistical analysis	37
Chapter 4: Results and Discussion.....	38
4.1. Green synthesis and characterization of AgNPs.....	38
4.1.1. UV-vis and DLS analyses of green AgNPs.....	39
4.2. Cytotoxicity of green AgNPs.....	41
4.2.1. Effect of green AgNPs on the cellular morphology.....	44
4.2.2. Determination of the IC ₅₀ of GA-AgNPs and SAL-AgNPs.....	47
4.3. Real-time analysis of the effects of SAL-AgNPs and GA-AgNPs.....	50
4.4. Molecular effects of GA-AgNPs on PC-3 cells.....	55
4.4.1. RNA and cDNA Analysis using Agarose gel Electrophoresis	55
4.5. Gene expression analysis using RT-qPCR	57
4.6. STRING Analysis of DEGs.....	69
4.7 Conclusion.....	70
References	72



List of Figures

Chapter 2

Figure 1. Synthesis of NPs via the bottom-up and top-down approaches.

Figure 2. An overview of the synthesis of NPs using the chemical, physical and green synthesis methods.

Figure 3. Green synthesis AgNPs using plant extracts.

Figure 4. The anti-microbial action of AgNPs.

Figure 5. Anti-angiogenic effects of AgNPs in vivo using a matrigel plug model with BRECs.

Chapter 4

Figure 4.1: The UV-vis spectra of green AgNPs.

Figure 4.2: Screening of the cytotoxicity effects of green AgNPs using MTT assay on human cells.

Figure 4.3: Effects of green AgNPs on cell morphology.

Figure 4.4: MTT cell viability assay for SAL-AgNPs and GA-AgNPs.

Figure 4.5: Cellular morphological changes after exposure to SAL-AgNPs and GA-AgNPs, as well as 10% DMSO positive control on A375 cells.

Figure 4.6: Realtime analysis of the effects of SAL-AgNPs and GA-AgNPs on PC-3 cells using xCELLigence RTCA.

Figure 4.7: Realtime analysis of the effects of SAL-AgNPs and GA-AgNPs on MCF-7 cells using xCELLigence RTCA.

Figure 4.8: RTCA and MTT of GA-AgNPs on human cancer cell line PC-3.

Figure 4.9: Agarose gel analysis of RNA extracted from PC-3 cells.

Figure 4.10: Agarose gel analysis of cDNA of PC-3 cells.

Figure 4.11: Clustergram showing gene expression in untreated versus GA-AgNPs-treated PC-3 cells.

Figure 4.12: STRING Analysis showing PPIs of DEGs in PC-3 cells treated with 12.5µg/ml GA-AgNPs.

List of Tables

Chapter 1

Table 1.1: Conventional cancer therapies and their adverse effects.

Chapter 2

Table 1. AgNPs synthesized from various bacteria and fungi species.

Table 2. AgNPs synthesized from various plant extracts and algae cultures.

Table 3. Plant-synthesized AgNPs and their anti-bacterial activity.

Table 4. Anti-angiogenic agents and some of their inhibitory strategies.

Table 5. Plant extract-synthesized AgNPs with anti-cancer activity.

Table 6. Plant-synthesized AgNPs with anti-diabetic activity

Table 7. AgNPs-based products approved by FDA for clinical trials

Chapter 3

Table 3.1. Optimal conditions for select AgNPs synthesis

Table 3.2: List of Cell lines, Species, source and respective Media

Table 3.3: Genomic Elimination for RNA synthesized from all untreated and treated PC-3 cells:

Table 3.4: Reverse-transcription mix preparation for 7 reactions

Table 3.5: PCR Reaction for cDNA synthesis confirmation

Table 3.6: PCR conditions for confirmation and amplification of cDNA product

Table 3.7: Total volume of SYBR Mastermix reaction experiment

Table 3.8: Light Cycler Instrument PCR Setup Conditions

Chapter 4

Table 4.1: Surface plasmon resonance, and the hydrodynamic size of the green AgNPs

Table 4.2: The IC₅₀ of GA-AgNPs and SAL-AgNPs on numerous cell lines

Table 4.3: Differentially expressed genes in the PC-3 cells treated with GA-AgNPs

List of Abbreviations

A375	Human melanoma cell line
A549	Adenocarcinoma Human Alveolar basal epithelial cells (lung cancer)
AAI	α -amylase inhibition
AGI	α -glucosidase inhibition
AgNPs	Silver nanoparticles
ATM	Ataxia Telangiectasia Mutated
AUNPs	Gold nanoparticles
BRCA1	Breast Cancer Susceptibility Gene 1
BRECS	Bovine Retinal Endothelial cells
Caco-2	Cancer coli-2 (Human colorectal cancer)
cAuNPs	Citrate capped gold nanoparticles
CAM	Chick Chorioallantonic membranes
cDNA	Complementary Deoxyribonucleic acids
Cefe	<i>Carpobrotus edulis</i> fruit (sour fig)
Cefe-AgNPs	<i>Carpobrotus edulis</i> fruit (sour fig) nanoparticles
CO	<i>Cotyledon orbiculata</i>
CO-AgNPs	<i>Cotyledon orbiculata</i> nanoparticles
COX	Cyclooxygenase-2
D.nm	Diameter values in nanometers
DEG	Differentially Expressed Genes
DLS	Dynamic Light Scattering
DMEM	Dulbecco's Modified Eagle Medium
DMEM-F12	Dulbecco's Modified Eagle Medium F-12 Nutrient Mixture (Ham)

DMSO	Dimethyl sulfoxide
DNA	Deoxyribonucleic acids
EGFR	Epidermal Growth Factor Receptor
ESKAPE	<i>Enterococcus faecium</i> , <i>Staphylococcus aureus</i> , <i>Klebsiella pneumoniae</i> , <i>Acinetobacter baumannii</i> , <i>Pseudomonas aeruginosa</i> , and, <i>Enterobacter</i> spp
G1	Cell growth phase
GA	Gum arabic
GA-AgNPs	Gum Arabic silver nanoparticles
GAPDH	Glyceraldehyde-3-phosphate dehydrogenase
gDNA	Genomic Deoxyribonucleic acids
HaCaT	Human Epidermal Keratinocytes
HSPA8	Heat Shock Cognate 71 kDa Protein
HSPB1	Heat Shock Protein Family B (small) member 1
IC ₅₀	The concentration of a drug or inhibitor needed to inhibit a biological process or response by 50%
kDA	Kilodalton
KMST-6	Immortalized Human Fibroblast cell
MCF-7	Michigan Cancer Foundation – 7 (Human Breast Cancer cell)
MKI67	Marker of Proliferation Ki-67
MMP	Matrix metalloproteinase
MNPs	Metallic nanoparticles
MTT	Thiazolyl Blue Tetrazolium Bromide
NCOA7	Nuclear receptor coactivator 7
nm	nanometer
NP(s)	Nanoparticle(s)
PARP	poly-ADP ribose polymerase

PBS	Phosphate Buffered Saline
PC-3	Human Prostate cancer cell line
PCa	Prostate cancer
PPI	Protein-Protein interaction
RNA	Ribonucleic acids
ROS	Reactive Oxygen Species
RPMI	Roswell Park Memorial Institute medium
RTCA	Real Time Cell Analysis
RTCA	Real-time Cell analysis
RT-qPCR	Reverse transcription Real-time Quantitative Polymerase Chain Reaction
RW	Red Wine
RW-AgNPs	Red wine silver nanoparticles
SAL	<i>Salvia Africana lutea</i>
SAL-AgNPs	<i>Salvia Africana lutea</i> nanoparticles
SPR	Surface plasmon resonance
SREBF1	Sterol Regulatory Element Binding Transcription Factor 1
STRING	Search Tool for the Retrieval of Interaction Genes
TBE	Tris/Borate/EDTA
TRIB3	Tribbles Pseudokinase 3
TXNL4B	Thioredoxin Like 4B
UHRF1	Ubiquitin like with PHD and Ring Finger Domains 1
UV-vis	Ultraviolet-visible Spectroscopy
VEGF	Vascular Endothelial Growth Factor

Chapter 1: Project overview

1.1. Introduction

Cancer is the second leading cause of death globally [1], For example, in 2023 there is an estimated projection of 20 million new cancer cases and 10 million deaths [2]. In 2020, cancer accounted for 10 million deaths with a staggering total of 19 million new cases of cancer [3]. The most common types of cancer were breast, lung, colorectum and prostate cancers. A global annual increase in cancer cases has been estimated at approximately 25 million cases by 2032. The alarming rise of cancer cases increases pressure on the health care facilities, especially in less developed countries where relative increase of cancer cases is higher and health care facilities are scarce [3].

The available cancer treatments for patients have been limited to a few options over many decades, that is, surgery and radiotherapy which are mainly used for solid localized tumors, and chemotherapy used to treat blood-related cancers and solid metastatic tumors (Table 1.1). These treatment strategies have been used alone or in combination with one another [4].

Table 1.1: Conventional cancer therapies and their adverse effects.

Cancer Therapy	Side effects
Chemotherapy	Mouth sores, Hair loss, Nausea/Vomiting, Fatigue, Sexual problems, Appetite loss, Anemia, Thrombocytopenia, Memory, and concentration problems
Radiotherapy	Fatigue, Hair loss, Diarrhea, Fertility problems, Urinary and bladder problems, Less active thyroid gland, Nausea/Vomiting, Swelling, Shortness of breath, Sexual problems, Lymphedema
Surgery	Lymphedema, Pain in areas of surgery, Prone to infections, Bleeding/damage to nearby tissues, Fertility problems

The conventional treatment strategies for cancer such as chemo- and radiotherapy are associated with a wide-array of side effects, ranging from discomfort to development of secondary tumors and severe off-site toxicity (Table 1.1) [5]. Drawbacks associated with conventional strategies such as; lack of specificity, toxicity and multi-drug resistance pose a huge challenge for cancer treatment. The demand for novel treatment strategies have increasingly gained attention in the recent years with the emergence of the use of NPs. Researchers have set out on a quest to address the limitations of the existing or conventional cancer treatment strategies [6]. Nanotechnology has been increasingly studied and applied over the last few decades in medicine, especially in applications for diagnosis, treatment, and tumor targeting in a safer and more effective manner [7].

NPs within the size range of 10-100nm are considered the gold standard for cancer therapy, as these small sized-NPs can effectively deliver drugs and achieve enhanced permeability and retention (EPR) effect [7]. NP-based strategies have demonstrated precise targeting, reduced side effects, and drug sensitizing effects [6]. There are various types of NPs including MNPs such as, iron, gold, silver, cerium, platinum, thallium etc. AgNPs are one of the extensively studied MNPs due to their unique physiochemical properties, such as; incredible SPR, toxicity against pathogens, ease of modification with different types of ligands, large surface area to volume ratio, etc. [8].

Green synthesized AgNPs proved to be eco-friendly, cost-effective and simple to produce as opposed to chemically synthesized AgNPs [9]. A recent study showed the anticancer activity of green synthesized AgNPs using fruit extract of *Azadirachta indica*. The AgNPs demonstrated a dose dependent activity on A549 cancer cells [10]. In another study, AgNPs synthesized using *Nepeta deflersiana* plant extract also showed dose dependent toxicity on HeLA cells [11]. Similarly, AgNPs synthesized using *Ginkgo Biloba* extract demonstrated toxicity on HeLA and SiHa cells. The AgNPs at $<2\mu\text{g/ml}$ has shown no cytotoxic effect on either of the cell lines, however, concentrations $>2\mu\text{g/ml}$ had a concentration dependent cytotoxic effect [12]. Therefore, green AgNPs are a potential treatment strategy for different kinds of tumors and can be further investigated for other applications involved in cancer treatment.

1.2. Aims and Objectives of the study

The aim of this study was to evaluate the anticancer activity and molecular effects of selected green synthesized AgNPs on a panel of cancer cell lines.

The objectives of this study were:

1. To compare bioactivity of various green synthesized AgNPs previously studied in the laboratory.
2. To investigate the cytotoxicity of green AgNPs on cancer and normal cells using the MTT assay.
3. To evaluate the real-time effects of selected green AgNPs on cell viability of cancer cells using xCELLigence Real-time cell analysis (RTCA).
4. To determine the molecular effects of highly potent green AgNPs on prostate cancer (PCa).

1.3. Thesis Outline

Chapter 1: Project Overview: Introduces the topic of this study and its relevance, by highlighting the importance of and role of green AgNPs and their potential in cancer treatment.

Chapter 2: Literature Review: It was published as a review paper. It provides a background of the study, which includes nanotechnology, the role of green-synthesized silver nanoparticles (AgNPs) and their biomedical applications.

Chapter 3: Materials and Methods: Describes the methods used for characterization and biological assays of green AgNPs in this study.

Chapter 4: Results and Discussion: Describes and discusses experimental results obtained from all biological assays and characterizations done.

Chapter 5: Conclusion: Summarizes the findings of the study, and gives recommendations for future work.

Chapter 2: Literature Review

Biomedical Applications of Plant Extract-Synthesized Silver Nanoparticles

Publication Reference:

Simon, S.; Sibuyi, N.R.S.; Fadaka, A.O.; Meyer, S.; Josephs, J.; Onani, M.O.; Meyer, M.; Madiehe, A.M. Biomedical Applications of Plant Extract-Synthesized Silver Nanoparticles. *Biomedicines* 2022, 10, 2792. <https://doi.org/10.3390/biomedicines10112792>

Thesis page numbers: 4 -27





Review

Biomedical Applications of Plant Extract-Synthesized Silver Nanoparticles

Sohail Simon ^{1,2}, Nicole Remaliah Samantha Sibuyi ^{1,3,*} , Adewale Oluwaseun Fadaka ¹ , Samantha Meyer ⁴ ,
Jamie Josephs ², Martin Opiyo Onani ⁵ , Mervin Meyer ^{1,*} and Abram Madimabe Madiehe ^{1,2,*}

- ¹ Department of Science and Innovation (DSI)/Mintek Nanotechnology Innovation Centre (NIC), Biolabels Research Node, Department of Biotechnology, University of the Western Cape, Bellville 7535, South Africa
² Nanobiotechnology Research Group, Department of Biotechnology, University of the Western Cape, Bellville 7535, South Africa
³ Health Platform Diagnostic Unit, Advanced Materials Division, Mintek, Randburg 2194, South Africa
⁴ Department of Biomedical Sciences, Faculty of Health and Wellness Sciences, Cape Peninsula University of Technology, Bellville 7535, South Africa
⁵ Organometallics and Nanomaterials, Department of Chemical Sciences, University of the Western Cape, Bellville 7535, South Africa
* Correspondence: nsibuyi@uwc.ac.za (N.R.S.S.); memeyer@uwc.ac.za (M.M.); amadiehe@uwc.ac.za (A.M.M.)

Abstract: Silver nanoparticles (AgNPs) have attracted a lot of interest directed towards biomedical applications due in part to their outstanding anti-microbial activities. However, there have been many health-impacting concerns about their traditional synthesis methods, i.e., the chemical and physical methods. Chemical methods are commonly used and contribute to the overall toxicity of the AgNPs, while the main disadvantages of physical synthesis include high production costs and high energy consumption. The biological methods provide an economical and biocompatible option as they use microorganisms and natural products in the synthesis of AgNPs with exceptional biological properties. Plant extract-based synthesis has received a lot of attention and has been shown to resolve the limitations associated with chemical and physical methods. AgNPs synthesized using plant extracts provide a safe, cost-effective, and environment-friendly approach that produces biocompatible AgNPs with enhanced properties for use in a wide range of applications. The review focused on the use of plant-synthesized AgNPs in various biomedical applications as anti-microbial, anti-cancer, anti-inflammatory, and drug-delivery agents. The versatility and potential use of green AgNPs in the bio-medicinal sector provides an innovative alternative that can overcome the limitations of traditional systems. Thus proving green nanotechnology to be the future for medicine with continuous progress towards a healthier and safer environment by forming nanomaterials that are low- or non-toxic using a sustainable approach.

Keywords: anti-microbial activity; anti-cancer activity; anti-angiogenesis activity; green synthesis; nanotechnology; metallic nanoparticles; phytochemicals; phytonanotechnology; plant-synthesized AgNPs; silver nanoparticles



Citation: Simon, S.; Sibuyi, N.R.S.; Fadaka, A.O.; Meyer, S.; Josephs, J.; Onani, M.O.; Meyer, M.; Madiehe, A.M. Biomedical Applications of Plant Extract-Synthesized Silver Nanoparticles. *Biomedicines* **2022**, *10*, 2792. <https://doi.org/10.3390/biomedicines10112792>

Academic Editor: Ali Nokhodchi

Received: 26 September 2022

Accepted: 28 October 2022

Published: 2 November 2022

Publisher's Note: MDPI stays neutral with regard to jurisdictional claims in published maps and institutional affiliations.



Copyright: © 2022 by the authors. Licensee MDPI, Basel, Switzerland. This article is an open access article distributed under the terms and conditions of the Creative Commons Attribution (CC BY) license (<https://creativecommons.org/licenses/by/4.0/>).

1. Introduction

Nanotechnology is a thriving field of science that incorporates materials at a nanoscale ranging in size from 1–100 nm [1,2]. Due to their small size, these nanoparticles (NPs) have unique physicochemical properties and exhibit extraordinary activities [3] with the potential to solve most of the health challenges faced by the globe. Metallic nanoparticles (MNPs) are among the nanomaterials that have been broadly used in the biomedical fields [4] to fight against infectious and chronic diseases. MNPs have admirable physicochemical properties such as magnetic, catalytic, photochemical, and mechanical attributes [5] that ensure and improve cellular response towards treatments [6].

MNPs are synthesized by using various metals such as gold, silver, iron, zinc, copper, palladium, platinum, and metal oxides [4,7]. However, more attention has been focused on the health-related activities of AgNPs [8]. The bio-activities of AgNPs are associated with their physical, chemical, and biological characteristics stemming from their shape, size, composition, and crystallinity compared with the bulk material [4]. Initially, AgNPs attracted global attention due to their anti-microbial activities [8] and are now widely found in commercial products, such as food packaging, soaps, cosmetics, plastics, and textiles [9,10]. However, the chemically synthesized AgNPs (cAgNPs) used in these products, together with their by-products, can be toxic and harmful to humans [11] and the environment [12,13]. In an effort to counteract these limitations, green synthesis methods were used to produce biogenic AgNPs that are biocompatible and have reduced bystander toxic effects [14]. Herein, the different approaches used for the synthesis of AgNPs were discussed with a strong focus on the plant-extract-synthesized AgNPs. Plant-synthesized AgNPs present a fresh perspective and a sustainable approach for the development of improved or new therapeutic strategies. AgNPs can be synthesized from easily accessible and renewable plant materials such as vegetables [15], fruits [16], and medicinal plants [17,18]. The phytochemicals in the extracts serve as reducing and capping agents [19] and are responsible for the stabilization of the AgNPs and their bioactivities. The phytochemicals as the capping agents will promote the biocompatibility of the AgNPs by preventing the Ag^+ ions from leaching out. Moreover, the plant-synthesized AgNPs demonstrated similar and improved bioactivities to those of the cAgNPs, such as anti-microbial [20], anti-angiogenesis [21,22], anti-cancer [23] and anti-diabetic [24,25] agents. As such, they can be used to replace the cAgNPs found in consumer products and ones in clinical trials. The biocompatibility demonstrated by the green AgNPs suggests the possibility of their application in health as therapeutic agents. Exposure to AgNPs is inevitable as they are already used for both cosmetic- and health-related purposes, and the use of biogenic AgNPs can offer some form of confidence in using these products.

2. Synthesis of AgNPs

Synthesis of AgNPs, just like other MNPs, can follow the top-down or bottom-up approaches [7,26,27]. The major difference between these two methods is the starting materials involved in the synthesis process. In the top-down approach, the bulk material is used as a starting material, which is then broken down into NPs via various physical and chemical processes, as shown in Figure 1 [4]. In contrast, the bottom-up approach uses atoms as starting material, which is then built up into larger NPs using chemical or green synthesis methods [7].

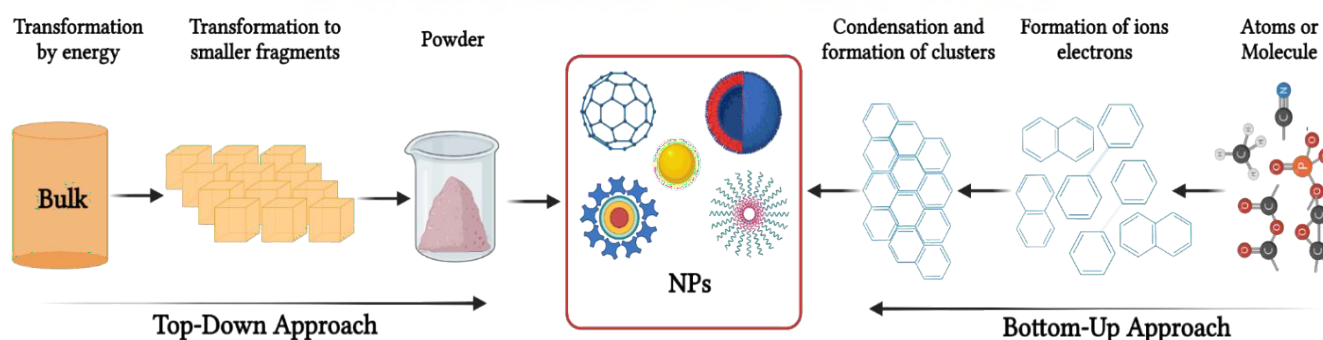


Figure 1. Synthesis of NPs via the bottom-up and top-down approaches. Bulk materials are broken down into small particles using physical methods in the top-down approach, while the bottom-up approach uses wet chemistry to assemble smaller atoms into NPs.

An overview of the physical, chemical, and green synthesis methods used for the synthesis of NPs is highlighted in Figure 2. The physical approach includes methods such as evaporation, condensation, and laser ablation [28]. These techniques are capable of

synthesizing larger quantities of AgNPs at high purity in the absence of any chemical-reducing agents [6]. Unfortunately, these physical methods have some drawbacks, such as high power consumption and time-consuming processes [29]. Additionally, complex equipment is required for the synthesis process, thus increasing the operating costs [4].

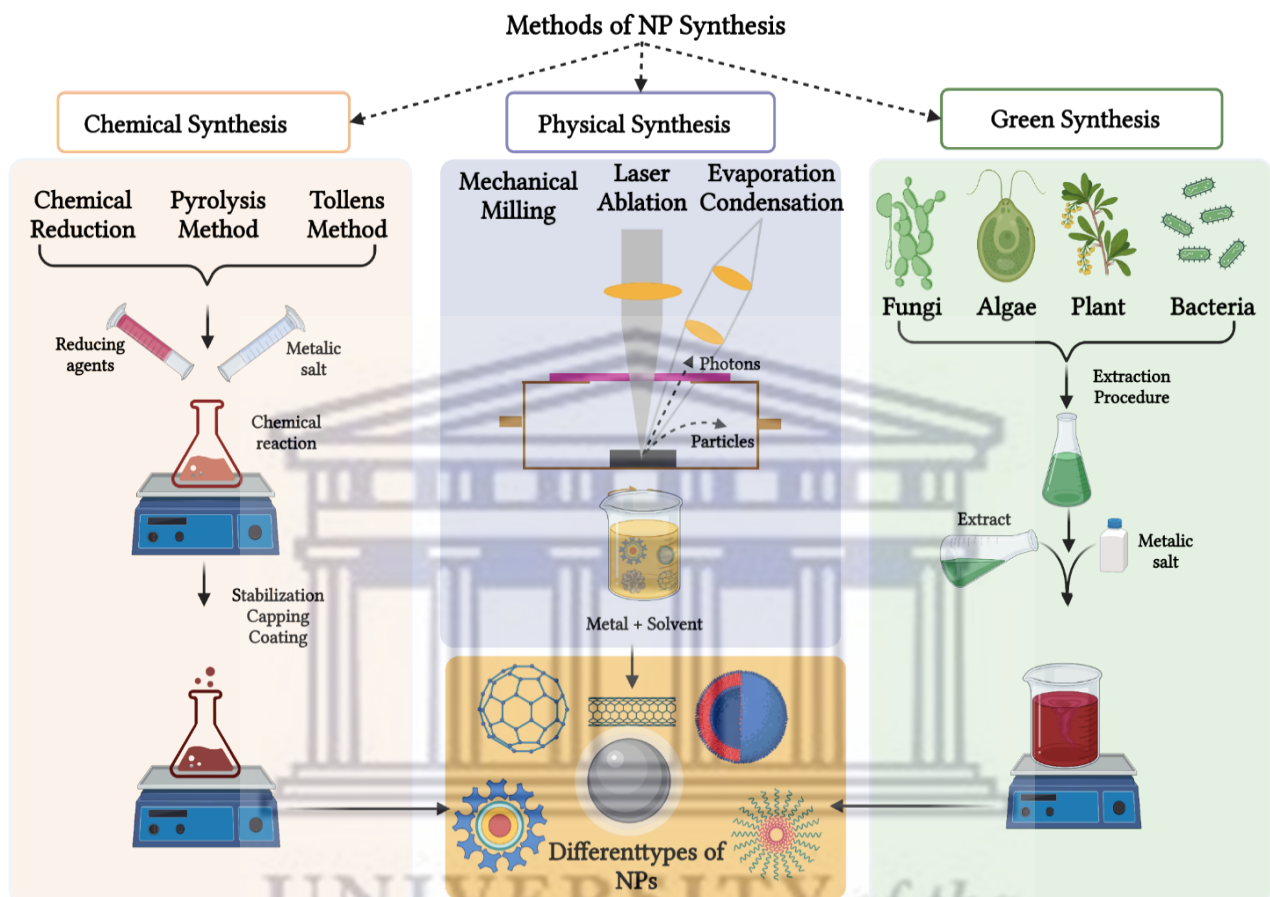


Figure 2. An overview of the synthesis of NPs using the chemical, physical and green synthesis methods. The bulk materials are crushed by physical methods to produce NPs, whereas the chemicals and natural products are used to reduce metal precursors into their respective NPs.

The chemical synthesis methods use chemicals such as sodium citrate and sodium borohydride to reduce the metal precursors into their respective MNPs. Chemical synthesis methods have been widely used in the production of MNPs by using chemical reducing agents to synthesize their respective MNPs [4]. However, chemical synthesis routes are also associated with drawbacks such as increased toxicity and high reactivity, which pose harmful threats to human and animal health and the environment [30]. Thus, there is a need for an improved synthesis strategy for MNPs in terms of sustainability, eco-friendliness, and non-toxicity. Green synthesis of AgNPs, using bio-reducing agents from natural sources such as microbial and plant extracts, can attain such properties [31].

2.1. Green Synthesis of MNPs

The green or biological synthesis methods of MNPs are a cost-effective and eco-friendly alternative to the physical and chemical methods [32]. Another benefit of biological synthesis for MNPs is that waste streams of costly materials such as gold or silver salts can be recycled, ultimately reducing the overall costs of production [30]. Green synthesis makes use of biological or natural entities such as plant or microbial extracts as reducing, capping, and stabilizing agents in the synthesis of NPs.

2.2. AgNPs Synthesis Using Microbes

Microorganisms (bacteria, fungi, and yeast) and their components are used in a biological approach to synthesize various MNPs, including AgNPs [14]. The use of microorganisms to synthesize MNPs has been extensively studied for more than three decades, and it has many advantages over chemical and physical methods, including simplicity, low cost, and the use of non-toxic reducing agents. The biomolecules from these microorganisms, such as proteins, polymers, sugars, enzymes, and others, are the ones responsible for reducing and stabilizing the metal precursors to produce biogenic MNPs [33,34].

Microbes can produce AgNPs in two ways through in vitro or in vivo methods. The in vitro method produces NPs through the extracellular process, which usually involves Ag^+ reduction by cell wall-reducing enzymes or biomolecules secreted in the culture medium. The in vivo method involves the intracellular production of AgNPs with the bio-reduction occurring within the cells [35]. When using microorganisms as a biological source, the growth medium parameters, such as pH, temperature, metal concentration, and exposure time, affect the size and shape of MNPs [30]. Table 1 shows some of the AgNPs synthesized by bacteria and fungi, resulting in different sizes and shapes [36,37]. However, the use of microbes in NP synthesis can be challenging, as both the reducing and stabilizing agents are highly dependent on their growth and maintenance [38]. The AgNPs synthesized using bacteria [36,39] and fungi [37,40] also require rigorous purification steps [41].

Table 1. AgNPs synthesized from various bacteria and fungi species.

Microbes	Strain	AgNPs Size (nm)	AgNPs Shape	References
Bacteria	<i>Arthrospira indica</i>	48–67	Spherical	[39]
	<i>Pseudomonas mandelii</i>	1.9–10	Spherical, irregular	[36]
Fungi	<i>Penicillium expansum</i>	14–25	Spherical, irregular	[37]
	<i>Aspergillus niger</i>	25–175	Spherical	[40]

2.3. AgNPs Synthesis Using Plant Extracts

Plant-mediated synthesis methods provide a sustainable alternative for the synthesis of AgNPs, as plant materials are readily available, eco-friendly, renewable, and affordable [14,42,43]. The phytochemicals in plant (roots, stems, leaves, etc.) extracts are key building blocks in the plant-mediated synthesis of AgNPs [19]. These plant extracts contain an abundance of molecules with carboxyl, amino, carbonyl, hydroxyl, and phenol groups and, thus, have the ability to reduce metals such as silver [44], gold [43], and platinum [45]. Antioxidants are strongly implicated as reducing and capping agents in these processes [46], especially the flavonoids (flavonols, flavan-3-ols), phenolic acids (benzoic, hydroxycinnamic, and ellagic acids) [33], and anthocyanins [16,33].

AgNPs are synthesized using plant extracts in a relatively simple method schematically shown in Figure 3, where the plant extracts obtained from the plant materials (vegetables, fruits, herbs, medicinal plants, etc.) are mixed with an aqueous AgNO_3 solution in various reaction conditions to produce biogenic AgNPs. The reaction parameters include the type and concentration of the extracts, metal salt concentration, temperature, and pH [47]. In most cases, a color change to brown or yellow signifies the formation of AgNPs. The wide range of phytochemicals present in plant extracts are responsible for the bio-reduction of metal cations, and other plant metabolites such as proteins and chlorophyll are responsible for stabilization of the NPs [47]. The major phytochemicals responsible for the bio-reduction process are aldehydes, ketones, flavones, sugars, terpenoids, carboxylic acids, and amides [27]. Table 2 illustrates bioactive AgNPs synthesized from various extracts obtained from different parts of plant species, such as vegetables [15], fruits [16], and medicinal plants [17,18].

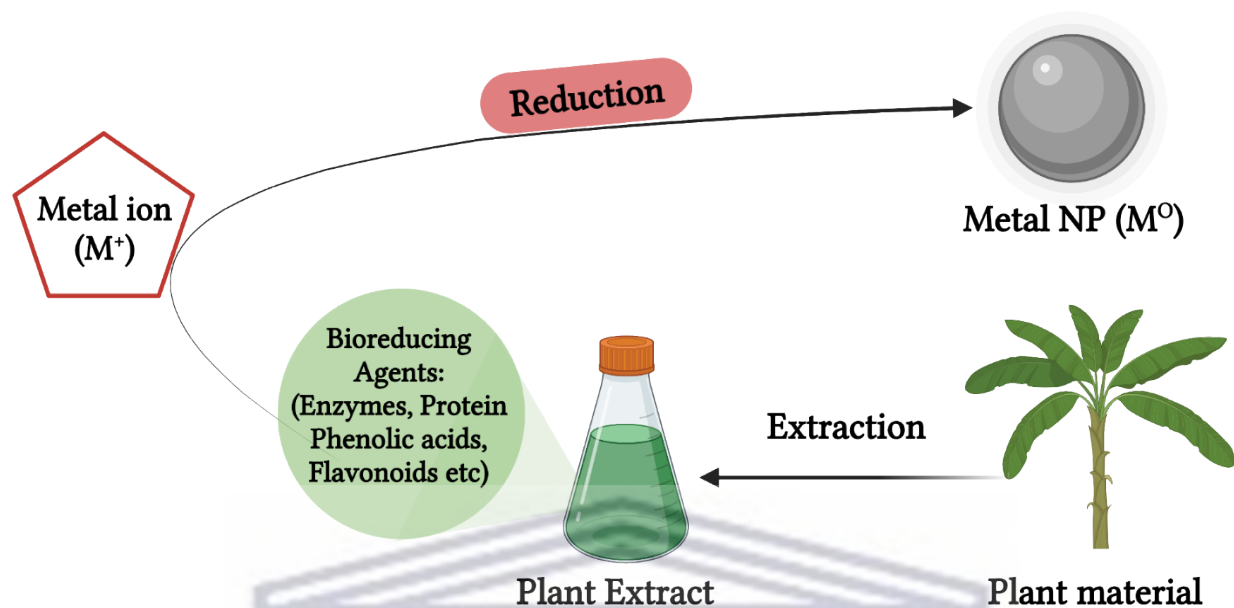


Figure 3. Green synthesis AgNPs using plant extracts. Extracts obtained from various parts of plants are used for bio-reducing and stabilizing AgNPs in a one-step synthesis method.

Table 2. AgNPs synthesized from various plant extracts and algae cultures.

Species	Type	Plant Source	Hydrodynamic Size (nm)	References
	<i>Allium cepa</i>	Onion	5–80	[15]
	<i>Solanum lycopersicum</i> L.	Tomato	2–50	
	<i>Acacia catechu</i>	<i>Acacia catechu</i> powder	5–80	
Plants	<i>Cotyledon orbiculata</i>	Plant leaves	100–140	[17]
	<i>Pyrus communis</i> L. cultivars	Fruit pulp and skins	110–190	[16]
	<i>Terminalia mantaly</i>	Root, stem bark, leaves	11–83	[18]
	<i>Coelastrum</i> sp.		19.2	
Algae	<i>Spirulina</i> sp.	Algae cultures	13.85	[48]
	<i>Botryococcus braunii</i>		15.67	

3. Biomedical Applications of Biogenic AgNPs

The anti-bacterial efficacy of AgNPs against a diverse spectrum of therapeutically relevant planktonic and sessile pathogenic microorganisms (bacteria, viruses, fungi, and yeasts) has led to tremendous interest in biomedical applications of AgNPs [8] as either therapeutic or drug delivery agents. There have been numerous reports and studies that illustrated that green AgNPs have superior potency and biocompatibility compared with cAgNPs. As a result, the biogenic or green AgNPs have been used in many preclinical and medical applications as anti-microbial, anti-cancer, drug delivery, anti-angiogenesis agents, etc. [8,44]. Although the mode of action of the green AgNPs is not well understood, their anti-bacterial and anti-cancer properties might follow similar mechanisms to that of other MNPs. For example, the induction of reactive oxygen species (ROS) within the cells in both bacteria and cells induces toxicity that ultimately causes their death [8]. Some of these applications are explored herein, and in some cases, compared with cAgNPs to weigh in on their advantages and disadvantages.

3.1. Anti-Microbial Applications of Biogenic AgNPs

Antibiotics have been used for many decades to combat infectious diseases. Antibiotics provide a strong baseline for much available modern-day medicine; however, misuse and wrong prescription of antibiotics have lowered their efficiency. These factors have led to the emergence of multi-drug-resistant microorganisms, which have become a worldwide medical concern. As such, the search for non-traditional approaches to combat multi-drug-resistant microorganisms has received increased attention. This has led to the development of novel green nanotechnology-based approaches [49]. AgNPs have been shown to be effective against over 650 microorganisms, including Gram-negative or -positive bacteria, fungi, and viruses. After decades of research, the biogenic AgNPs demonstrated attributes that make them suitable as alternative anti-microbial agents to combat multi-drug resistance [50]. Plant extracts synthesized AgNPs exhibited anti-microbial activities that were comparable and, at times, superior to that of the conventional anti-microbial agents [51]. Additionally, when the green AgNPs were used in combination with the conventional drugs, synergistic effects or improved activity were observed [52].

The exact anti-microbial mechanism of the biogenic AgNPs is not fully elucidated [53] and is speculated to follow the four well-defined mechanisms for various nanomaterials, as illustrated in Figure 4. The biogenic AgNPs can adhere to the surface of the cell wall and membrane; penetrate the cell and damage intracellular structures such as the mitochondria, ribosomes, and biomolecules (DNA and protein); induce cellular cytotoxicity and oxidative stress by generating ROS; and lastly, modulate the signal transduction pathway [53]. The AgNPs are perceived to attach to the surface of bacterial cells through electrostatic interaction between the Ag^+ ions and the negatively charged surface of the cell wall or membrane due to the presence of carboxyl, phosphate, and amino groups. As such, the Ag^+ ions will then penetrate the membrane, which will, in turn, cause structural and permeability changes leading to the dissipation of the proton motive force and destruction of the cell membrane [51]. Consequently, AgNPs can dissociate and release the Ag^+ ions into the bacterial cell, which will enhance the anti-microbial activity and cause their death [46].

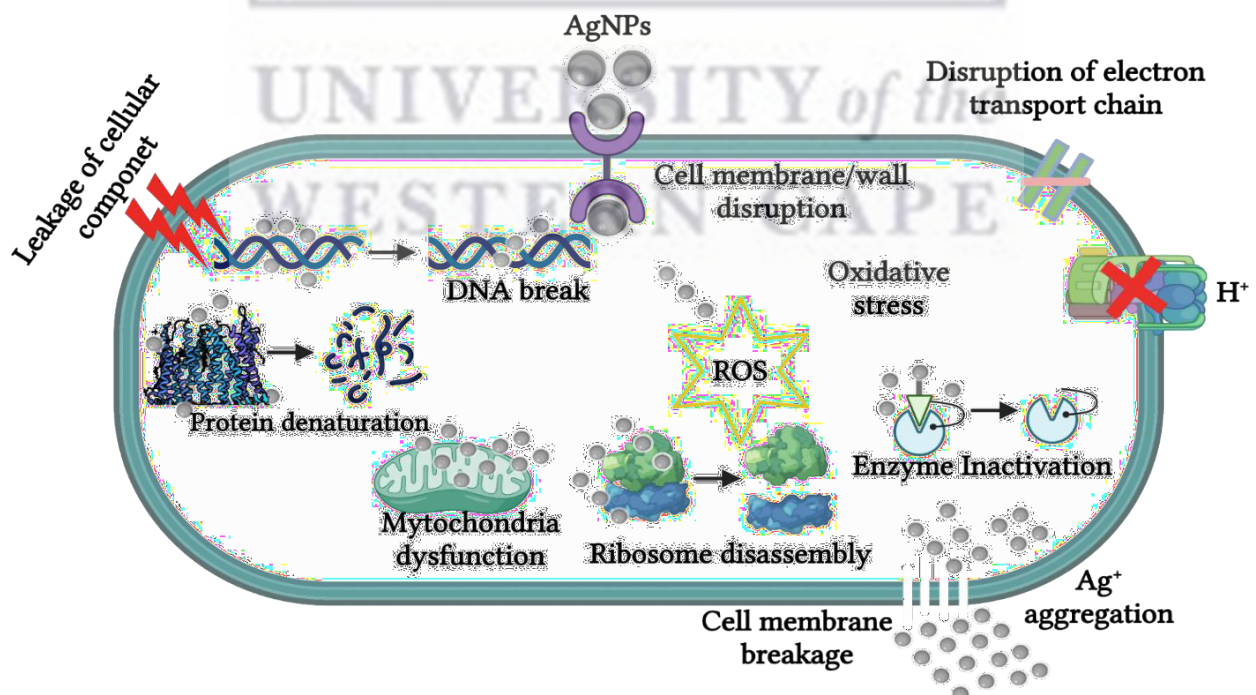


Figure 4. The anti-microbial action of AgNPs. The AgNPs can disrupt and penetrate the bacterial cell wall or membrane. The Ag^+ ions are then released into the bacterial cell and disrupt the functions of the cellular components and systems, leading to bacterial cell death.

3.1.1. Anti-Bacterial Activity

At present, many bacterial species from genera, such as *Streptococcus*, *Pseudomonas*, *Escherichia*, *Salmonella*, etc., have developed resistance to many well-known antibiotics, which present major health threats [51]. For example, *Enterococcus faecium*, *S. aureus*, *K. pneumoniae*, *Acinetobacter baumannii*, *P. aeruginosa*, and *Enterobacter* species, collectively termed ESKAPE, are considered the most virulent and classified as high-priority pathogens for human health [49,54]. Medicinal plants have been successfully used in inhibiting the growth of drug-resistant strains, including the ESKAPE pathogens, and thus have the potential to combat anti-microbial drug resistance [55]. Therefore, using these plant extracts in the synthesis of AgNPs provides an attractive strategy to produce alternative anti-bacterial agents that can kill drug-resistant pathogens [50]. The anti-bacterial activity of plant-synthesized AgNPs was somewhat comparable with that of standard antibiotics and, at times, has shown enhanced activity [51]. Moreover, synergistic effects were observed when the plant-synthesized AgNPs were used in combination with the anti-bacterial agents, implying that they can also be used as drug sensitizers [52]. Table 3 summarizes some of the plant-synthesized AgNPs and the type of microorganisms they were tested against [20]. The plant-synthesized AgNPs showed anti-bacterial activity that was comparable to that of the standard antibiotics or drugs such as penicillin-streptomycin, ampicillin, amoxicillin, vancomycin, streptomycin, etc.

Table 3. Plant-synthesized AgNPs and their anti-bacterial activity.

Plant Material	Plant Extract	Test Bacteria	Shape of AgNPs	Size of AgNPs (nm)	References
<i>Curcuma Longa</i>	Turmeric powder extract	<i>E. coli</i> <i>Listeria monocytogenes</i>	Mostly spherical with quasi-spherical, decahedral, ellipsoidal, and triangular shapes	5–35	[56]
<i>Pyrus communis</i> L. cultivars	Fruit peel and pulp	<i>S. aureus</i> , MRSA, <i>P. aeruginosa</i> , <i>E. coli</i>	Spherical	110–190	[16]
<i>Terminalia Mantaly</i>	Stem bark, leaves, and roots	<i>S. aureus</i> , <i>Streptococcus pneumoniae</i> , <i>K. pneumoniae</i> , <i>Salmonella enterica</i> , <i>Shigella flexneri</i> , <i>Hoemophilus influenza</i>	Polydispersed	11–83	[18]
<i>Salvia Africana Lutea</i>	Leaves	<i>Staphylococcus epidermidis</i> , <i>P. aeruginosa</i>	Polygon and spherical	25–40	[57]
<i>Sutherlandia frutescens</i>	Leaves	<i>S. epidermidis</i> , <i>P. aeruginosa</i>	Spherical	200–400	[57]
<i>Sapindus mukorossi</i>	fruit pericarp extract	<i>S. Aureus</i> , <i>P. aeruginosa</i>	Spherical	≤30	[58]
Grape fruit	peel extract	<i>E. coli</i> , <i>S. aureus</i> , <i>Enterococcus faecalis</i>	-	0–100	[59]
<i>Areca catechu</i>	fruits extract	<i>E. faecalis</i> , Vancomycin-resistant <i>E. faecalis</i> , <i>P. aeruginosa</i> , Multidrug-resistant <i>P. aeruginosa</i> , <i>Acinetobacter baumannii</i> , Multidrug-resistant <i>Acinetobacter baumannii</i>	Spherical	100–300	[20]
<i>Ipomoea aquatica</i>	leaf extract	<i>Salmonella</i> , <i>Staphylococcus</i> sp., <i>E. coli</i>	Spherical	5–30	[60]
<i>Acacia lignin</i>	wood dust	<i>Bacillus subtilis</i> , <i>Bacillus circulans</i> , <i>S. aureus</i> , <i>E. coli</i> , <i>Ralstonia eutropha</i> , <i>P. aeruginosa</i>	Spherical	2–26	[61]
<i>Amaranthus Tricolor</i> L.	Red spinach leaf extract	<i>E. coli</i>	Spherical	5–40	[62]

3.1.2. Anti-Fungal Activity

Fungal infections have increased at a higher rate and, together with it, the drug-resistant fungi strains, thus requiring more potent anti-fungal agents for treatment. AgNPs have received plenty of attention due to their remarkable anti-bacterial activities, which

could also present themselves as promising anti-fungal agents [63]. The anti-fungal activity of green AgNPs is not as extensively studied as that of their anti-bacterial activity. However, the limited studies so far have reported that AgNPs produced from plant extracts possess fungicidal properties. AgNPs from three medicinal plant extracts (*Boswellia ovalifoliolata*, *Shorea tumbuggaia*, and *Svensonia hyderbadensis*) had higher activity against *A. flavus*, *A. niger*, *Curvularia sp.*, *Fusarium sp.*, and *Rhizopus sp.* Among these, AgNPs derived from *Svensonia hyderbadensis* showed more activity than AgNPs derived from the other two plants [64]. AgNPs synthesized from stems and flowers of *Teucrium polium* had anti-fungal activity against *Fusarium oxysporum* [65]. *Amaranthus retroflexus*-synthesized AgNPs were reported to have anti-fungal activity against several pathogenic fungal species, especially against *Macrophomina phaseolina* and *F. oxysporum* [66]. AgNPs synthesized from strawberry waste were also reported to have anti-fungal activity against *F. oxysporum*, a plant fungus [67], further demonstrating the importance of AgNPs in both plant and human health.

3.1.3. Anti-Viral Activity

Outbreaks of infectious diseases triggered by newly emerging pathogenic viruses or those that have acquired resistance to currently available anti-viral drugs have prompted the search for novel anti-viral agents [68]. Viral infections are dependent on the virus's ability to enter and attach to host cells through the binding of viral ligands to the host's cellular proteins. The best approach for creating new anti-viral agents is to disrupt the interactions between the virus and host cell, thus preventing the virus from attaching and entering the cells. The ideal anti-viral agent should have broad-spectrum activity against pathogenic viral species to be employed as a first-class anti-viral agent against current and future viral epidemics or pandemics. As such, the anti-viral arsenal is in dire need of novel and improved anti-viral agents. AgNPs have emerged as one of the most promising anti-viral candidates, especially since AgNPs have shown broad activity against most microbes [68]. As a result of their unique intrinsic features, AgNPs have shown anti-viral activity against a variety of viruses [69], including HIV-1, monkeypox, hepatitis B, Tacaribe, Rift Valley fever, and influenza (H3N2 and H1N1) [70] viruses. However, the precise anti-viral mechanism of AgNPs, as well as the precise stage of infection at which AgNPs exert anti-viral activity, are still unknown [69].

Preclinical studies have shown that interactions between viruses and NPs result in direct or indirect anti-viral activity. Nanomaterials with indirect activity do not inhibit viruses on their own; instead, they are used as delivery agents to improve the bioavailability of anti-viral treatments and to boost their activity. Furthermore, nanomaterials can elicit an immune response, resulting in either short- or long-term immunity. Nanomaterials with direct action, on the other hand, serve as the active compound and inactivate viruses on their own, most often by modifying the viral structure or genetic material [70].

Three major elements can be derived from previous research on the anti-viral capabilities of AgNPs: (1) AgNPs have shown anti-viral activity against prokaryotic and eukaryotic organisms; thus, making them a viable broad-spectrum anti-viral candidate [71,72]. (2) Smaller AgNPs have higher anti-viral activity in most cases [73,74], and (3) AgNPs generally exert their effect at the early stage of infection of the virus [75].

Biogenic AgNPs were also reported to be potent against several viruses. *Cinnamomum cassia* synthesized AgNPs inhibited the H7N3 virus from infecting the Vero cells [76]. AgNPs synthesized from three medicinal plants, namely *Andrographis paniculata*, *Phyllanthus niruri*, and *Tinospora cordifolia*, prevented the Chikungunya virus from infecting Vero cells in a dose-dependent manner. The *A. paniculata* AgNPs were the most active, followed by *T. cordifolia* AgNPs. The *P. niruri* AgNPs did not show as significant an inhibitory effect as the other two AgNPs [77], signifying that the phytochemicals indeed influence the function and activity of the AgNPs. AgNPs synthesized from aqueous and hexane extracts of *Lampranthus coccineus* and *Malephora lutea* also prevented infection of Vero cells with HSV-1, HAV-10, and Coxsackie B4 viruses. Furthermore, the *L. coccineus* hexane AgNPs showed

higher anti-viral activity against all three viruses, while the *L. coccineus* aqueous AgNPs had weaker anti-viral activity against HSV-1 and no anti-viral activity against HAV-10 and CoxB4 viruses. The *M. lutea* AgNPs showed anti-viral activity against HAV-10 and CoxB4 viruses, with no activity against HSV-1 [78].

3.2. Anti-Angiogenesis Activity

Angiogenesis is the process of creating new blood vessels from pre-existing ones [79]. It is required for various physiological processes such as embryo development, ovulation, and wound healing. The combination of several pro-angiogenic and anti-angiogenic factors regulates this process. While the physiological angiogenesis is well controlled, disruptions in this process have been reported in cancer and obesity development and progression, resulting in excessive blood vessel proliferation [80]. The first angiogenesis hypothesis was proposed nearly four decades ago, stating that tumor growth is reliant on its blood vessels to supply nutrients and oxygen to the tumors, for removal of waste and to spread to other tissues [81]; and that cutting off the blood supply can be used as a therapeutic intervention. Strategies targeting factors that contribute to tumor development could successfully treat cancer and other diseases caused by dysfunctional angiogenesis [82].

Vascular Endothelial Growth Factor (VEGF) is one of the well-studied angiogenesis activators which was shown to be overexpressed during tumor growth and metastasis [83]. VEGF expression is upregulated by nuclear factor-kappa B transcription factor, which in turn promotes the expression of anti-apoptotic proteins such as Bcl-2; and prevents cancer cell death [84]. As a result, anti-angiogenesis strategies were used to prevent the development of new blood vessels and supply of blood to the tumor [79] and stop cancer growth and progression [85]. Consequently, anti-angiogenesis strategies inhibited tumor growth, and the tumors were unable to grow larger than 1–2 mm³ in size and died as a result of hypoxia [86]. Monoclonal antibodies (mAB) against pro-angiogenic factors or their receptors, matrix metalloproteinase (MMP) inhibitors, and signal transduction blocking are some of the methods that were reported to inhibit angiogenesis. Anti-angiogenic drugs or chemotherapy (Table 4) have been shown to improve cancer outcomes [81]. However, there are several drawbacks associated with the use of angiogenesis inhibitors, including drug resistance, the disruption of VEGF-dependent angiogenesis, and the reduction of radiotherapy response, among others [82]. As such, using monotherapy to prevent angiogenesis could be ineffective [87]. Improvements in the efficacy and biocompatibility of the drugs (angiogenesis inhibitors) were reported when a drug carrier was used. NPs, among others, have done a stellar job in this regard, serving as both a drug carrier and/or angiogenesis inhibitor.

Table 4. Anti-angiogenic agents and some of their inhibitory strategies.

Anti-Angiogenesis Drugs	Angiogenesis Inhibitory Strategies	References
Bevacizumab (Avastin)	Target VEGF and inhibits formations of VEGF complexes such as VEGF-A and VEGF-2	[88]
Semaxanib, Sunitinib, Sorafenib, Vatalanib	Inhibition of receptor tyrosine kinase	[89–91]
GEM 220	Inhibition of VEGF	[92,93]
Endostatin	Inhibition of endothelial-cell survival	[94]
Erlotinib, Gefitinib	Inhibitors of EGFR	[95]
Celecoxib, Rofecoxib	COX-2 inhibitors	[96,97]

The anti-angiogenic properties of nanomaterials have been reported and provide an alternative candidate for anti-angiogenetic therapy for a variety of diseases [81], including cancers and obesity. NPs may be a useful treatment option as anti-angiogenic or drug-delivery agents. And through antibodies, aptamers, microRNAs, and peptides, among others, the nanomaterials can be targeted to specific tissues [98]. The anti-angiogenic

activity of cAgNPs has been reported. In one study, it was associated with the inhibition of hypoxia-inducible factor-1 expression in breast cancer (MCF-7) cells, consequently affecting the expression of anti-angiogenic factors such as VEGF-A and glucose transporter-1 [99,100]. *Bacillus licheniformis* AgNPs inhibited the proliferation and migration of bovine retinal endothelial cells (BRECs) as a model system for angiogenesis after 24 h. The AgNPs activated caspase-3 activity and DNA fragmentation, which in turn inhibited the VEGF-induced PI3K/Akt pathway in BRECs [101]. AgNPs synthesized from *Saliva officinalis* extracts were also shown to have anti-angiogenic activity in vivo. The *Saliva officinalis* AgNPs had a dose dependent anti-angiogenic activity on chick chorioallantoic membranes (CAM). Ross fertilized eggs were exposed to the *Saliva officinalis* AgNPs on day 8. After 4 days, the AgNPs demonstrated dose-dependent anti-angiogenetic effects [80]. Similarly, other plant-extract-synthesized AgNPs reduced blood vessel formation in a CAM assay, these included AgNPs from *Azadirachta indica* leaf [22] and *Ceropegia juncea* [21] extracts. Although the mechanism was not clearly defined, using the matrigel plug model with BRECs in mice, it was shown that AgNPs might induce anti-angiogenic effects by inhibiting the expression of VEGF, as illustrated in Figure 5 [99]. These strategies might also be of health benefit to other diseases with excessive angiogenesis, such as atherosclerosis, arthritis, obesity, pulmonary hypertension, diabetic retinopathy, and age-related macular degeneration [102].

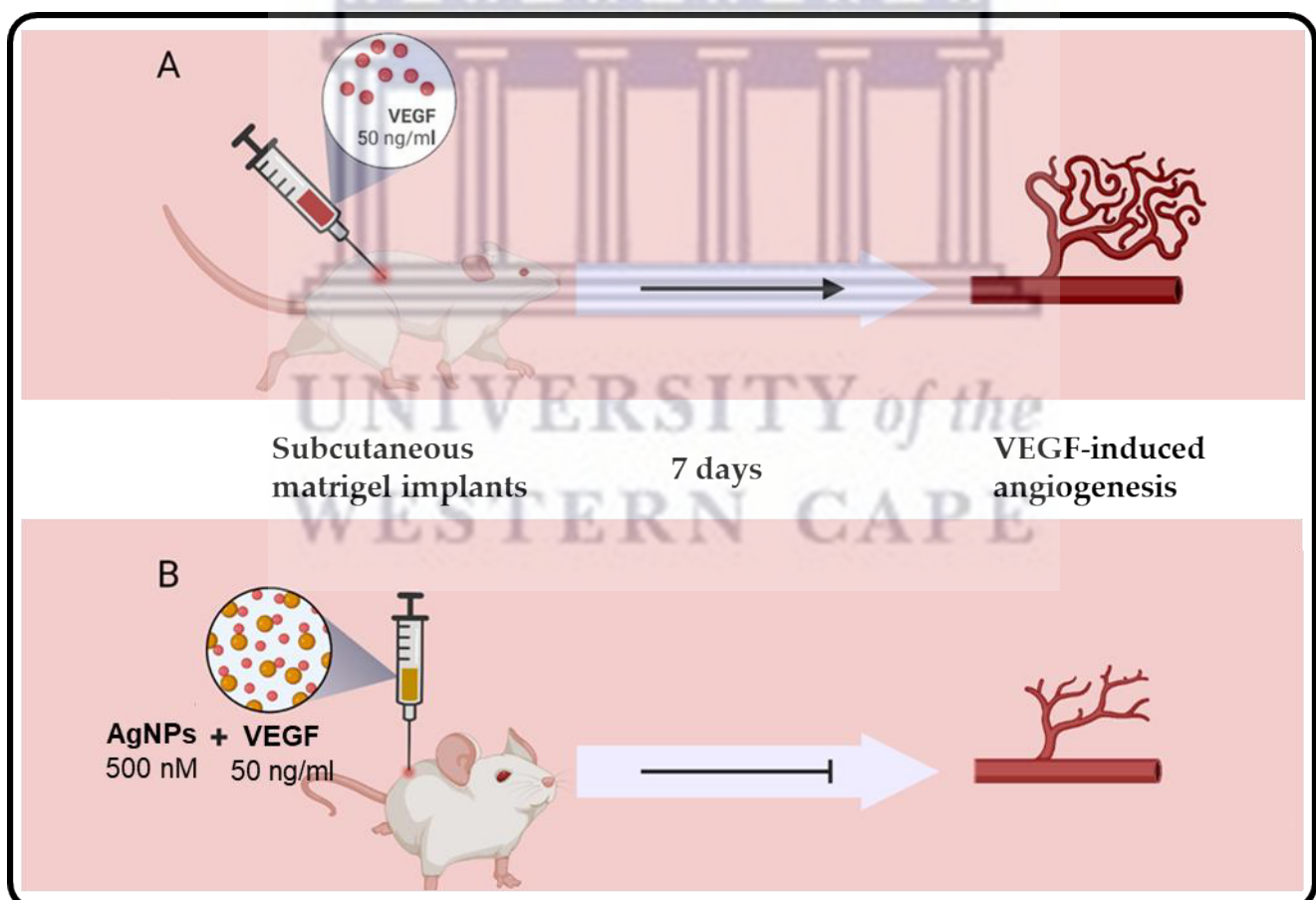


Figure 5. Anti-angiogenic effects of AgNPs in vivo using a matrigel plug model with BRECs. Matrigel plugs containing BRECs with and without 50 ng/mL VEGF were implanted into mice for 7 days. Angiogenesis occurred in mice treated with VEGF alone (A). The AgNPs inhibited the VEGF-induced angiogenesis in mice implanted with matrigel plugs containing BRECs with 50 ng/mL VEGF and 500 nM AgNPs after 7 days (B). Adapted from [99].

3.3. Anti-Cancer Activity

Cancer remains one of the highest killers in the world, with 18.1 million cancer cases reported in 2020. Of these cases, 9.3 million cases were men, and 8.8 million cases were women [103]. The basic problems of early detection and treatment need to be addressed to combat cancer [69]. Moreover, the ability to reach the target site at a sufficient concentration and have efficacious activity without causing harm to healthy cells and tissues are crucial points regarding the effectiveness of anti-cancer drugs [69].

Cancer treatment strategies employ the use of radiation therapy, chemotherapy, surgery, immunotherapy, photodynamic therapy, and stem cell transformation, individually or in combination. However, there are side effects that accompany these treatment strategies, such as non-specificity, limited bioavailability, toxicity, and early drug clearance [104]. The use of chemotherapeutic agents can cause toxic side effects. For example, 5-fluorouracil and doxorubicin, the commonly used chemotherapeutic agents, are linked to renal toxicity, cardiotoxicity, myelotoxicity, and blood vessel constriction [104].

Research into newer technologies to prevent systemic and bystander side effects, as well as to improve on the existing drugs, has led to the development of nanotechnology-based therapeutics [105]. Doxil (doxorubicin encapsulated in liposomes) [106] and Abraxane (paclitaxel bound with albumin) [107] are the first organic nano-formulations to be FDA-approved for the treatment of cancer. The AuNPs were the first MNPs to be approved for human trials as drug delivery and diagnostic agents [1,108]; AgNPs followed suit as anti-microbial agents [109]. Several studies have demonstrated the potential anti-cancer activity of AgNPs, including AgNPs synthesized from various plant extracts [23]. Table 5 highlights some of the plant-synthesized AgNPs and their anti-cancer effects on multiple cancer cell lines, namely breast (MCF-7) [110], lung (A549) [111], cervical (HeLa) [112], colon (HT-29, Caco-2) [113], prostate (PC-3) [26], and VCaP [114] cancer cell lines. The half-maximal inhibitory concentration (IC₅₀) of AgNPs was comparable to that of standard anti-cancer drugs [23] and a validation that AgNPs could be useful as anti-cancer agents.

Table 5. Plant extract-synthesized AgNPs with anti-cancer activity.

Cancer	Plant	AgNPs Size (nm)	AgNPs Shape	Cell Line	IC ₅₀ (µg/mL)	References
Breast cancer	<i>Achillea biebersteinii</i>	12	Spherical, pentagonal	MCF-7	20	[80]
	<i>Melia dubia</i>	7.3	Irregular		31.2	[110]
	<i>Ulva lactuca</i>	56	Spherical		37	[115]
Liver cancer	<i>Cucumis prophetarum</i>	30–50	Polymorphic shape (ellipsoidal, irregular)	HepG-2	94.2	[116]
Lung cancer	<i>Rosa damascene</i>	15–27	Spherical	A549	80	[117]
	<i>Gossypium hirsutum</i>	13–40	Spherical		40	[118]
	<i>Syzygium aromaticum</i>	5–20	Spherical		70	[111]
Cervical cancer	<i>Podophyllum hexandrum</i>	14	Spherical	HeLa	20	[112]
	<i>Heliotropium indicum</i>	80–120	Spherical	Siha	20	[119]
	<i>Azadirachta indica</i>	2–18	Triangular and hexagonal		≤4.25	[120]
Colon cancer	Gum arabic	1–30	Spherical	HT-29	1.55	[113]
				Caco-2	1.26	
Prostate cancer	<i>Alternanthera sessilis</i>	50–300	Spherical	PC-3	6.85	[26]
	<i>Gracilaria edulis</i>	55–99	Spherical	PC-3	53.99	[121]
	<i>Dimocarpus longan</i>	8–22	Spherical	VCaP	87.33	[114]

The working principles and mechanisms of action of AgNPs are critical and unique to each cell type. Many factors influence their cytotoxicity and genotoxicity, including size, shape, surface charge, surface coating, solubility, concentration, media, surface composition, distribution into cells, method of entry, and cell type [122]. Their biological activities are also dependent on their possible interaction with proteins in cell culture media or in vivo, forming a protein corona that might enable interactions between AgNPs and cells to induce or ameliorate toxicity [123]. AgNPs can penetrate the cell through the assistance of cellular components, such as the endosomes and lysosomes, or through passive or active transport modes, such as pinocytosis, phagocytosis, etc. [124].

The interaction of AgNPs with biomolecules can cause a variety of physiological and metabolic changes, including oxidative stress, conformational changes, enhanced membrane permeability, mutations, signaling pathway activation, ionic exchange disorder, and exposure to novel protein epitopes [125]. Several in vitro models demonstrated that ROS-mediated toxicity is more apparent and results in cellular and metabolic changes. As such, oxidative stress is the most likely mechanism of AgNPs-induced toxicity [126]. The formation of peroxide (H_2O_2) and superoxide (O_2) radicals changes the trans-membrane potential of mitochondria, allowing the respiration mechanism to become uncoupled, thus causing oxidative stress [127]. ROS is one of the mechanisms commonly followed by plant-based AgNPs; it alters the signal transduction pathway and induces cell death by apoptosis [128–130]. AgNPs trigger intrinsic apoptosis by releasing cytochrome c into the cytosol and translocation of Bax to the mitochondria, as well as cell cycle arrest in the G1 (cell growth) and S (DNA synthesis) phases [131]. Plant-based AgNPs are also capable of inducing cell death by upregulating the expression of genes that causes apoptosis, such as the p53, Bax, and poly-ADP ribose polymerase (PARP)-1, p21. *Mentha arvensis* AgNPs activated breast cancer cell death following different pathways, indicating the ability of green AgNPs to overcome drug resistance. *Mentha arvensis* AgNPs induced caspase-3-dependent death in MDA-MB-231 cells due to mutations in p53, and through caspase 9-dependent apoptosis in p53-expressing MCF-7 cells [132].

3.4. Anti-Diabetic Activity

Diabetes is a chronic disease in which blood sugar levels rise due to inadequate insulin output or when the cells do not respond well to insulin. As a result, diabetes can be either insulin-dependent or insulin-independent [52]. Several enzymes are involved in this complex disease, with two of the most important regulators being α -glucosidase, which is responsible for the breakdown of disaccharides to monosaccharides, and α -amylase, which is responsible for the breakdown of the long-chain carbohydrates (polysaccharides to disaccharides). Thus, inhibition of these enzymes would provide an effective anti-diabetic strategy [51].

The anti-diabetic effect of plant-synthesized AgNPs has been reported for both in vitro and in vivo studies. In vitro, the potential of the AgNPs to reduce blood glucose levels was tested based on their ability to block the secretion of the two enzymes [52] and, in some instances, the dipeptidyl peptidase IV [133]. Some of the plant-based AgNPs able to inhibit the activity of the three enzymes are summarized in Table 6. AgNPs synthesized from *Calophyllum tomentosum* [133], *Punica granatum* [134], *Ficus palmata* [24], and *Lonicera japonica* [135] leaf extracts demonstrated α -amylase inhibition (AAI) and α -glucosidase inhibition (AGI) in vitro. The green AgNPs were found to have high levels of AAI and AGI; as such, the green synthesized AgNPs might have strong anti-diabetic activity [24,25,134,136]. In vivo, the anti-diabetic activity of these AgNPs was measured based on their ability to reduce blood glucose levels and their effect on other blood biochemical events (cholesterol and triglycerides). The *Solanum nigrum* AgNPs reduced blood glucose levels in alloxan-induced diabetic rats [136]. *Eysenhardtia polystachya* AgNPs also protected the pancreatic β cells from oxidative cellular damage, enhanced secretion of insulin and hypolipidemia. These effects were also replicated in a glucose-induced diabetic zebrafish [137]. *Cassia auriculata* AgNPs, in a similar manner, were shown to reduce blood glucose levels and

normalized other markers associated with diabetes in streptozotocin-induced diabetic rats [138].

Table 6. Plant-synthesized AgNPs with anti-diabetic activity.

Plant Type	Core Size (nm)	Hydrodynamic Size (nm)	AgNPs Inhibitory Effect	Test Sample	References
<i>Calophyllum tomentosum</i> leaves extract	-	24	α -amylase	Starch	[133]
			Dipeptidyl peptidase IV	Gly-Pro-P-Nitroanilide	
			α -glucosidase	4-nitrophenyl- α -D-glycopyranoside	
<i>Punica granatum</i> leaves	20–45	35–60	α -amylase	Starch	[134]
			α -glucosidase	para-nitrophenyl- α -D-glycopyranoside	
Grape Pomace	5–40	-	inhibits α -amylase and α -glucosidase	α -amylase and α -glucosidase	[25]
<i>Solanum nigrum</i>	4–25	-	Glucose inhibition	alloxan-induced diabetic rats	[136]
Bark of <i>Eysenhardtia polystachya</i>	5–25	36.2	Promote pancreatic β -cell survival; Restores insulin secretion in INS-1 cells	Glucose-induced adult Zebrafish (hyperglycemia)	[137]

Note: -, not reported.

3.5. Anti-Inflammatory Activity

Inflammation is a vital defensive mechanism in which the body reacts to external stimuli such as bacteria, irritants, or damaged cells. Various cells, including molecular mediators, immune, and blood cells, are involved in this complicated process [139]. Chronic inflammation, on the other hand, can also do more damage than good and can last for longer periods. Prolonged inflammation is a major problem for many metabolic diseases such as obesity, insulin resistance, and diabetes [140,141], as well as in wound healing. It is classified as the second phase of the wound-healing process [10,142]. As such, the quest for compounds that can stop chronic inflammation may be beneficial in the treatment of these diseases and in human health.

AgNPs are among the MNPs that were demonstrated to have anti-inflammatory properties [10]. AgNPs have shown anti-inflammatory response during wound healing by modulating the expressions of various inflammatory response genes in vitro such as tumor necrosis factor (TNF)- α , interferons, interleukin 1, cyclooxygenase (COX)-2, and matrix metalloproteinases-3 [27,133,143,144]. A number of plant-based AgNPs with anti-inflammatory effects that are beneficial to wounds have been reviewed elsewhere [142] and show potential for the treatment of metabolic and autoimmune disorders. *C. orbiculata* AgNPs inhibited pro-inflammatory cytokines (TNF- α , IL-6, and IL-1 β) in THP-1 differentiated macrophages and NK cells [17]. *Piper nigrum* AgNPs selectively inhibited the expression of IL-1 β and IL-6 [145], suggesting the anti-inflammatory activity of these green AgNPs. Another anti-inflammatory activity was demonstrated by the *Viburnum opulus* L fruit AgNPs on skin keratinocytes (HaCaT). The IL-1 α was released due to irradiation of the cells indicating the anti-inflammatory activity of the AgNPs. The phenomenon was further investigated in vivo in carrageenan-induced hind paw edema and found that injecting AgNPs into the skin of Wistar rats moderated cytokine release within 2 h. The AgNPs demonstrated inhibitory activity against COX-2, which is one of the main causes of inflammation [146]. Overall, these studies demonstrated that green-synthesized AgNPs could be used as a valuable therapeutic method for the treatment of inflammation.

3.6. AgNPs as Drug Delivery Agents

Drug delivery via MNPs is an effective strategy for the treatment of a variety of diseases [147]. The two most important strategies for effective drug delivery systems are: slow and sustained drug release, and delivery to specific targets. These conditions can be

met through active or passive delivery methods [148]. Conventional strategies for cancer treatment, such as chemotherapy and radiotherapy, come with various side effects, such as drug toxicity, lack of specificity, unpredictability, and drug resistance [149].

Since one of the most studied topics for improving current human healthcare practice has been the precise and selective delivery and action of therapeutic agents, NPs have received a lot of attention when it comes to the design and development of novel and improved drug-delivery systems [8]. More specifically, green synthesized AgNPs could overcome the disadvantages associated with conventional therapies by reducing their side effects and enhancing their efficacy [149]. Green nanotechnology is an innovative approach that can improve disease treatment, and when green AgNPs are coupled with anti-cancer drugs can directly deliver the drugs to the tumor tissues due to the ability of the AgNPs to pass through various biological barriers [149]. The size of the NPs influences drug uptake and distribution in the cells via endocytosis. AgNPs synthesized from the *Aerva javanica* extract coupled with the anti-cancer agent (gefitinib) had higher apoptotic potency than gefitinib alone on the MCF-7 cells. Gefitinib delivery by the AgNPs improved the drug efficacy while reducing the negative effects [150].

Outside of oncology, AgNPs conjugated with the anti-seizure drugs against brain-eating amoebae (*Naegleria fowleri*) were used to treat central nervous system infection. Anti-seizure drugs (diazepam, phenobarbitone, and phenytoin) that are known to pass through the blood-brain barrier were added on the surface of AgNPs as capping agents and demonstrated general anti-amoebic activity against both trophozoite and cyst phases. The AgNPs-drug conjugates showed a considerable increase in fungicidal activity against both trophozoite and cyst amoebic stages, as compared with the drugs alone [4].

4. Perspectives and Concerns for Clinical Application of AgNPs

Nanotechnology is gaining worldwide recognition due to the growing capacity and applications of engineered NPs [151]. Over the last few decades, the wide distribution and use of nanomaterials in medical imaging, disease diagnosis, drug delivery, and a variety of consumer-based products have been on the rise. This is attributed to their novel properties [44,152], which are influenced by their small size, large surface area to volume ratio, drug loading capacity, and ease of functionalization of the NP surface. However, the extensive application of these nanomaterials has raised concerns regarding potential health and environmental effects [151]. Despite the numerous advantages offered by the NPs, the potential health hazards cannot be overlooked due to their uncontrollable release into the natural environment and possibly deleterious effects on organisms that are continually subjected to exposure to these nanomaterials [153]. Hence, toxicity studies are perpetually conducted to make the application of NPs more environmentally friendly. Among the most frequently studied nanomaterials are fullerenes, carbon nanotubes, gold, titanium oxide, iron oxide, and silver NPs [151].

The increase in the number of commercial AgNPs-based products without any regulatory restraints and risk assessment policies is a major issue that can turn into a health scare. The lack of proper health hazard assessments is mainly due to the historical use of silver-based products for health purposes, which must be regarded as a call for concern because prolonged use of silver-based compounds in wound care was associated with argyria, bacteria resistance, and toxicity. Since these were topically administered, the effects were easy and quick to observe [10]. However, unlike the bulk silver compounds, AgNPs are smaller in size, and their route of administration can differ based on the intended application. All these might alter their uptake, distribution and ultimately their biological effects. Studies have reported on the size, shape, surface composition, and dose of the AgNPs as the major contributing factors to their toxicity; some external factors include time, suspension media, cell, and species type [11,154].

AgNPs have demonstrated a remarkable potential for the development of novel anti-microbial, biosensing, imaging, drug-delivery, and therapeutic agents [8] and are used to improve or as alternatives to the current therapies [155]. The incorporation of AgNPs within

the biomedical sector [10,109,156] is attributed to their biocompatibility and anti-bacterial activity. Several cAgNPs-based formulations were approved for clinical trials by the FDA (Table 7) as anti-microbial and wound healing agents [10] for topical and oral applications in humans [109]. In fact, 37 AgNPs-based clinical trials are registered in the U.S. National Library of Medicine ClinicalTrials.gov database to date. The majority of these products were for dental and wound healing applications, although there were some registered for rhinosinusitis, pain management and COVID-19. The completion of 51% of the trials validates that AgNPs have been ingested, inhaled, or absorbed by human beings, including children from 1–12 years of age. Their incorporation in dental composite resins, such as restorative, prosthetic, endodontics, implantology, and periodontology, has undoubtedly shown notable anti-microbial properties and reduced microleakage in the root canal system. When used in dental irrigation, AgNPs-based formulations showed similar potency to that of sodium hypochlorite against *E. faecalis* [157]. Nonetheless, exposure to AgNPs can be lethal even at low levels [154], and these detrimental effects can be long-lasting and passed to future generations [11]. In animals, administration of AgNPs exposed them to vital organs such as the kidneys, lungs, spleen, and liver, and their accumulation in these organs has been associated with an altered expression of genes involved in oxidative stress, apoptosis, and ion transport [158]. Although the biogenic AgNPs are considered to have a reduced risk of toxicity compared with cAgNPs, they are also non-selective. The toxicity of biogenic AgNPs is also influenced by a number of parameters, among others being the size [113].

Colloidal stability is considered a significant factor affecting the fate of AgNPs. When introduced into the environment, AgNPs possess a high affinity for biomolecules, such as DNA, proteins; leading to the formation of AgNPs-protein corona, which can alter the activity of the NPs. Furthermore, AgNPs can be affected by pH, where if the environmental pH corresponds to the isoelectric point (pI) of biomolecules on the AgNPs, the NPs become unstable and ultimately form aggregates [159]. The release of Ag⁺ ions into the environment greatly impacts the toxicity of AgNPs [12]. Importantly, their fate after being released into the environment and interaction with the surroundings is of serious concern [13]. The most commonly known process related to AgNPs transformation is oxidative dissolution [12] when subjected to oxygen-rich conditions [13]. The capping agents in the green AgNPs, which act as stabilizers, might protect the AgNPs against agglomeration and reduce their cytotoxicity. The biomolecules on the surface of the AgNPs are likely to enhance their biocompatibility and render them safe for use in various biomedical applications [160].

Table 7. AgNPs-based products approved by FDA for clinical trials.

Status	Study Title	ClinicalTrials.gov Identifier	AgNPs Formulation	Condition	Participants	Administration Route	Phase
Active, recruiting	Colloidal silver, treatment for COVID-19	NCT04978025	AgNPs	Severe acute respiratory syndrome	50	Oral and inhalation	N/A
	Topical application of silver nanoparticles and oral pathogens in ill patients	NCT02761525	12 ppm of AgNPs- innocuous gel	Critical illness	50	Oral mucosa	N/A
	Silver nanoparticles in multi-drug-resistant bacteria	NCT04431440	AgNPs	Methicillin and vancomycin-resistant S.	150	Tested on clinical isolates	N/A
	Nano-silver fluoride to prevent dental biofilms growth	NCT01950546	5% nanosilver fluoride (390 mg/mL 9 nm AgNPs, 21 mg/mL chitosan, 22 mg/mL NaF)	Dental caries	30	Applied on cervical vestibular surfaces of incisors and canines	1
	The anti-bacterial effect of nano-silver fluoride on primary teeth	NCT05221749	Nano-silver fluoride	Dental caries in children (1–12 years old)	50	Oral	3
Completed	Evaluation of silver nanoparticles for the prevention of COVID-19	NCT04894409	ARGOVIT® AgNPs (Mouthwash and nose rinse)	COVID-2019	231	Mouthwash and nose rinse	N/A
	Assessment of postoperative pain after using various intracanal medications in patients with necrotic pulp	NCT03692286	AgNPs and calcium hydroxide vs. AgNPs in gel form	Necrotic pulp (postoperative pain)	30	Intracanal medication	4
	Effect of thyme and carvacrol nanoparticles on aspergillus fumigatus isolate from intensive care patients	NCT04431804	AgNPs	Aspergillosis	210	Aspergillus isolates	N/A
	Evaluation of diabetic foot wound healing using hydrogel and nano silver-based dressing vs. traditional dressing	NCT04834245	Hydrogel and nano silver-based dressing	Diabetic wounds	30	Topical wound dressing	N/A
	Comparison of central venous catheters (CVC) with silver nanoparticles versus conventional catheters	NCT00337714	CVC impregnated with AgNPs (AgTive®)	CVC related infections	472	Cannulation	4
	Topical silver nanoparticles for microbial activity	NCT03752424	AgNPs-cream	Fungal infection (Tinea pedis, Capitis and Versicolor)	30	Topical	1
	Research on the key technology of burn wound treatment	NCT03279549	Nano-silver ion gel and dressings	Burns	200	Topical	N/A
Unknown	Addition of silver nanoparticles to an orthodontic primer in preventing enamel demineralisation adjacent brackets	NCT02400957	AgNPs incorporated into the primer orthodontic Transbond XT	Tooth demineralisation	40	Dental application	3
	Fluor varnish with silver nanoparticles for dental remineralisation in patients with Trisomy 21	NCT01975545	25% of 50 nm AgNPs in fluor varnish	Dental remineralisation in patients with Down syndrome	20	Oral varnish	2
	Efficacy of silver nanoparticle gel versus a common anti-bacterial hand gel	NCT00659204	Nano-silver gel (SilvaSorb® gel)	Healthy	40	Topical on hands	3

5. Conclusions

Plant-extract-synthesized AgNPs can be used as an alternative to cAgNPs and conventional treatment strategies, as well as in combination with current treatments to enhance their efficacy. Due to their size-dependent physicochemical properties, eco-friendliness, availability, and cost-effectiveness; green AgNPs have been used in a variety of biomedical applications, such as anti-bacterial, anti-fungal, anti-viral, anti-cancer, anti-angiogenesis, anti-inflammatory, and drug delivery agents. There is a large amount of research describing the benefits of green AgNPs in novel biomedical strategies. As such, their long- and short-term toxicity requires a much more thorough investigation to alleviate the fear of their societal and environmental impacts. This review demonstrated the versatility of green AgNPs in many innovative therapeutic strategies that can help fight against current and future pandemics due to their multifaceted activities.

Author Contributions: A.M.M., S.M., M.O.O., and M.M.—conceptualization, student supervision, and funding acquisition; S.S., N.R.S.S., A.O.F., and J.J.—writing the initial draft; S.S., N.R.S.S., A.O.F., S.M., M.O.O., M.M. and A.M.M.—writing—review and editing, methodology, and resources. All authors have read and agreed to the published version of the manuscript.

Funding: Authors state no external funding was involved.

Institutional Review Board Statement: Not applicable.

Informed Consent Statement: Not applicable.

Data Availability Statement: Not applicable.

Conflicts of Interest: Authors state no conflict of interest.

References

1. Sibuyi, N.R.S.; Moabelo, K.L.; Fadaka, A.O.; Meyer, S.; Onani, M.O.; Madiehe, A.M.; Meyer, M. Multifunctional Gold Nanoparticles for Improved Diagnostic and Therapeutic Applications: A Review. *Nanoscale Res. Lett.* **2021**, *16*, 174. [[CrossRef](#)] [[PubMed](#)]
2. Raj, S.; Singh, H.; Trivedi, R.; Soni, V. Biogenic Synthesis of AgNPs Employing Terminalia Arjuna Leaf Extract and Its Efficacy towards Catalytic Degradation of Organic Dyes. *Sci. Rep.* **2020**, *10*, 9616. [[CrossRef](#)] [[PubMed](#)]
3. Krishnan, P.D.; Banas, D.; Durai, R.D.; Kabanov, D.; Hosnedlova, B.; Kepinska, M.; Fernandez, C.; Ruttkay-Nedecky, B.; Nguyen, H.V.; Farid, A.; et al. Silver Nanomaterials for Wound Dressing Applications. *Pharmaceutics* **2020**, *12*, 821. [[CrossRef](#)] [[PubMed](#)]
4. Lee, S.H.; Jun, B.H. Silver Nanoparticles: Synthesis and Application for Nanomedicine. *Int. J. Mol. Sci.* **2019**, *20*, 865. [[CrossRef](#)] [[PubMed](#)]
5. Calderón-Jiménez, B.; Johnson, M.E.; Montoro Bustos, A.R.; Murphy, K.E.; Winchester, M.R.; Baudrit, J.R.V. Silver Nanoparticles: Technological Advances, Societal Impacts, and Metrological Challenges. *Front. Chem.* **2017**, *5*, 6. [[CrossRef](#)]
6. Beyene, H.D.; Werkneh, A.A.; Bezaab, H.K.; Ambaye, T.G. Synthesis Paradigm and Applications of Silver Nanoparticles (AgNPs), a Review. *Sustain. Mater. Technol.* **2017**, *13*, 18–23. [[CrossRef](#)]
7. Jamkhande, P.G.; Ghule, N.W.; Bamer, A.H.; Kalaskar, M.G. Metal Nanoparticles Synthesis: An Overview on Methods of Preparation, Advantages and Disadvantages, and Applications. *J. Drug Deliv. Sci. Technol.* **2019**, *53*, 101174. [[CrossRef](#)]
8. Burdus, el, A.C.; Gherasim, O.; Grumezescu, A.M.; Mogoantă, L.; Fica, A.; Andronescu, E. Biomedical Applications of Silver Nanoparticles: An up-to-Date Overview. *Nanomaterials* **2018**, *8*, 681. [[CrossRef](#)]
9. Haider, A.; Kang, I.K. Preparation of Silver Nanoparticles and Their Industrial and Biomedical Applications: A Comprehensive Review. *Adv. Mater. Sci. Eng.* **2015**, *2015*, 165257. [[CrossRef](#)]
10. Nqakala, Z.B.; Sibuyi, N.R.S.; Fadaka, A.O.; Meyer, M.; Onani, M.O.; Madiehe, A.M. Advances in Nanotechnology towards Development of Silver Nanoparticle-Based Wound-Healing Agents. *Int. J. Mol. Sci.* **2021**, *22*, 11272. [[CrossRef](#)]
11. Zhang, J.; Liu, S.; Han, J.; Wang, Z.; Zhang, S. On the Developmental Toxicity of Silver Nanoparticles. *Mater. Des.* **2021**, *203*, 109611. [[CrossRef](#)]
12. Levard, C.; Hotze, E.M.; Lowry, G.V.; Brown, G.E. Environmental Transformations of Silver Nanoparticles: Impact on Stability and Toxicity. *Environ. Sci. Technol.* **2012**, *46*, 6900–6914. [[CrossRef](#)] [[PubMed](#)]
13. Tortella, G.R.; Rubilar, O.; Durán, N.; Diez, M.C.; Martínez, M.; Parada, J.; Seabra, A.B. Silver Nanoparticles: Toxicity in Model Organisms as an Overview of Its Hazard for Human Health and the Environment. *J. Hazard. Mater.* **2020**, *390*, 121974. [[CrossRef](#)]
14. Aboyewa, J.A.; Sibuyi, N.R.S.; Meyer, M.; Oguntibeju, O.O. Green Synthesis of Metallic Nanoparticles Using Some Selected Medicinal Plants from Southern Africa and Their Biological Applications. *Plants* **2021**, *10*, 1929. [[CrossRef](#)] [[PubMed](#)]
15. Chand, K.; Cao, D.; Eldin Fouad, D.; Hussain Shah, A.; Qadeer Dayo, A.; Zhu, K.; Nazim Lakhan, M.; Mehdi, G.; Dong, S. Green Synthesis, Characterization and Photocatalytic Application of Silver Nanoparticles Synthesized by Various Plant Extracts. *Arab. J. Chem.* **2020**, *13*, 8248–8261. [[CrossRef](#)]

16. Simon, S.; Sibuyi, N.R.S.; Fadaka, A.O.; Meyer, M.; Madiehe, A.M.; du Preez, M.G. The Antimicrobial Activity of Biogenic Silver Nanoparticles Synthesized from Extracts of Red and Green European Pear Cultivars. *Artif. Cells Nanomed. Biotechnol.* **2021**, *49*, 614–625. [[CrossRef](#)]
17. Tyavambiza, C.; Elbagory, A.M.; Madiehe, A.M.; Meyer, M.; Meyer, S. The Antimicrobial and Anti-Inflammatory Effects of Silver Nanoparticles Synthesized from Cotyledon Orbiculata Aqueous Extract. *Nanomaterials* **2021**, *11*, 1343. [[CrossRef](#)]
18. Majoumouo, M.S.; Sibuyi, N.R.S.; Tincho, M.B.; Mbekou, M.; Boyom, F.F.; Meyer, M. Enhanced Anti-Bacterial Activity of Biogenic Silver Nanoparticles Synthesized from Terminalia Mantaly Extracts. *Int. J. Nanomed.* **2019**, *14*, 9031–9046. [[CrossRef](#)]
19. Karmous, I.; Pandey, A.; Haj, K.; Ben; Chaoui, A. Efficiency of the Green Synthesized Nanoparticles as New Tools in Cancer Therapy: Insights on Plant-Based Bioengineered Nanoparticles, Biophysical Properties, and Anticancer Roles. *Biol. Trace Elem. Res.* **2020**, *196*, 330–342. [[CrossRef](#)]
20. Choi, J.S.; Jung, H.C.; Baek, Y.J.; Kim, B.Y.; Lee, M.W.; Kim, H.D.; Kim, S.W. Antibacterial Activity of Green-Synthesized Silver Nanoparticles Using Areca Catechu Extract against Antibiotic-Resistant Bacteria. *Nanomaterials* **2021**, *11*, 205. [[CrossRef](#)]
21. Subramaniam, P.; Nisha, K.M.J.; Vanitha, A.; Kiruthika, M.L.; Sindhu, P.; Elesaw, B.H.; Brindhadevi, K.; Kalimuthu, K. Synthesis of Silver Nanoparticles from Wild and Tissue Cultured Ceropogia Juncea Plants and Its Antibacterial, Anti-Angiogenesis and Cytotoxic Activities. *Appl. Nanosci.* **2021**, *1*, 1–15. [[CrossRef](#)]
22. Kitimu, S.R.; Kirira, P.; Abdille, A.A.; Sokei, J.; Ochwang'i, D.; Mwitari, P.; Makanya, A.; Maina, N.; Kitimu, S.R.; Kirira, P.; et al. Anti-Angiogenic and Anti-Metastatic Effects of Biogenic Silver Nanoparticles Synthesized Using Azadirachta Indica. *Adv. Biosci. Biotechnol.* **2022**, *13*, 188–206. [[CrossRef](#)]
23. Ratan, Z.A.; Haidere, M.F.; Nurunnabi, M.; Shahriar, S.M.; Ahammad, A.J.S.; Shim, Y.Y.; Reaney, M.J.T.; Cho, J.Y. Green Chemistry Synthesis of Silver Nanoparticles and Their Potential Anticancer Effects. *Cancers* **2020**, *12*, 855. [[CrossRef](#)] [[PubMed](#)]
24. Sati, S.C.; Kour, G.; Bartwal, A.S.; Sati, M.D. Biosynthesis of Metal Nanoparticles from Leaves of Ficus Palmata and Evaluation of Their Anti-Inflammatory and Anti-Diabetic Activities. *Biochemistry* **2020**, *59*, 3019–3025. [[CrossRef](#)]
25. Saratale, R.G.; Saratale, G.D.; Ahn, S.; Shin, H.S. Grape Pomace Extracted Tannin for Green Synthesis of Silver Nanoparticles: Assessment of Their Antidiabetic, Antioxidant Potential and Antimicrobial Activity. *Polymer* **2021**, *13*, 4355. [[CrossRef](#)]
26. Firdhouse, M.J.; Lalitha, P. Biosynthesis of Silver Nanoparticles and Its Applications. *J. Nanotechnol.* **2015**, *2015*, 829526. [[CrossRef](#)]
27. Singh, P.; Ahn, S.; Kang, J.P.; Veronika, S.; Huo, Y.; Singh, H.; Chokkaligam, M.; El-Agamy Farh, M.; Aceituno, V.C.; Kim, Y.J.; et al. In Vitro Anti-Inflammatory Activity of Spherical Silver Nanoparticles and Monodisperse Hexagonal Gold Nanoparticles by Fruit Extract of Prunus Serrulata: A Green Synthetic Approach. *Artif. Cells Nanomed. Biotechnol.* **2018**, *46*, 2022–2032. [[CrossRef](#)]
28. Natsuki, J. A Review of Silver Nanoparticles: Synthesis Methods, Properties and Applications. *Int. J. Mater. Sci. Appl.* **2015**, *4*, 325. [[CrossRef](#)]
29. Abbasi, B.H.; Nazir, M.; Muhammad, W.; Hashmi, S.S.; Abbasi, R.; Rahman, L.; Hano, C. A Comparative Evaluation of the Antiproliferative Activity against HepG2 Liver Carcinoma Cells of Plant-Derived Silver Nanoparticles from Basil Extracts with Contrasting Anthocyanin Contents. *Biomolecules* **2019**, *9*, 320. [[CrossRef](#)]
30. Hussain, I.; Singh, N.B.; Singh, A.; Singh, H.; Singh, S.C. Green Synthesis of Nanoparticles and Its Potential Application. *Biotechnol. Lett.* **2016**, *38*, 545–560. [[CrossRef](#)]
31. Chugh, H.; Sood, D.; Chandra, I.; Tomar, V.; Dhawan, G.; Chandra, R. Role of Gold and Silver Nanoparticles in Cancer Nano-Medicine. *Artif. Cells Nanomed. Biotechnol.* **2018**, *46*, 1210–1220. [[CrossRef](#)] [[PubMed](#)]
32. Teimuri-mofrad, R.; Hadi, R.; Tahmasebi, B.; Farhoudian, S.; Mehravar, M.; Nasiri, R. Green Synthesis of Gold Nanoparticles Using Plant Extract: Mini-Review. *Nanochem. Res.* **2017**, *2*, 8–19. [[CrossRef](#)]
33. Khodadadi, B.; Bordbar, M.; Yeganeh-Faal, A.; Nasrollahzadeh, M. Green Synthesis of Ag Nanoparticles/Clinoptilolite Using Vaccinium Macrocarpon Fruit Extract and Its Excellent Catalytic Activity for Reduction of Organic Dyes. *J. Alloys Compd.* **2017**, *719*, 82–88. [[CrossRef](#)]
34. Ballottin, D.; Fulaz, S.; Souza, M.L.; Corio, P.; Rodrigues, A.G.; Souza, A.O.; Gaspari, P.M.; Gomes, A.F.; Gozzo, F.; Tasic, L. Elucidating Protein Involvement in the Stabilization of the Biogenic Silver Nanoparticles. *Nanoscale Res. Lett.* **2016**, *11*, 1–9. [[CrossRef](#)] [[PubMed](#)]
35. Zhao, P.; Li, N.; Astruc, D. State of the Art in Gold Nanoparticle Synthesis. *Coord. Chem. Rev.* **2013**, *257*, 638–665. [[CrossRef](#)]
36. Mageswari, A.; Subramanian, P.; Ravindran, V.; Yesodharan, S.; Bagavan, A.; Rahuman, A.A.; Karthikeyan, S.; Gothandam, K.M. Synthesis and Larvicidal Activity of Low-Temperature Stable Silver Nanoparticles from Psychrotolerant Pseudomonas Mandelii. *Environ. Sci. Pollut. Res.* **2015**, *22*, 5383–5394. [[CrossRef](#)]
37. Ammar, H.A.M.; El-Desouky, T.A. Green Synthesis of Nanosilver Particles by Aspergillus Terreus HA1N and Penicillium Expansum HA2N and Its Antifungal Activity against Mycotoxigenic Fungi. *J. Appl. Microbiol.* **2016**, *121*, 89–100. [[CrossRef](#)]
38. Dawadi, S.; Katuwal, S.; Gupta, A.; Lamichhane, U.; Thapa, R.; Jaisi, S.; Lamichhane, G.; Bhattarai, D.P.; Parajuli, N. Current Research on Silver Nanoparticles: Synthesis, Characterization, and Applications. *J. Nanomater.* **2021**, *2021*, 6687290. [[CrossRef](#)]
39. Husain, S.; Sardar, M.; Fatma, T. Screening of Cyanobacterial Extracts for Synthesis of Silver Nanoparticles. *World J. Microbiol. Biotechnol.* **2015**, *31*, 1279–1283. [[CrossRef](#)]
40. Zomorodian, K.; Pourshahid, S.; Sadatsharifi, A.; Mehryar, P.; Pakshir, K.; Rahimi, M.J.; Arabi Monfared, A. Biosynthesis and Characterization of Silver Nanoparticles by Aspergillus Species. *Biomed. Res. Int.* **2016**, *2016*, 5435397. [[CrossRef](#)] [[PubMed](#)]
41. Gahlawat, G.; Choudhury, A.R. A Review on the Biosynthesis of Metal and Metal Salt Nanoparticles by Microbes. *RSC Adv.* **2019**, *9*, 12944–12967. [[CrossRef](#)]

42. Hamouda, R.A.; Hussein, M.H.; Abo-elmagd, R.A.; Bawazir, S.S. Synthesis and Biological Characterization of Silver Nanoparticles Derived from the Cyanobacterium *Oscillatoria Limnetica*. *Sci. Rep.* **2019**, *9*, 1–17. [[CrossRef](#)]
43. Aboyewa, J.A.; Sibuyi, N.R.S.; Meyer, M.; Oguntibeju, O.O. Gold Nanoparticles Synthesized Using Extracts of *Cyclopia Intermedia*, Commonly Known as Honeybush, Amplify the Cytotoxic Effects of Doxorubicin. *Nanomaterials* **2021**, *11*, 132. [[CrossRef](#)]
44. Rafique, M.; Sadaf, I.; Rafique, M.S.; Tahir, M.B. A Review on Green Synthesis of Silver Nanoparticles and Their Applications. *Artif. Cells Nanomed. Biotechnol.* **2017**, *45*, 1272–1291. [[CrossRef](#)]
45. Fahmy, S.A.; Preis, E.; Bakowsky, U.; Azzazy, H.M.E.S. Platinum Nanoparticles: Green Synthesis and Biomedical Applications. *Molecules* **2020**, *25*, 4981. [[CrossRef](#)]
46. Ashour, A.A.; Raafat, D.; El-Gowell, H.M.; El-Kamel, A.H. Green Synthesis of Silver Nanoparticles Using Cranberry Powder Aqueous Extract: Characterization and Antimicrobial Properties. *Int. J. Nanomed.* **2015**, *10*, 7207. [[CrossRef](#)]
47. Srikar, S.K.; Giri, D.D.; Pal, D.B.; Mishra, P.K.; Upadhyay, S.N. Green Synthesis of Silver Nanoparticles: A Review. *Green Sustain. Chem.* **2016**, *6*, 34–56. [[CrossRef](#)]
48. Patel, V.; Berthold, D.; Puranik, P.; Gantar, M. Screening of Cyanobacteria and Microalgae for Their Ability to Synthesize Silver Nanoparticles with Antibacterial Activity. *Biotechnol. Rep.* **2015**, *5*, 112–119. [[CrossRef](#)]
49. Fadaka, A.O.; Sibuyi, N.R.S.; Madiehe, A.M.; Meyer, M. Nanotechnology-Based Delivery Systems for Antimicrobial Peptides. *Pharmaceutics* **2021**, *13*, 1795. [[CrossRef](#)]
50. Bélteky, P.; Rónavári, A.; Igaz, N.; Szerencsés, B.; Tóth, I.Y.; Pfeiffer, I.; Kiricsi, M.; Kónya, Z. Silver Nanoparticles: Aggregation Behavior in Biorelevant Conditions and Its Impact on Biological Activity. *Int. J. Nanomed.* **2019**, *14*, 667–687. [[CrossRef](#)]
51. Mikhailova, E.O. Silver Nanoparticles: Mechanism of Action and Probable Bio-Application. *J. Funct. Biomater.* **2020**, *11*, 84. [[CrossRef](#)]
52. Kotcherlakota, R.; Das, S.; Patra, C.R. *Therapeutic Applications of Green-Synthesized Silver Nanoparticles*; Elsevier Inc.: Amsterdam, The Netherlands, 2019; ISBN 9780081025796.
53. Dakal, T.C.; Kumar, A.; Majumdar, R.S.; Yadav, V. Mechanistic Basis of Antimicrobial Actions of Silver Nanoparticles. *Front. Microbiol.* **2016**, *7*, 1831. [[CrossRef](#)]
54. De Oliveira, D.M.P.; Forde, B.M.; Kidd, T.J.; Harris, P.N.A.; Schembri, M.A.; Beatson, S.A.; Paterson, D.L.; Walker, M.J. Antimicrobial Resistance in ESKAPE Pathogens. *Clin. Microbiol. Rev.* **2020**, *33*, e00181-19. [[CrossRef](#)]
55. Schultz, F.; Anywar, G.; Tang, H.; Chassagne, F.; Lyles, J.T.; Garbe, L.A.; Quave, C.L. Targeting ESKAPE Pathogens with Anti-Infective Medicinal Plants from the Greater Mpigi Region in Uganda. *Sci. Rep.* **2020**, *10*, 11935. [[CrossRef](#)]
56. Alsammarráie, F.K.; Wang, W.; Zhou, P.; Mustapha, A.; Lin, M. Green Synthesis of Silver Nanoparticles Using Turmeric Extracts and Investigation of Their Antibacterial Activities. *Colloids Surf. B Biointerfaces* **2018**, *171*, 398–405. [[CrossRef](#)]
57. Dube, P.; Meyer, S.; Madiehe, A.; Meyer, M. Antibacterial Activity of Biogenic Silver and Gold Nanoparticles Synthesized from *Salvia Africana*-Lutea and *Sutherlandia Frutescens*. *Nanotechnology* **2020**, *31*, 505607. [[CrossRef](#)]
58. Thi Lan Huong, V.; Nguyen, N.T. Green Synthesis, Characterization and Antibacterial Activity of Silver Nanoparticles Using *Sapindus Mukorossi* Fruit Pericarp Extract. *Mater. Today Proc.* **2021**, *42*, 88–93. [[CrossRef](#)]
59. Arsène, M.M.J.; Podoprigora, I.V.; Davares, A.K.L.; Razan, M.; Das, M.S.; Senyagin, A.N. Antibacterial Activity of Grapefruit Peel Extracts and Green-Synthesized Silver Nanoparticles. *Vet. World* **2021**, *14*, 1330. [[CrossRef](#)]
60. Khan, M.R.; Hoque, S.M.; Hossain, K.F.B.; Siddique, M.A.B.; Uddin, M.K.; Rahman, M.M. Green Synthesis of Silver Nanoparticles Using *Ipomoea Aquatica* Leaf Extract and Its Cytotoxicity and Antibacterial Activity Assay. *Green Chem. Lett. Rev.* **2020**, *13*, 39–51. [[CrossRef](#)]
61. Aadil, K.R.; Pandey, N.; Mussatto, S.I.; Jha, H. Green Synthesis of Silver Nanoparticles Using Acacia Lignin, Their Cytotoxicity, Catalytic, Metal Ion Sensing Capability and Antibacterial Activity. *J. Environ. Chem. Eng.* **2019**, *7*, 103296. [[CrossRef](#)]
62. Fatimah, I.; Afrid, Z.H.V.I. Characteristics and Antibacterial Activity of Green Synthesized Silver Nanoparticles Using Red Spinach (*Amaranthus tricolor* L.) Leaf Extract. *Green Chem. Lett. Rev.* **2019**, *12*, 25–30. [[CrossRef](#)]
63. Ahmad, S.; Munir, S.; Zeb, N.; Ullah, A.; Khan, B.; Ali, J.; Bilal, M.; Omer, M.; Alamzeb, M.; Salman, S.M.; et al. Green Nanotechnology: A Review on Green Synthesis of Silver Nanoparticles—An Ecofriendly Approach. *Int. J. Nanomed.* **2019**, *14*, 5087. [[CrossRef](#)] [[PubMed](#)]
64. Savithamma, N.; Rao, M.; Rukmini, K.; Suvarnalatha-Devi, P. Antimicrobial Activity of Silver Nanoparticles Synthesized by Using Medicinal Plants. *Int. J. ChemTech Res.* **2011**, *3*, 1394–1402.
65. Ghosvandi, S.; Madani, M.; Karimi, J. Green Synthesis, Characterization and Antifungal Activity of Silver Nanoparticles Using Stems and Flowers of Felty Germander. *J. Inorg. Organomet. Polym. Mater.* **2020**, *30*, 2987–2997. [[CrossRef](#)]
66. Bahrami-Teimoori, B.; Nikparast, Y.; Hojatiannar, M.; Akhlaghi, M.; Ghorbani, R.; Pourianfar, H.R. Characterisation and Antifungal Activity of Silver Nanoparticles Biologically Synthesised by *Amaranthus Retroflexus* Leaf Extract. *J. Exp. Nanosci.* **2017**, *12*, 129–139. [[CrossRef](#)]
67. Khan, M.; Khan, A.U.; Bogdanchikova, N.; Garibo, D. Antibacterial and Antifungal Studies of Biosynthesized Silver Nanoparticles against Plant Parasitic Nematode *Meloidogyne Incognita*, Plant Pathogens *Ralstonia Solanacearum* and *Fusarium Oxysporum*. *Molecules* **2021**, *26*, 2462. [[CrossRef](#)]
68. Salleh, A.; Naomi, R.; Utami, N.D.; Mohammad, A.W.; Mahmoudi, E.; Mustafa, N.; Fauzi, M.B. The Potential of Silver Nanoparticles for Antiviral and Antibacterial Applications: A Mechanism of Action. *Nanomaterials* **2020**, *10*, 1566. [[CrossRef](#)]

69. Rai, M.; Kon, K.; Ingle, A.; Duran, N.; Galdiero, S.; Galdiero, M. Broad-Spectrum Bioactivities of Silver Nanoparticles: The Emerging Trends and Future Prospects. *Appl. Microbiol. Biotechnol.* **2014**, *98*, 1951–1961. [[CrossRef](#)]
70. Vazquez-Munoz, R.; Lopez-Ribot, J. Nanotechnology as an Alternative to Reduce the Spread of COVID-19. *Challenges* **2020**, *11*, 15. [[CrossRef](#)]
71. De Gusseme, B.; Sintubin, L.; Baert, L.; Thibo, E.; Hennebel, T.; Vermeulen, G.; Uyttendaele, M.; Verstraete, W.; Boon, N. Biogenic Silver for Disinfection of Water Contaminated with Viruses. *Appl. Environ. Microbiol.* **2010**, *76*, 1082–1087. [[CrossRef](#)]
72. Narasimha, G. Antiviral Activity of Silver Nanoparticles Synthesized by Fungal Strain *Aspergillus Niger*. *Nano Sci. Nano Technol. Indian J.* **2012**, *6*, 18–20.
73. Lara, H.H.; Ixtepan-Turrent, L.; Garza-Treviño, E.N.; Rodriguez-Padilla, C. PVP-Coated Silver Nanoparticles Block the Transmission of Cell-Free and Cell-Associated HIV-1 in Human Cervical Culture. *J. Nanobiotechnol.* **2010**, *8*, 15. [[CrossRef](#)] [[PubMed](#)]
74. Sheshock, J.L.; Murdock, R.C.; Braydich-Stolle, L.K.; Schrand, A.M.; Hussain, S.M. Interaction of Silver Nanoparticles with Tacaribe Virus. *J. Nanobiotechnol.* **2010**, *8*, 19. [[CrossRef](#)]
75. Trefry, J.C.; Wooley, D.P. Silver Nanoparticles Inhibit Vaccinia Virus Infection by Preventing Viral Entry through a Macropinocytosis-Dependent Mechanism. *J. Biomed. Nanotechnol.* **2013**, *9*, 1624–1635. [[CrossRef](#)]
76. Fatima, M.; Zaidi, N. us S.S.; Amraiz, D.; Afzal, F. In Vitro Antiviral Activity of Cinnamomum Cassia and Its Nanoparticles Against H7N3 Influenza A Virus. *J. Microbiol. Biotechnol.* **2016**, *26*, 151–159. [[CrossRef](#)] [[PubMed](#)]
77. Sharma, V.; Kaushik, S.; Pandit, P.; Dhull, D.; Yadav, J.P.; Kaushik, S. Green Synthesis of Silver Nanoparticles from Medicinal Plants and Evaluation of Their Antiviral Potential against Chikungunya Virus. *Appl. Microbiol. Biotechnol.* **2019**, *103*, 881–891. [[CrossRef](#)]
78. Haggag, E.G.; Elshamy, A.M.; Rabeh, M.A.; Gabr, N.M.; Salem, M.; Youssif, K.A.; Samir, A.; Bin Muhsinah, A.; Alsayari, A.; Abdelmohsen, U.R. Antiviral Potential of Green Synthesized Silver Nanoparticles of *Lampranthus Coccineus* and *Malephora Lutea*. *Int. J. Nanomed.* **2019**, *14*, 6217–6229. [[CrossRef](#)]
79. Saeed, B.A.; Lim, V.; Yusof, N.A.; Khor, K.Z.; Rahman, H.S.; Samad, N.A. Antiangiogenic Properties of Nanoparticles: A Systematic Review. *Int. J. Nanomed.* **2019**, *14*, 5135. [[CrossRef](#)]
80. Baharara, J.; Namvar, F.; Mousavi, M.; Ramezani, T.; Mohamad, R. Anti-Angiogenesis Effect of Biogenic Silver Nanoparticles Synthesized Using *Saliva Officinalis* on Chick Chorioalantoic Membrane (CAM). *Molecules* **2014**, *19*, 13498–13508. [[CrossRef](#)]
81. Goradel, N.H.; Ghiyami-Hour, F.; Jahangiri, S.; Negahdari, B.; Sahebkar, A.; Masoudifar, A.; Mirzaei, H. Nanoparticles as New Tools for Inhibition of Cancer Angiogenesis. *J. Cell. Physiol.* **2018**, *233*, 2902–2910. [[CrossRef](#)]
82. Mukherjee, S. Recent Progress toward Antiangiogenesis Application of Nanomedicine in Cancer Therapy. *Futur. Sci. OA* **2018**, *4*, 9–12. [[CrossRef](#)] [[PubMed](#)]
83. Dvorak, H.F. Vascular Permeability Factor/Vascular Endothelial Growth Factor: A Critical Cytokine in Tumor Angiogenesis and a Potential Target for Diagnosis and Therapy. *J. Clin. Oncol.* **2002**, *20*, 4368–4380. [[CrossRef](#)] [[PubMed](#)]
84. Gerber, H.P.; Dixit, V.; Ferrara, N. Vascular Endothelial Growth Factor Induces Expression of the Antiapoptotic Proteins Bcl-2 and A1 in Vascular Endothelial Cells. *J. Biol. Chem.* **1998**, *273*, 13313–13316. [[CrossRef](#)]
85. Carmeliet, P. Angiogenesis in Life, Disease and Medicine. *Nature* **2005**, *438*, 932–936. [[CrossRef](#)] [[PubMed](#)]
86. Folkman, J. What Is the Evidence That Tumors Are Angiogenesis Dependent? *J. Natl. Cancer Inst.* **1990**, *82*, 4–7. [[CrossRef](#)] [[PubMed](#)]
87. Jain, P.K.; Lee, K.S.; El-Sayed, I.H.; El-Sayed, M.A. Calculated Absorption and Scattering Properties of Gold Nanoparticles of Different Size, Shape, and Composition: Applications in Biological Imaging and Biomedicine. *J. Phys. Chem. B* **2006**, *110*, 7238–7248. [[CrossRef](#)] [[PubMed](#)]
88. Kong, D.H.; Kim, M.R.; Jang, J.H.; Na, H.J.; Lee, S. A Review of Anti-Angiogenic Targets for Monoclonal Antibody Cancer Therapy. *Int. J. Mol. Sci.* **2017**, *18*, 1786. [[CrossRef](#)]
89. Dragovich, T.; Laheru, D.; Dayyani, F.; Bolejack, V.; Smith, L.; Seng, J.; Burris, H.; Rosen, P.; Hidalgo, M.; Ritch, P.; et al. Phase II Trial of Vatalanib in Patients with Advanced or Metastatic Pancreatic Adenocarcinoma after First-Line Gemcitabine Therapy (PCRT 04-001). *Cancer Chemother. Pharmacol.* **2014**, *74*, 379–387. [[CrossRef](#)]
90. Motzer, R.J.; Escudier, B.; Gannon, A.; Figlin, R.A. Sunitinib: Ten Years of Successful Clinical Use and Study in Advanced Renal Cell Carcinoma. *Oncologist* **2017**, *22*, 41–52. [[CrossRef](#)]
91. Fan, G.; Wei, X.; Xu, X. Is the Era of Sorafenib over? A Review of the Literature. *Ther. Adv. Med. Oncol.* **2020**, *12*, 1758835920927602. [[CrossRef](#)]
92. Garcia, J.; Hurwitz, H.I.; Sandler, A.B.; Miles, D.; Coleman, R.L.; Deurloo, R.; Chinot, O.L. Bevacizumab (Avastin®) in Cancer Treatment: A Review of 15 Years of Clinical Experience and Future Outlook. *Cancer Treat. Rev.* **2020**, *86*, 102017. [[CrossRef](#)] [[PubMed](#)]
93. Le, B.T.; Raguraman, P.; Kosbar, T.R.; Fletcher, S.; Wilton, S.D.; Veedu, R.N. Antisense Oligonucleotides Targeting Angiogenic Factors as Potential Cancer Therapeutics. *Mol. Ther.-Nucleic Acids* **2019**, *14*, 142–157. [[CrossRef](#)] [[PubMed](#)]
94. Walia, A.; Yang, J.F.; Huang, Y.H.; Rosenblatt, M.I.; Chang, J.H.; Azar, D.T. Endostatin's Emerging Roles in Angiogenesis, Lymphangiogenesis, Disease, and Clinical Applications. *Biochim. Biophys. Acta-Gen. Subj.* **2015**, *1850*, 2422–2438. [[CrossRef](#)] [[PubMed](#)]
95. Truong, D.H.; Le, V.K.H.; Pham, T.T.; Dao, A.H.; Pham, T.P.D.; Tran, T.H. Delivery of Erlotinib for Enhanced Cancer Treatment: An Update Review on Particulate Systems. *J. Drug Deliv. Sci. Technol.* **2020**, *55*, 101348. [[CrossRef](#)]

96. Punganuru, S.R.; Madala, H.R.; Mikelis, C.M.; Dixit, A.; Arutla, V.; Srivenugopal, K.S. Conception, Synthesis, and Characterization of a Rofecoxib-Combretastatin Hybrid Drug with Potent Cyclooxygenase-2 (COX-2) Inhibiting and Microtubule Disrupting Activities in Colon Cancer Cell Culture and Xenograft Models. *Oncotarget* **2018**, *9*, 26109–26129. [CrossRef]
97. Tołoczko-Iwaniuk, N.; Dziemiańczyk-Pakieła, D.; Nowaszewska, B.K.; Celińska-Janowicz, K.; Milyk, W. Celecoxib in Cancer Therapy and Prevention—Review. *Curr. Drug Targets* **2018**, *20*, 302–315. [CrossRef]
98. Alsaab, H.O.; Al-Hibs, A.S.; Alzhrani, R.; Alrabighi, K.K.; Alqathama, A.; Alwithenani, A.; Almalki, A.H.; Althobaiti, Y.S.; Alsaab, H.O.; Al-Hibs, A.S.; et al. Nanomaterials for Antiangiogenic Therapies for Cancer: A Promising Tool for Personalized Medicine. *Int. J. Mol. Sci.* **2021**, *22*, 1631. [CrossRef]
99. Gurunathan, S.; Lee, K.J.; Kalishwaralal, K.; Sheikpranbabu, S.; Vaidyanathan, R.; Eom, S.H. Antiangiogenic Properties of Silver Nanoparticles. *Biomaterials* **2009**, *30*, 6341–6350. [CrossRef]
100. Yang, T.; Yao, Q.; Cao, F.; Liu, Q.; Liu, B.; Wang, X.H. Silver Nanoparticles Inhibit the Function of Hypoxia-Inducible Factor-1 and Target Genes: Insight into the Cytotoxicity and Antiangiogenesis. *Int. J. Nanomed.* **2016**, *11*, 6679–6692. [CrossRef]
101. Kalishwaralal, K.; Banumathi, E.; Pandian, S.B.R.K.; Deepak, V.; Muniyandi, J.; Eom, S.H.; Gurunathan, S. Silver Nanoparticles Inhibit VEGF Induced Cell Proliferation and Migration in Bovine Retinal Endothelial Cells. *Colloids Surf. B Biointerfaces* **2009**, *73*, 51–57. [CrossRef]
102. Fallah, A.; Sadeghinia, A.; Kahroba, H.; Samadi, A.; Heidari, H.R.; Bradaran, B.; Zeinali, S.; Molavi, O. Therapeutic Targeting of Angiogenesis Molecular Pathways in Angiogenesis-Dependent Diseases. *Biomed. Pharmacother.* **2019**, *110*, 775–785. [CrossRef] [PubMed]
103. World Cancer Research Fund International Worldwide Cancer Data, Global Cancer Statistics for the Most Common Cancers in the World. Available online: <https://www.wcrf.org/cancer-trends/worldwide-cancer-data/> (accessed on 29 July 2022).
104. Ovais, M.; Khalil, A.T.; Raza, A.; Khan, M.A.; Ahmad, I.; Islam, N.U.; Saravanan, M.; Ubaid, M.F.; Ali, M.; Shinwari, Z.K. Green Synthesis of Silver Nanoparticles via Plant Extracts: Beginning a New Era in Cancer Theranostics. *Nanomedicine* **2016**, *12*, 3157–3177. [CrossRef] [PubMed]
105. Zhang, X.-F.; Liu, Z.-G.; Shen, W.; Gurunathan, S. Silver Nanoparticles: Synthesis, Characterization, Properties, Applications, and Therapeutic Approaches. *Int. J. Mol. Sci.* **2016**, *17*, 1534. [CrossRef] [PubMed]
106. Barenholz, Y. Doxil®—The First FDA-Approved Nano-Drug: Lessons Learned. *J. Control. Release* **2012**, *160*, 117–134. [CrossRef] [PubMed]
107. Gianni, L.; Mansutti, M.; Anton, A.; Calvo, L.; Bisagni, G.; Bermejo, B.; Semiglazov, V.; Thill, M.; Chacon, J.I.; Chan, A.; et al. Comparing Neoadjuvant Nab-Paclitaxel vs. Paclitaxel Both Followed by Anthracycline Regimens in Women With ERBB2/HER2-Negative Breast Cancer—The Evaluating Treatment With Neoadjuvant Abraxane (ETNA) Trial: A Randomized Phase 3 Clinical Trial. *JAMA Oncol.* **2018**, *4*, 302. [CrossRef] [PubMed]
108. Singh, P.; Pandit, S.; Mokkapati, V.R.S.S.; Garg, A.; Ravikumar, V.; Mijakovic, I. Gold Nanoparticles in Diagnostics and Therapeutics for Human Cancer. *Int. J. Mol. Sci.* **2018**, *19*, 1979. [CrossRef]
109. Ahmed, O.; Sibuyi, N.R.S.; Fadaka, A.O.; Madiehe, M.A.; Maboza, E.; Meyer, M.; Geerts, G. Plant Extract-Synthesized Silver Nanoparticles for Application in Dental Therapy. *Pharmaceutics* **2022**, *14*, 380. [CrossRef]
110. Kathiravan, V.; Ravi, S.; Ashokkumar, S. Synthesis of Silver Nanoparticles from Melia Dubia Leaf Extract and Their in Vitro Anticancer Activity. *Spectrochim. Acta Part A Mol. Biomol. Spectrosc.* **2014**, *130*, 116–121. [CrossRef]
111. Venugopal, K.; Rather, H.A.; Rajagopal, K.; Shanthi, M.P.; Sheriff, K.; Illiyas, M.; Rather, R.A.; Manikandan, E.; Uvarajan, S.; Bhaskar, M.; et al. Synthesis of Silver Nanoparticles (Ag NPs) for Anticancer Activities (MCF 7 Breast and A549 Lung Cell Lines) of the Crude Extract of Syzygium Aromaticum. *J. Photochem. Photobiol. B Biol.* **2017**, *167*, 282–289. [CrossRef]
112. Jeyaraj, M.; Rajesh, M.; Arun, R.; MubarakAli, D.; Sathishkumar, G.; Sivanandhan, G.; Dev, G.K.; Manickavasagam, M.; Premkumar, K.; Thajuddin, N.; et al. An Investigation on the Cytotoxicity and Caspase-Mediated Apoptotic Effect of Biologically Synthesized Silver Nanoparticles Using Podophyllum Hexandrum on Human Cervical Carcinoma Cells. *Colloids Surf. B Biointerfaces* **2013**, *102*, 708–717. [CrossRef]
113. Fadaka, A.O.; Meyer, S.; Ahmed, O.; Geerts, G.; Madiehe, M.A.; Meyer, M.; Sibuyi, N.R.S. Broad Spectrum Anti-Bacterial Activity and Non-Selective Toxicity of Gum Arabic Silver Nanoparticles. *Int. J. Mol. Sci.* **2022**, *23*, 1799. [CrossRef]
114. He, Y.; Du, Z.; Ma, S.; Liu, Y.; Li, D.; Huang, H.; Jiang, S.; Cheng, S.; Wu, W.; Zhang, K.; et al. Effects of Green-Synthesized Silver Nanoparticles on Lung Cancer Cells in Vitro and Grown as Xenograft Tumors in Vivo. *Int. J. Nanomed.* **2016**, *11*, 1879. [CrossRef] [PubMed]
115. Devi, J.S.; Bhimba, B.V. Anticancer Activity of Silver Nanoparticles Synthesized by the Seaweed Ulva Lactuca In Vitro. *Open Access Sci. Rep.* **2012**, *1*, 242. [CrossRef]
116. Hemlata; Meena, P.R.; Singh, A.P.; Tejavath, K.K. Biosynthesis of Silver Nanoparticles Using Cucumis Prophetarum Aqueous Leaf Extract and Their Antibacterial and Antiproliferative Activity against Cancer Cell Lines. *ACS Omega* **2020**, *5*, 5520–5528. [CrossRef] [PubMed]
117. Venkatesan, B.; Subramanian, V.; Tumala, A.; Vellaichamy, E. Rapid Synthesis of Biocompatible Silver Nanoparticles Using Aqueous Extract of Rosa Damascena Petals and Evaluation of Their Anticancer Activity. *Asian Pac. J. Trop. Med.* **2014**, *7*, S294–S300. [CrossRef]

118. Kanipandian, N.; Thirumurugan, R. A Feasible Approach to Phyto-Mediated Synthesis of Silver Nanoparticles Using Industrial Crop *Gossypium Hirsutum* (Cotton) Extract as Stabilizing Agent and Assessment of Its in Vitro Biomedical Potential. *Ind. Crops Prod.* **2014**, *55*, 1–10. [[CrossRef](#)]
119. Meenatchi, R.; Vijistella Bai, G. Green Synthesis of Silver Nanostructures against Human Cancer Cell Lines and Certain Pathogens. *IJPCBS* **2014**, *4*, 101–111.
120. Mishra, A.; Mehdi, S.J.; Irshad, M.; Ali, A.; Sardar, M.; Rizvi, M.M.A. Effect of Biologically Synthesized Silver Nanoparticles on Human Cancer Cells. *Sci. Adv. Mater.* **2012**, *4*, 1200–1206. [[CrossRef](#)]
121. Priyadharshini, R.I.; Prasannaraj, G.; Geetha, N.; Venkatachalam, P. Microwave-Mediated Extracellular Synthesis of Metallic Silver and Zinc Oxide Nanoparticles Using Macro-Algae (*Gracilaria Edulis*) Extracts and Its Anticancer Activity Against Human PC3 Cell Lines. *Appl. Biochem. Biotechnol.* **2014**, *174*, 2777–2790. [[CrossRef](#)]
122. Liu, M.; Zhang, J.; Zhu, X.; Shan, W.; Li, L.; Zhong, J.; Zhang, Z.; Huang, Y. Efficient Mucus Permeation and Tight Junction Opening by Dissociable “Mucus-Inert” Agent Coated Trimethyl Chitosan Nanoparticles for Oral Insulin Delivery. *J. Control. Release* **2016**, *222*, 67–77. [[CrossRef](#)]
123. Durán, N.; Silveira, C.P.; Durán, M.; Martinez, D.S.T. Silver Nanoparticle Protein Corona and Toxicity: A Mini-Review. *J. Nanobiotechnol.* **2015**, *13*, 55. [[CrossRef](#)] [[PubMed](#)]
124. AshaRani, P.V.; Mun, G.L.K.; Hande, M.P.; Valiyaveetil, S. Cytotoxicity and Genotoxicity of Silver Nanoparticles in Human Cells. *ACS Nano* **2009**, *3*, 279–290. [[CrossRef](#)] [[PubMed](#)]
125. Xia, T.; Li, N.; Nel, A.E. Potential Health Impact of Nanoparticles. *Annu. Rev. Public Health* **2009**, *30*, 137–150. [[CrossRef](#)]
126. Chairuangkitti, P.; Lawanprasert, S.; Roytrakul, S.; Aueviriyavit, S.; Phummiratch, D.; Kulthong, K.; Chanvorachote, P.; Maniratanachote, R. Silver Nanoparticles Induce Toxicity in A549 Cells via ROS-Dependent and ROS-Independent Pathways. *Toxicol. Vitro* **2013**, *27*, 330–338. [[CrossRef](#)]
127. Zhang, X.F.; Shen, W.; Gurunathan, S. Silver Nanoparticle-Mediated Cellular Responses in Various Cell Lines: An in Vitro Model. *Int. J. Mol. Sci.* **2016**, *17*, 1603. [[CrossRef](#)]
128. Hsin, Y.H.; Chen, C.F.; Huang, S.; Shih, T.S.; Lai, P.S.; Chueh, P.J. The Apoptotic Effect of Nanosilver Is Mediated by a ROS- and JNK-Dependent Mechanism Involving the Mitochondrial Pathway in NIH3T3 Cells. *Toxicol. Lett.* **2008**, *179*, 130–139. [[CrossRef](#)]
129. Park, E.J.; Yi, J.; Kim, Y.; Choi, K.; Park, K. Silver Nanoparticles Induce Cytotoxicity by a Trojan-Horse Type Mechanism. *Toxicol. Vitro* **2010**, *24*, 872–878. [[CrossRef](#)]
130. Hembram, K.C.; Kumar, R.; Kandha, L.; Parhi, P.K.; Kundu, C.N.; Bindhani, B.K. Therapeutic Prospective of Plant-Induced Silver Nanoparticles: Application as Antimicrobial and Anticancer Agent. *Artif. Cells Nanomed. Biotechnol.* **2018**, *46*, S38–S51. [[CrossRef](#)]
131. McShan, D.; Ray, P.C.; Yu, H. Molecular Toxicity Mechanism of Nanosilver. *J. Food Drug Anal.* **2014**, *22*, 116–127. [[CrossRef](#)]
132. Banerjee, P.P.; Bandyopadhyay, A.; Harsha, S.N.; Policegoudra, R.S.; Bhattacharya, S.; Karak, N.; Chattopadhyay, A. *Mentha Arvensis* (Linn.)-Mediated Green Silver Nanoparticles Trigger Caspase 9-Dependent Cell Death in MCF7 and MDA-MB-231 Cells. *Breast Cancer* **2017**, *9*, 265. [[CrossRef](#)]
133. Govindappa, M.; Hemashekhar, B.; Arthikala, M.K.; Ravishankar Rai, V.; Ramachandra, Y.L. Characterization, Antibacterial, Antioxidant, Antidiabetic, Anti-Inflammatory and Antityrosinase Activity of Green Synthesized Silver Nanoparticles Using *Calophyllum Tomentosum* Leaves Extract. *Results Phys.* **2018**, *9*, 400–408. [[CrossRef](#)]
134. Saratale, R.G.; Shin, H.S.; Kumar, G.; Benelli, G.; Kim, D.S.; Saratale, G.D. Exploiting Antidiabetic Activity of Silver Nanoparticles Synthesized Using *Punica Granatum* Leaves and Anticancer Potential against Human Liver Cancer Cells (HepG2). *Artif. Cells Nanomed. Biotechnol.* **2018**, *46*, 211–222. [[CrossRef](#)] [[PubMed](#)]
135. Balan, K.; Qing, W.; Wang, Y.; Liu, X.; Palvannan, T.; Wang, Y.; Ma, F.; Zhang, Y. Antidiabetic Activity of Silver Nanoparticles from Green Synthesis Using *Lonicera Japonica* Leaf Extract. *RSC Adv.* **2016**, *6*, 40162–40168. [[CrossRef](#)]
136. Sengottaiyan, A.; Aravinthan, A.; Sudhakar, C.; Selvam, K.; Srinivasan, P.; Govarthanan, M.; Manoharan, K.; Selvankumar, T. Synthesis and Characterization of *Solanum Nigrum*-Mediated Silver Nanoparticles and Its Protective Effect on Alloxan-Induced Diabetic Rats. *J. Nanostruct. Chem.* **2015**, *6*, 41–48. [[CrossRef](#)]
137. Campoy, A.H.G.; Gutierrez, R.M.P.; Manriquez-Alvirde, G.; Ramirez, A.M. Original Research [Highly-Accessed] Protection of Silver Nanoparticles Using *Eisenhardtia Polystachya* in Peroxide-Induced Pancreatic β -Cell Damage and Their Antidiabetic Properties in Zebrafish. *Int. J. Nanomed.* **2018**, *13*, 2601–2612. [[CrossRef](#)] [[PubMed](#)]
138. Grace, B.; Viswanathan, M.; Wilson, D.D. A New Silver Nano-Formulation of *Cassia Auriculata* Flower Extract and Its Anti-Diabetic Effects. *Recent Pat. Nanotechnol.* **2021**, *16*, 160–169. [[CrossRef](#)] [[PubMed](#)]
139. Ferrero-Miliani, L.; Nielsen, O.H.; Andersen, P.S.; Girardin, S.E. Chronic Inflammation: Importance of NOD2 and NALP3 in Interleukin-1 β Generation. *Clin. Exp. Immunol.* **2007**, *147*, 227. [[CrossRef](#)] [[PubMed](#)]
140. Hu, R.; Xie, Y.; Lu, B.; Li, Q.; Chen, F.; Li, L.; Hu, J.; Huang, Y.; Li, Q.; Ye, W.; et al. Metabolic Inflammatory Syndrome: A Novel Concept of Holistic Integrative Medicine for Management of Metabolic Diseases. *AME Med. J.* **2018**, *3*, 51. [[CrossRef](#)]
141. Lee, Y.S.; Olefsky, J. Chronic Tissue Inflammation and Metabolic Disease. *Genes Dev.* **2021**, *35*, 307–328. [[CrossRef](#)]
142. Tyavambiza, C.; Dube, P.; Goboza, M.; Meyer, S.; Madiehe, A.M.; Meyer, M. Wound Healing Activities and Potential of Selected African Medicinal Plants and Their Synthesized Biogenic Nanoparticles. *Plants* **2021**, *10*, 2635. [[CrossRef](#)]
143. Franková, J.; Pivodová, V.; Vágnerová, H.; Juráňová, J.; Ulrichová, J. Effects of Silver Nanoparticles on Primary Cell Cultures of Fibroblasts and Keratinocytes in a Wound-Healing Model. *J. Appl. Biomater. Funct. Mater.* **2016**, *14*, e137–e142. [[CrossRef](#)] [[PubMed](#)]

144. Alkhalaf, M.I.; Hussein, R.H.; Hamza, A. Green Synthesis of Silver Nanoparticles by Nigella Sativa Extract Alleviates Diabetic Neuropathy through Anti-Inflammatory and Antioxidant Effects. *Saudi J. Biol. Sci.* **2020**, *27*, 2410–2419. [[CrossRef](#)] [[PubMed](#)]
145. Aparna, M.K.; Seethalakshmi, S.; Gopal, V. Evaluation of In-Vitro Anti-Inflammatory Activity of Silver Nanoparticles Synthesised Using Piper Nigrum Extract. *J. Nanomed. Nanotechnol.* **2015**, *6*, 268. [[CrossRef](#)]
146. Moldovan, B.; David, L.; Vulcu, A.; Olenic, L.; Perde-Schrepler, M.; Fischer-Fodor, E.; Baldea, I.; Clichici, S.; Filip, G.A. In Vitro and in Vivo Anti-Inflammatory Properties of Green Synthesized Silver Nanoparticles Using Viburnum Opulus L. Fruits Extract. *Mater. Sci. Eng. C* **2017**, *79*, 720–727. [[CrossRef](#)] [[PubMed](#)]
147. Ghiuț, I.; Cristea, D. Silver Nanoparticles for Delivery Purposes. *Nanoeng. Biomater. Adv. Drug Deliv.* **2020**, 347–371. [[CrossRef](#)]
148. Mitchell, M.J.; Billingsley, M.M.; Haley, R.M.; Wechsler, M.E.; Peppas, N.A.; Langer, R. Engineering Precision Nanoparticles for Drug Delivery. *Nat. Rev. Drug Discov.* **2020**, *20*, 101–124. [[CrossRef](#)] [[PubMed](#)]
149. Ivanova, N.; Gugleva, V.; Dobрева, M.; Pehlivanov, I.; Stefanov, S.; Andonova, V. Silver Nanoparticles as Multi-Functional Drug Delivery Systems. In *Nanomedicines*; IntechOpen: London, UK, 2019.
150. Khalid, S.; Hanif, R. Green Biosynthesis of Silver Nanoparticles Conjugated to Gefitinib as Delivery Vehicle. *Int. J. Adv. Sci. Eng. Technol.* **2017**, *5*, 2321–9009.
151. Ferdous, Z.; Nemmar, A. Health Impact of Silver Nanoparticles: A Review of the Biodistribution and Toxicity Following Various Routes of Exposure. *Int. J. Mol. Sci.* **2020**, *21*, 2375. [[CrossRef](#)]
152. Sun, X.; Shi, J.; Zou, X.; Wang, C.; Yang, Y.; Zhang, H. Silver Nanoparticles Interact with the Cell Membrane and Increase Endothelial Permeability by Promoting VE-Cadherin Internalization. *J. Hazard. Mater.* **2016**, *317*, 570–578. [[CrossRef](#)]
153. Lekamge, S.; Miranda, A.F.; Abraham, A.; Li, V.; Shukla, R.; Bansal, V.; Nugegoda, D. The Toxicity of Silver Nanoparticles (AgNPs) to Three Freshwater Invertebrates with Different Life Strategies: Hydra Vulgaris, Daphnia Carinata, and Paratya Australiensis. *Front. Environ. Sci.* **2018**, *6*, 152. [[CrossRef](#)]
154. Mao, B.H.; Chen, Z.Y.; Wang, Y.J.; Yan, S.J. Silver Nanoparticles Have Lethal and Sublethal Adverse Effects on Development and Longevity by Inducing ROS-Mediated Stress Responses. *Sci. Rep.* **2018**, *8*, 2445. [[CrossRef](#)] [[PubMed](#)]
155. Khan, S.U.; Saleh, T.A.; Wahab, A.; Khan, M.H.U.; Khan, D.; Khan, W.U.; Rahim, A.; Kamal, S.; Khan, F.U.; Fahad, S. Nanosilver: New Ageless and Versatile Biomedical Therapeutic Scaffold. *Int. J. Nanomed.* **2018**, *13*, 733–762. [[CrossRef](#)] [[PubMed](#)]
156. Bruna, T.; Maldonado-Bravo, F.; Jara, P.; Caro, N. Silver Nanoparticles and Their Antibacterial Applications. *Int. J. Mol. Sci.* **2021**, *22*, 7202. [[CrossRef](#)] [[PubMed](#)]
157. González-Luna, P.I.; Martínez-Castanon, G.A.; Zavala-Alonso, N.V.; Patiño-Marin, N.; Niño-Martínez, N.; Morán-Martínez, J.; Ramírez-González, J.H. Bactericide Effect of Silver Nanoparticles as a Final Irrigation Agent in Endodontics on Enterococcus Faecalis: An Ex Vivo Study. *J. Nanomater.* **2016**, *2016*, 7597295. [[CrossRef](#)]
158. Falconer, J.L.; Grainger, D.W. In Vivo Comparisons of Silver Nanoparticle and Silver Ion Transport after Intranasal Delivery in Mice. *J. Control. Release* **2018**, *269*, 1–9. [[CrossRef](#)] [[PubMed](#)]
159. Jorge de Souza, T.A.; Rosa Souza, L.R.; Franchi, L.P. Silver Nanoparticles: An Integrated View of Green Synthesis Methods, Transformation in the Environment, and Toxicity. *Ecotoxicol. Environ. Saf.* **2019**, *171*, 691–700. [[CrossRef](#)]
160. Wypij, M.; Je, drzejewski, T.; Trzcińska-Wencel, J.; Ostrowski, M.; Rał, M.; Golińska, P. Green Synthesized Silver Nanoparticles: Antibacterial and Anticancer Activities, Biocompatibility, and Analyses of Surface-Attached Proteins. *Front. Microbiol.* **2021**, *12*, 888. [[CrossRef](#)]

WESTERN CAPE

Chapter 3: Materials and Methods

3.1. Synthesis and characterization of green AgNPs

The green synthesized AgNPs namely, Gum Arabic (GA-AgNPs), *Salvia Africana-lutea* (SAL-AgNPs), *Carpobrotus edulis* (Cefe-AgNPs), *Cotyledon Orbiculata* (CO-AgNPs), and Red Wine AgNPs (RW-AgNPs) were obtained from the laboratory, already synthesized using their optimal concentration of plant extracts, concentration of AgNO₃ and temperature, which are summarized in Table 3.1. The intended applications for the selected AgNPs are also highlighted in Table 3.1.

Table 3.1: Optimal conditions for select AgNPs synthesis.

Type of AgNPs	Intended application	[plant extract] (mg/ml)	[AgNO ₃] (mM)	Temperature for synthesis (°C)	Ref
GA-AgNPs	Antimicrobial agent for dental caries	4	0.05	121	[13]
SAL-AgNPs	Antimicrobial agent	3.125	3	70	[14]
Cefe-AgNPs	Anti-cancer agent	12.5	1	80	-
CO-AgNPs	Antimicrobial and anti-inflammatory agent for wound healing	3	3	70	[15]
RW-AgNPs	Anti-cancer agent	6.25	3	70	-

Note: -, Data not published yet

The AgNPs were washed twice in dH₂O and spun at 14000 rpm for 15 minutes using the Centrifuge 5417 (Eppendorf, Germany), except the GA-AgNPs which were spun down at 9000 rpm for 1 hour. All AgNPs were resuspended in equal volume of dH₂O and characterized by UV-vis on a POLARstar Omega microplate reader (BMG Labtech, Offenburg, Germany) and DLS using Zetasizer (Malvern Instruments Ltd., Malvern, UK) as previously described [15].

All AgNPs samples were freeze dried using the VirTis Freeze Dryer – BenchTop Pro with Omnitronics (SP Scientific, Pennsylvania, USA) in a total volume of 1 ml and weighed.

The dry weights were then used to calculate concentration in the stock volumes of the AgNPs samples.

3.2. Evaluation of the anti-cancer effects of green AgNPs

3.2.1. Cell culture and maintenance

A panel of normal and cancer cell lines listed in Table 3.2 were randomly selected to study the effects of green AgNPs in this study. The cells were purchased from American Type Culture Collection (ATCC, Manassas, USA). Cryovials of frozen stocks were obtained from the cryofreezer (-120 °C) which contained 1-2 ml of cells suspended in freezing media with 5% DMSO (Sigma-Aldrich, MO, USA). The cells were thawed and transferred into a 15 ml tube containing 5 ml of complete media and centrifuged for 5 minutes at 3000 rpm using an E-C4.5-6.50 CP centrifuge (Eins Sci, United Kingdom). The supernatant was removed, and the pellet was resuspended in 1 ml of cell media which was then transferred into T25 cell culture flasks in their respective media supplemented with 10% of FBS and 1% Pen-strep (complete media). The flasks were then labelled and incubated at 37 °C in a Forma series II Water Jacketed CO₂ incubator (Thermo Fisher Scientific, MA, USA). The cells were regularly checked on an Evos XL Core inverted microscope (Thermo Fisher Scientific, MA, USA) for growth and contamination. Media was changed every 2 to 3 days as required.

Table 3.2: List of cell lines, species, source and respective media

Cell lines	Species	Source	Condition	Media
KMST-6	Human	Skin Fibroblast	Normal	Complete DMEM
HaCaT	Human	Skin Keratinocytes	Normal	Complete DMEM
Caco-2	Human	Colon tissue	Cancer	Complete DMEM
A375	Human	Skin Tissue	Cancer	Complete DMEM
A549	Human	Lung tissue	Cancer	Complete DMEM-F12
PC-3	Human	Prostate tissue	Cancer	Complete RPMI
MCF-7	Human	Breast tissue	Cancer	Complete DMEM

3.2.2. Trypsinization

Trypsin (Sigma-Aldrich, MO, USA) was used to detach adherent cells from T25 cell culture flasks when the cells were 70-80%. The media were removed from the cell culture flasks and the flasks were then washed with 5 ml of Phosphate Buffered Saline (PBS, Thermo Fisher Scientific, MA, USA). A volume of 3 ml of trypsin was added to the culture flasks and incubated at 37 °C. The flasks were observed using an Evos XL Core inverted microscope and analyzed to determine if the cells were detached. Then twice the volume of media was added to the flasks, transferred into 15 ml tubes and spun down for 5 minutes at 3000 rpm. The pellets were resuspended in 1-2 ml of complete media.

3.2.3. Cryo-preservation of cells

After the cells were trypsinized, and spun down, as described in section 3.2.2, the pellets were resuspended in a total of 10 ml of freezing media containing 5% DMSO. Once resuspended, 1- 2 ml of the cells were aliquoted into cryovials. The cryovials were labelled and stored at - 120 °C in a liquid nitrogen freezer.

3.2.4. Cell count

Once the cells were resuspended in media following the protocol described in subsection 3.2.2, 20 µl of the cell suspension was mixed with 20 µl of trypan blue dye (Thermo Fisher Scientific, MA, USA) on parafilm paper. An aliquot of the mixture (20 µl) was transferred into a Countess cell counting chamber slide (Thermo Fisher Scientific, MA, USA) and read on a countess automated cell counter (Thermo Fisher Scientific, MA, USA). Once read, the cells were diluted in complete media to have a desired concentration for further analysis.

3.3. Investigation of the biocompatibility and cytotoxicity of the green AgNPs

3.3.1. MTT (3-(4,5-Dimethylthiazol-2-yl)-2,5-diphenyltetrazolium bromide) assay

The effect of the green AgNPs (GA-AgNPs, SAL-AgNPs, Cefe-AgNPs, CO-AgNPs, and RW-AgNPs) was investigated on human non-cancer (KMST-6 and, HaCaT) and cancer (MCF-7,

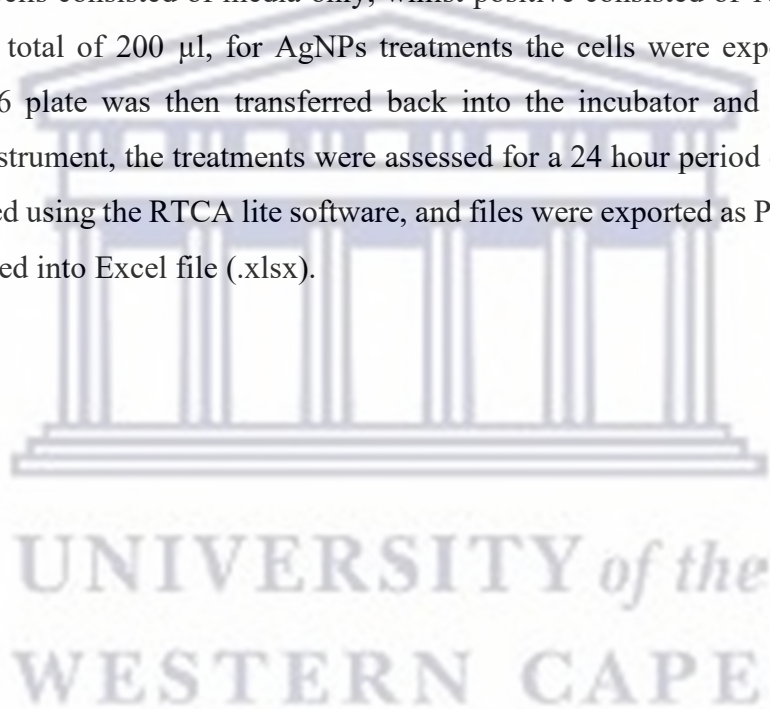
PC-3, A549, A375, and Caco-2) cells using MTT assay as previously reported [13]. Briefly, the cells were seeded in 96 well plates at a cell density of 1×10^5 cells/ml, a volume of 100 μ l of the cell suspension per well. The plates were incubated at 37 °C for 24 hours and treated with increasing concentrations of the AgNPs (0–1000 μ g/ml) prepared in their respective media. 10% DMSO was used as a positive control and untreated cells were included as a negative control. The untreated cells contained 100 μ l of fresh media. The treatments were done in quadruplicates and incubated at 37 °C for 24 hours. The media was then removed from the 96 well plate and new media containing 10% of 0.5 mg/ml MTT dye at a total volume of 100 μ l was added into each well. The plate was then covered with foil and incubated at 37 °C for 24 hours. After the incubation period, the media/MTT mixture was removed from all wells and a volume of 100 μ l of DMSO was added to each well and incubated at 37 °C for 30 minutes. The absorbance was then read at 570 nm with a reference wavelength of 690 nm.

3.3.2. xCELLigence Real Time Cell Analyzer (RTCA)

The xCELLigence RTCA system supports real time analysis of cell behavior or response to treatments without a need of colorimetric reagent, the response can be monitored as soon as the treatments are added. It is thus very accurate and does not require any alteration or adjustments to the medium or additions of any markers that may alter cellular function during the experimental run. The cells can also be harvested after the experiment for successive analysis [16]. The xCELLigence RTCA system utilizes gold microelectrodes which are located at the bottom of microtiter wells and able to monitor the status of either adherent or suspension cells at the bottom of the plate. The principle behind the assay is that the cells at the bottom of the plate, act as insulators, which in turn prevents the flow of alternating microampere electric current between the electrodes. Prevention of the signal is measured automatically at set intervals which then provides an incredibly sensitive reading of cell size, number, and cell-substrate strength [48].

The real time effect of GA-AgNPs on cell viability was also assessed using the xCELLigence RTCA (Agilent, CA, USA) and according to the manufacturer's guidelines described elsewhere [16] with some modifications in an E16-plate. Changes were made to the protocol as the guide did not provide optimal growth for specific cell lines therefore concentration of MCF-7 and PC-3 cells were optimized first. Software setup was kept as the guide provided, however changes made were as follows: MCF-7 and PC-3 cells were grown up until 75-85%

confluency. Prior to harvesting after the growth period, the E-plate 16 wells were filled with 100 μ l of media and the E-16 plate was run on the xCELLigence RTCA for 30 minutes with just media as a background for 1 minute. Once background was completed, the cells were added at optimized concentrations on the E-16 plate. PC-3 cells were seeded at 10000 cells per well and MCF-7 cells at 3500 cells per well by adding 100 μ l of cell suspension into each well which resulted in a total of 200 μ l in each well. Followed by a 15-30 minute waiting period inside the laminar flow for the cells to settle into the E-16 plate. The E-16 plate was then transferred into the incubator and inserted into the xCELLigence instrument; the cells were allowed to grow for 24 hours. After which, all media was removed from the E-16 plate, a blank, untreated and positive was accounted for in the allocated wells. Blank consisted of media only, untreated cells consisted of media only, whilst positive consisted of 10% DMSO. Each treatment was a total of 200 μ l, for AgNPs treatments the cells were exposed to 6.25-100 μ g/ml. The E-16 plate was then transferred back into the incubator and inserted into the xCELLigence instrument, the treatments were assessed for a 24 hour period of treatment. The data was analyzed using the RTCA lite software, and files were exported as Perl files (.pl files) and then converted into Excel file (.xlsx).



3.4. Molecular effects of green AgNPs on PC-3 cells

3.4.1. Cell culture and treatment

PC-3 cells were seeded in six T25 flasks at a cell density of 2×10^5 cells/ml. After 24 hours, the media was removed from the flasks, and three of the flasks were treated with 12.5 $\mu\text{g/ml}$ GA-AgNPs and in the other three media was replaced with fresh media and used as untreated. After 24 hours of treatment, the cells were harvested by trypsinization as described in 3.2.2, and the harvested pellets were washed three times with PBS. The washing step was repeated thrice. The cell pellets were stored at -80°C until further use.

3.4.2. RNA Extraction using RNeasy Plus Mini Kit

RNA samples were extracted from both the treated and untreated cells using RNeasy Plus Mini Kit [17] (Qiagen, Hilden, Germany) following manufacturer's instructions. Cell pellets were disrupted using 18-19 gauge needle and syringe by adding 600 μl of RLT Plus Buffer and 10 μl of β -mercaptoethanol. The pellets were homogenized by gently drawing it up and down the syringe to disrupt the cell. The homogenized lysate was transferred to a gDNA Eliminator Spin Column placed in a 2 ml collection tube. The column was centrifuged for 30 seconds at 12 000 rpm. The flow-through was kept, and 600 μl of 70% ethanol was added to the flow through. The sample was transferred into a RNeasy spin column placed in a 2 ml collection tube and spun for 15 seconds at 12 000 rpm. Flow-through was discarded and 700 μl of RW1 buffer was added to the RNeasy mini spin column. The tube was centrifuged for 15 seconds at 12 000 rpm. Flow-through was discarded and 500 μl of RPE buffer was added to the RNeasy spin column. The tube was centrifuged again as before. After discarding the flow-through, 500 μl of RPE buffer was added to the RNeasy spin column and spun again. The RNeasy Spin column was transferred in a new 1.5 ml collection tube and 30 μl of RNase-Free water was added directly to the spin column membrane. The mixture was then centrifuged for 1 minute at 12 000 rpm to elute the RNA. The RNA samples were aliquoted into 3 separate tubes (20 μl ,

5 μ l, 5 μ l) to prevent contamination. The aliquots were stored at -80°C for further use, to evaluate RNA quality and for cDNA synthesis.

3.4.3. RNA quantification using Qubit

The RNA samples were quantified by the Qubit RNA BR (Broad-Range) Assay Kit [17] (Invitrogen by Life Technologies, CA, USA) as recommended by the manufacturer's instructions. A qubit cocktail of the qubit buffer and reagent mix was prepared for 8 samples, for the 6 RNA samples from treated and untreated PC-3 cells and 2 standards. A total volume of 1.592 μ l of qubit buffer was added to 8 μ l of qubit reagent. The qubit buffer and reagent mix were then aliquoted into 8 separate 1.5 ml Eppendorf tubes. The standards were prepared by mixing 190 μ l of qubit cocktail with 10 μ l of either standard 1 or standard 2. The PC-3 RNA samples were prepared by adding 198 μ l of qubit cocktail with 2 μ l of RNA samples. All tubes were vortexed for a few seconds and incubated in the dark for 2 minutes. The concentration of the RNA samples was measured by the Qubit 2.0 fluorometer instrument [17] (Invitrogen by Life Technologies, CA, USA).

3.4.4. Agarose gel electrophoresis analysis of the RNA Sample

The agarose gel [18] (1%) was prepared in 1x TBE buffer, i.e. 0.33 mg of agarose powder in 30 ml of 1x TBE buffer (prepared from a 10x TBE buffer: 108 g of Tris, 55 g of Boric acid, and 40 ml of 0.5 M Na_2EDTA in 1l). The solution was allowed to cool, then 3 μ l of Ethidium bromide (EtBr) was added to the gel. It was mixed and then poured into the gel-casting tray and allowed to solidify. Once solidified, the gel was transferred to the electrophoresis tray, the tank was then filled with 1x TBE running buffer. The RNA samples and the marker were loaded on the gel and run at 90 mV. The gel was imaged and analyzed on a UVP Biospectrum Imaging system (The Scientific Group, California, USA).

3.4.5. cDNA Synthesis and confirmation by PCR

The cDNA was synthesized from RNA using RT2 First Strand Kit (Qiagen, Hilden, Germany). The total amount of RNA used for the genomic DNA elimination step from the RNA samples

was 25 ng in a total reaction volume of 10 μ l. Table 3.3 shows the total amount of each component used for the genomic elimination mix. The genomic DNA elimination mix was incubated for 5 minutes at 45 $^{\circ}$ C, then placed immediately on ice for at least 1 minute.

Table 3.3: Genomic elimination for RNA synthesized from untreated and GA-AgNPs treated PC-3 cells

PC-3 Samples	Volume of RNA (μ l)	Volume of Buffer GE (μ l)	Volume of RNase Free water (μ l)	Total Volume (μ l)
Untreated 1	5.3	2	2.7	10
Untreated 2	0.74	2	7.26	10
Untreated 3	1.06	2	6.94	10
Treated 1	5.4	2	2.6	10
Treated 2	3.67	2	4.33	10
Treated 3	1	2	7	10

cDNA synthesis was performed using the genomic DNA elimination samples. A total of 10 μ l reverse transcriptase mix was added to each reaction tube containing 10 μ l genomic DNA elimination mix and mixed gently with a pipette. A reverse transcription mix was prepared according to Table 3.4 for a total of 7 reactions (1 extra reaction was for margin of error).

Table 3.4: Reverse-transcription mix preparation for 7 reactions

Component	Volume for 7 reactions (μ l)
5x Buffer Bc3	28
Control P ₂ (Primer)	71
RE3 Reverse transcriptase mix	14
RNase free water	21
Total volume	70

Each reaction was prepared in PCR tubes. The reaction tubes were then incubated at 45 $^{\circ}$ C for 15 minutes, the reaction was incubated at 95 $^{\circ}$ C for 5 minutes. To each reaction tube, 91 μ l RNase-free water was added, mixed by pipetting up and down several times. The reaction was placed immediately on ice and then confirmed by the PCR through amplification of gene 1 and the house keeping gene (GAPDH). The PCR reactions were set up for the amplification of cDNA samples as shown in Table 3.5, with and without the primers for the genes of interest.

Table 3.5: PCR Reaction for cDNA synthesis confirmation

Reagents	Tube 1 (Gene 1)	Tube 2 (-ve gene 1)	Tube 3 (GAPDH)	Tube 4 (-ve GAPDH)
Nuclease free H ₂ O	7.2µl	7.2µl	7.2µl	7.2µl
Mastermix	10µl	10µl	10µl	10µl
GAPDH Forward Primer	0.4µl (gene1)	0.4µl (gene1)	0.4µl	0.4µl
GAPDH Reverse Primer	0.4µl (gene1)	0.4µl (gene1)	0.4µl	0.4µl
cDNA	2µl	0µl	2µl	0µl
RNase free water	0µl	2µl	0µl	2µl

The samples were mixed and placed on ice while the PCR programme was set up on a GeneAmp PCR system 2700 (Applied Biosystems by Life Technologies, USA) as in Table 3.6. The PCR products were analyzed on a 1% agarose gel electrophoresis to confirm the presence of the cDNA before proceeding to qPCR.

Table 3.6: PCR conditions for confirmation and amplification of cDNA product

Step	Temperature(°C)	Time
Initial Denaturation	95	5 minutes
Denaturation	95	15 seconds
Annealing	61	15 Seconds
Extension	72	30 Seconds
Final Extension	72	3 Minutes
Hold	10	∞

3.4.6. Analysis of gene expression by RT-qPCR

The RT² SYBR® Green Mastermix (Qiagen, Hilden, Germany) was centrifuged for 10-15 seconds for the contents to be collected at the bottom of the tube. The RT-qPCR [19] cocktail was prepared in a 15 ml tube by adding together the components in Table 3.7.

Table 3.7: Total volume of SYBR Mastermix reaction experiment

Array format	96-well A, C, D, F
2x RT ² SYBR® Green Mastermix	1350 µl
cDNA synthesis reaction	102 µl
RNase-free water	1248 µl
Total volume	2700 µl

Once the cocktail was mixed, a total volume of 25 µl was added to each well of the RT² Profiler PCR Array 96 well plate. The PCR array plate was then sealed with optical adhesive film. Once sealed, the array plate was centrifuged for 1 min at room temperature. The PCR array plate was placed on ice while setting up the RT-qPCR cycling program on a Roche® LightCycler® 480 RT-qPCR according to the RT-qPCR parameters shown in Table 3.8. The array plate was run for a total of 2 hours, this was done in triplicate for all samples. Once data was obtained, it was analyzed using the Qiagen data analysis tool.

Table 3.8: Light cycler instrument PCR setup conditions

Cycles	Duration	Temperature
1	10 min	95°C
45	15 s	95°C
45	1 min	60°C

3.3.7. Analysis of the interaction Differentially Expressed Genes

The Search Tool for the Retrieval of Interaction Genes (STRING) gathers and scores evidence from a variety of sources [20], including (i) automated text mining of scientific literature, (ii) databases of interaction experiments and annotated complexes/pathways, (iii) computational interaction predictions based on co-expression and conserved genomic context, and (iv) systematic transfers of interaction evidence from one organism to another [21]. The 10 DEGs were entered into the STRING tool (<https://string-db.org/>), with the settings for the minimum required interactions scored set to high confidence (0.700) and the MCL clustering coefficient set to 3.

3.4. Statistical analysis

The data presented are means from at least three replicates. Differences between means were significant if $p < 0.05$. Graph pad prism was used to obtain IC_{50} and 2 tailed T- tests were used to obtain p-values. DEGs were analyzed using the Qiagen geneglobe software (<https://geneglobe.qiagen.com/us/analyze>)



Chapter 4: Results and Discussion

There has been a peaked interest in bioapplication of green AgNPs as they provide a sustainable, eco-friendly and cheaper alternative to that of the traditional chemical AgNPs [22]. Green AgNPs have been reportedly used in many bioapplications as anti-microbial, anti-angiogenesis, anti-cancer, anti-diabetic, anti-inflammatory and drug delivery systems [23]. In the current study, the anticancer properties of a number of green AgNPs, namely; GA-AgNPs, SAL-AgNPs, Cefe-AgNPs, CO-AgNPs, and RW-AgNPs was investigated. These AgNPs were shown to have antimicrobial activities (GA-AgNPs [13], [14] [15] against a number of Gram-positive, Gram-negative and multi-drug resistant strains. CO-AgNPs was also shown to have anti-inflammatory and wound healing properties [15]. Therefore making these AgNPs potential candidates for anti-cancer and molecular activity studies. Ultimately, a single green AgNP will be selected based on it's cytotoxic affects in order to evaluate it's molecular and anti-cancer activity in a selected cell line.

4.1. Green synthesized AgNPs

Synthesis of the green AgNPs was optimized in the lab following independent studies for various applications. GA-AgNPs were shown to have anti-bacterial and anti-proliferative properties [13]. GA, derived from the Acacia Senegal tree, is the oldest and most well-known exudate gum, used commercially for over 5000 years in industries such as food, pharmaceuticals, cosmetics, textiles, paper, ink, adhesive, paint, and printing [24]. SAL-AgNPs [14] and CO-AgNPs [15] also demonstrated antimicrobial and immune-modulatory activities. SAL is used as an infusion to treat colds, and as a component of herbal tea mixtures for the treatments of tuberculosis and chronic bronchitis [25]. The succulent plant CO is native to Southern Africa, in folk medicine, it is used to treat skin rashes, abscesses, inflammation, boils, and acne [15]. The effects of RW-AgNPs and Cefe-AgNPs is still understudy in the lab. According to *in vitro* and *in vivo* researches, a moderate amount of daily consumption of wine may help prevent a variety of chronic diseases. This is due, in part, to the presence of important antioxidants in RW [26]. *Carpobrotus edulis* is a plant in the Aizoaceae family. It is a facultative halophytic invasive medicinal and edible succulent plant native to South Africa [27]. Its anti-proliferative, antioxidant, antifungal, antibacterial, antidiabetic, anti-inflammatory, and nutritional value have also been reported to be attributable to the plant's phytoconstituents [27] These properties made the plant extracts prospective plants for

synthesis of bio-active green AgNPs. The various green AgNPs were obtained from the NIC lab after synthesis, and further characterized by their optical and DLS properties.

4.1.1. UV-vis and DLS analyses of green AgNPs

UV-vis spectroscopy was used to measure the surface plasmon resonance (SPR), which is responsible for the optical characteristics of AgNPs and their color change during synthesis. The adsorption of the electrons on the surface of AgNPs and electromagnetic radiation by incident light produces oscillations, which are measurable by UV-vis. A confirmation of AgNPs synthesis is determined by a peak around 380 and 470 nm [24, 29, 30]. The Figure 4.1 represents the UV- vis spectra of the green AgNPs investigated in this study.

The SPR range for the AgNPs is based on their size and shape, as smaller AgNPs absorb at smaller wavelengths [30]. As seen in Figure 4.1A, GA-AgNPs had a narrow spectra with a SPR at 418 nm. The narrow peak suggested that the AgNPs were more uniform in size and therefore less polydisperse [31]. The SPR (418 nm) of the AgNPs also showed a blue-shift [32]. Cefe-AgNPs, RW-AgNPs, and CO-AgNPs represented by Figures 4.1(B, C and E) also exhibited blue-shifts with SPRs at 408, 410 and 410 nm respectively. Their narrow peaks indicated that the AgNPs are less poly disperse and were more uniform in size. SAL-AgNPs Figure 4.1(D), had a red-shift with a broader spectra and a SPR at 428 nm, the broad peak was a characteristic of polydisperse AgNPs, and less uniform in size. The polydispersity of the green AgNPs were confirmed in Table 4.1. All green AgNPs in Figure 4.1 have shown a SPR peak between wavelength 380-470 nm, a unique characteristic feature of AgNPs.

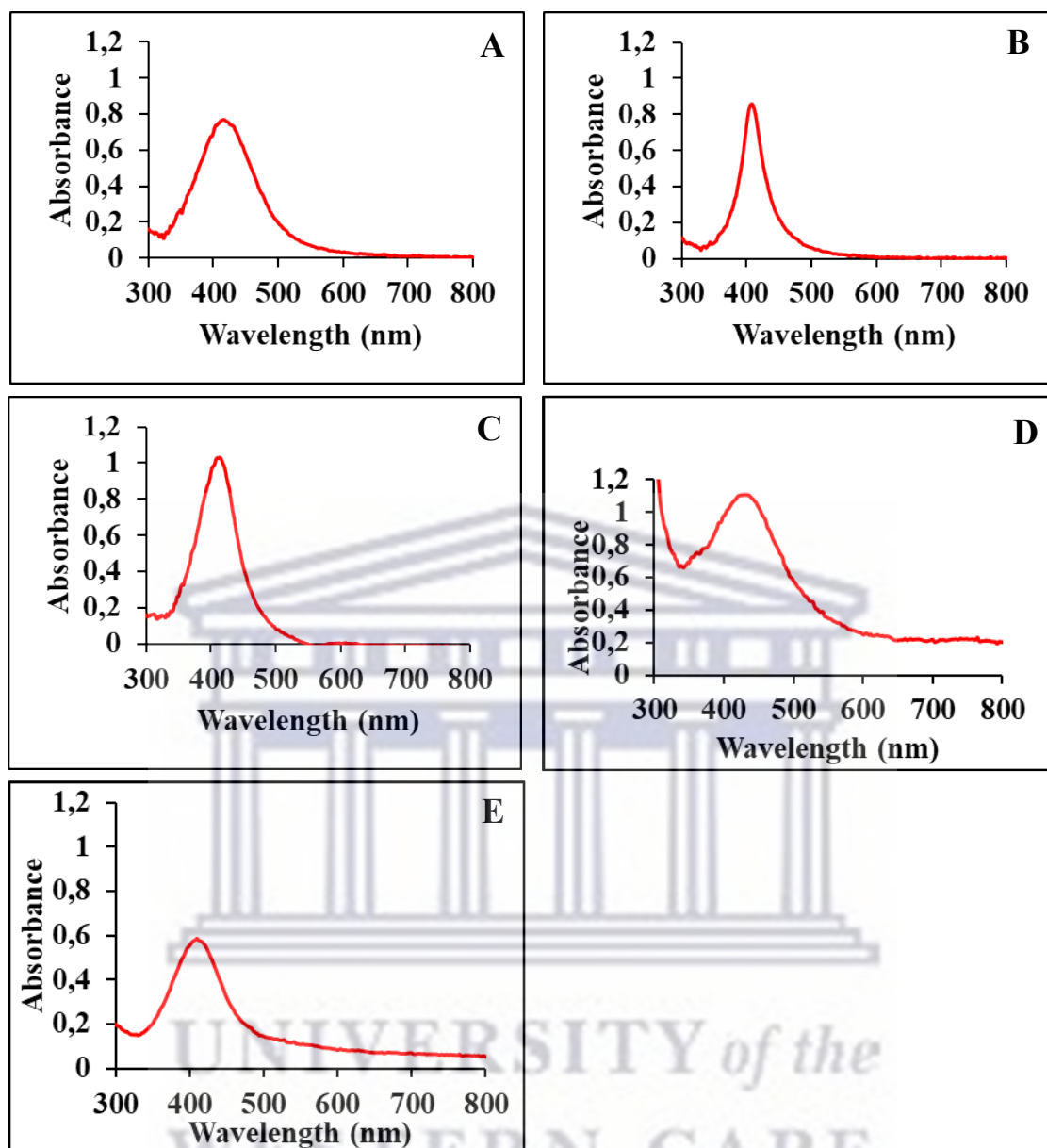


Figure 4.1: The UV-vis spectra of green AgNPs. Graphs represent UV-vis spectra of (A) GA-AgNPs, (B) Cefe-AgNPs, (C) RW-AgNPs, (D) SAL-AgNPs, and (E) CO-AgNPs.

DLS was also used to determine the size distribution (particle diameter) and PDI profile of AgNPs suspension in water. Table 4.1 shows the characteristics of the green AgNPs. GA-AgNPs had an absorbance of 0.769 at SPR 418 nm with a hydrodynamic size of 147.5 d.nm, SAL-AgNPs had an absorbance of 1.105 at SPR 428 nm and a hydrodynamic size of 34.63 d.nm, CO-AgNPs had an absorbance of 0.587 at SPR 410 and a hydrodynamic size of 110 d.nm, RW-AgNPs had an absorbance of 1.029 at SPR 410 nm and a hydrodynamic size of 138.3 d.nm, and Cefe-AgNPs had an absorbance of 0.856 at SPR 408 nm and, a hydrodynamic size of 66.27.

According to Beer-Lambert's law, absorption shares a linear relationship and is directly proportional to the concentration of the AgNPs [33], therefore, SAL-AgNPs, RW- AgNPs, and Cefe-AgNPs were more concentrated than GA-AgNPs and CO-AgNPs. PDI is the measurement of the average uniformity of particles in solution. Large PDI values correspond to a larger size distribution of particles in the total sample. When a sample has a PDI value < 0.1, it is considered monodispersed [34]. SAL-AgNPs has a PDI of 0.63 and are therefore polydispersed, while GA-AgNPs and RW-AgNPs have PDI values of 0.375 and 0.322 respectively, and considered to be less polydispersed than SAL-AgNPs. Cefe-AgNPs has a PDI value of 0.210 and is the second least polydispersed NPs, while the closet to being monodispersed as according to literature, were the CO-AgNPs with a PDI value of 0.15.

Table 4.1: SPR and the hydrodynamic size of the green AgNPs.

Types of AgNPs	Absorbance at SPR	SPR (nm)	Hydrodynamic size (d.nm)	PDI
GA-AgNPs	0.769	418	147.5	0.375
SAL-AgNPs	1.105	428	34.63	0.63
CO-AgNPs	0.587	410	110	0.15
RW-AgNPs	1.029	410	138.3	0.322
Cefe-AgNPs	0.856	408	66.27	0.210

4.2. Cytotoxicity of green AgNPs

Cytotoxicity assays provides information of how the cells respond when exposed to toxic substances, including their cell metabolism, survival and death [10]. In this study, the MTT assay was performed, the dye reagent is positively charged and capable of passing through the cell membrane and the mitochondrial inner membrane of viable cells. It is then reduced to formazan by metabolically active cells, the redox reaction has a chromogenic nature and provides a colorimetric-based measurement of intracellular formazan which is purple in color [35].

The biocompatibility and cytotoxicity of GA-AgNPs, SAL-AgNPs, Cefe-AgNPs, CO-AgNPs, and RW-AgNPs, was initially screened on the normal and cancerous cell lines which include KMST-6 (non-cancerous human fibroblast) cell line [36], PC-3 (PCa) cell line [37], Caco-2

(colorectal cancer) cell line [37], MCF-7 (human breast cancer) cell line [36] and A549 (lung cancer) cell line [37]. The cells were treated for 24 hours using increasing concentrations of AgNPs (0, 62.5, 125, 250, 500, and 1000 µg/ml, where 0 µg/ml represents the negative control or untreated cells).

Three of the AgNPs (Cefe-AgNPs, CO-AgNPs, and RW-AgNPs) were non-toxic to all cells at all concentrations (62.5-1000 µg/ml) as shown in Figure 4.2, and there were instances where each of these AgNPs have enhanced proliferating effects with cell viability that was higher than the untreated cells. Interestingly, CO-AgNPs have been reported to have enhanced proliferation of KMST-6 and HACAT cells. The wound healing effects of CO-AgNPs were attributed to their anti-inflammatory effects through the suppression of pro-inflammatory cytokines; Interleukin (IL)-1 beta, IL-Interleukin 6, and Tumor Necrosis Factor-alpha in THP-1 macrophages. CO-AgNPs were used to treat THP-1 cells at concentrations 5, 10 and 20 µg/ml, and reportedly had a cell viability of 84%, 52%, and 2% respectively. Thus, 5 µg/ml of CO- AgNPs was the least toxic and was used to evaluate immunomodulatory effects of the NPs. It has also been found that CO-AgNPs exhibited anti-microbial effects on multiple skin pathogens with MIC value of 5 µg/ml [15], and showed good antioxidant, growth-promoting, and cell migration properties at 2.5 µg/ml on KMST-6, HaCaT and CHO cells. The CO-AgNPs reportedly upregulated genes involved in cell proliferation, migration, and growth while downregulating pro-inflammatory genes [17]. This implied that these AgNPs were biocompatible and could be used at these concentrations as antimicrobial and wound healing agents, and not show toxicity to human cells. CO-AgNPs seemed to be not toxic at the concentration (≤ 1 mg/ml) used in this study, this discrepancy requires further studies.

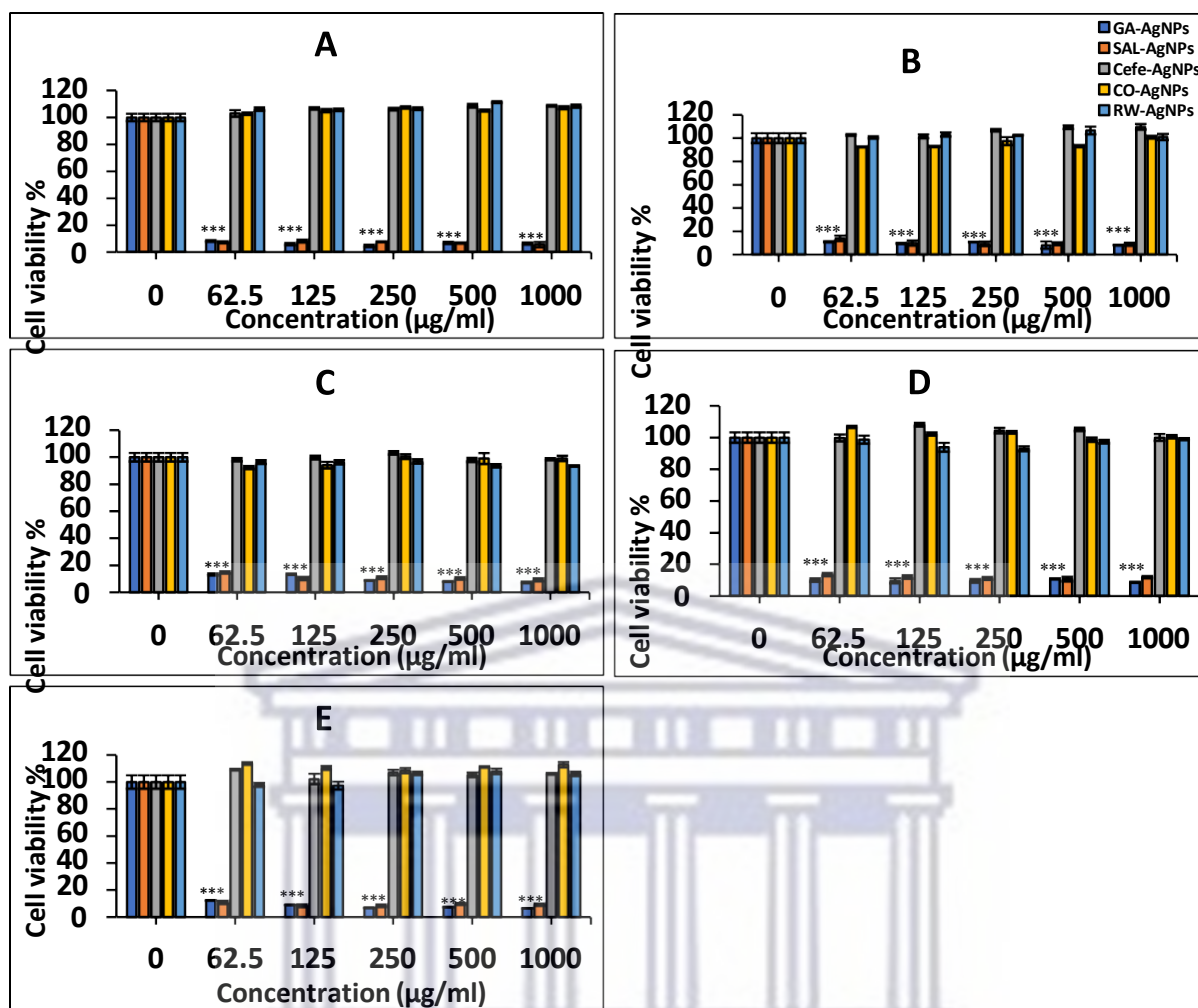


Figure 4.2: Screening of the cytotoxicity effects of green AgNPs using MTT assay on human cells: (A) KMST-6, (B) PC-3, (C) Caco-2, (D) MCF-7 and (E) A549. Each cell line was treated for 24 hours with GA-AgNPs, SAL-AgNPs, Cefe-AgNPs, CO-AgNPs and RW-AgNPs at concentration range 0 µg/ml–1000 µg/ml. Note: The level of significance is represented by $p^* < 0.05$, $p^{**} < 0.01$, $p^{***} < 0.001$.

While the biocompatibility of the green AgNPs have been reported by several studies [23], the current study demonstrated that AgNPs synthesized from plant extracts that have been deemed non-toxic in traditional medicine, have potential to be cytotoxic. Of the five studied green AgNPs, the GA-AgNPs and SAL-AgNPs showed non-selective toxicity to both normal and cancer cells with a cell viability of <20% at all concentrations. The GA-AgNPs were previously reported to be non-selective in nature, as they showed toxic effects on both normal (KMST-6 cells) and cancerous (Caco-2 and HT-29) cells. The cells were exposed to the GA-AgNPs at concentration range from 6.25-100 µg/ml, the AgNPs reduced cell viability to <15% at these concentrations. An IC_{50} value of 0.67 µg/ml was found in KMST-6 cells whilst in the 2 cancer cell lines, the IC_{50} were 0.82 and 1.16 µg/ml, respectively [13]. In a follow up study,

GA-AgNPs and a toothpaste (TP) formulated with GA-AgNPs using a commercial TP at a non-active concentration (GA-AgNPs_TP-1) were used in treatment of buccal mucosa fibroblasts (BMF) cells. The two treatments (GA-AgNPs and GA-AgNPs_TP-1) exhibited non-selective cytotoxicity by reducing BMF cell growth at the same concentrations they inhibited microbial growth [38]. These studies confirmed that the GA-AgNPs are highly toxic and nonspecific, even more so to the non-cancer cell line as it had a lower IC_{50} compared to the cancer cells [38,39]. Another study also illustrated the capabilities of SAL-AgNPs and its antibacterial activity against *Staphylococcus epidermis* and *Pseudomonas aeruginosa*. When the microorganisms were exposed to SAL-AgNPs, it was found that SAL-AgNPs had a MIC value of 0.1875 and 0.375 mg/ml for *S. epidermis* and *P. aeruginosa*, respectively. Thus, natural agents with a MIC value of 1 mg/ml or less are potential antimicrobial agents, and since SAL-AgNPs had MIC values below this value, they could be considered as antimicrobial agents [14]. Strategies are therefore warranted to reduce their cytotoxicity but still retain their anti-cancer activities. The cytotoxicity of GA-AgNPs to BMF cells was reduced by using the AgNPs in TP formulation [38], thus proving that it is possible to improve the biocompatibility of these nanomaterials.

4.2.1. Effect of green AgNPs on the cellular morphology

The morphological changes induced by the green AgNPs on the various cell types after 24 hours were observed using an inverted microscope. Cefe-AgNPs, CO-AgNPs, and RW-AgNPs had no visible toxic effects on all the cells, and showed no changes on cellular morphology or cell-density compared to the untreated cells (data not shown). Whereas, the non-selective toxic effects of GA-AgNPs and SAL-AgNPs were confirmed by the morphological changes in the shapes and number of cells. The changes are illustrated in Figure 4.3, compared to the untreated cells, cells treated with GA-AgNPs, SAL-AgNPs, and 10% DMSO (positive control) appeared to be stressed and unhealthy with drastic morphological changes (Figure 4.3). The morphologies of the cells were similar and had little to no difference in appearance in both the normal and cancerous cells.

A previous study showed the anti-cancer activity of AgNPs synthesized from the plant extract *Fagonia indica*. The MTT assay showed a concentration dependent inhibition of MCF-7 cells. Additionally, morphological changes were observed where the cells appeared in lower density, smaller in cell size, disfigured and more rounded than the untreated cells [40]. Green AgNPs synthesized from *Azadirachta indica* fruit extract had dose dependent inhibitory effects on A549 cells. Similarly, the same effect on morphological changes were seen on A549 cells, the cells appeared rounded, disfigured, and unhealthy [10].



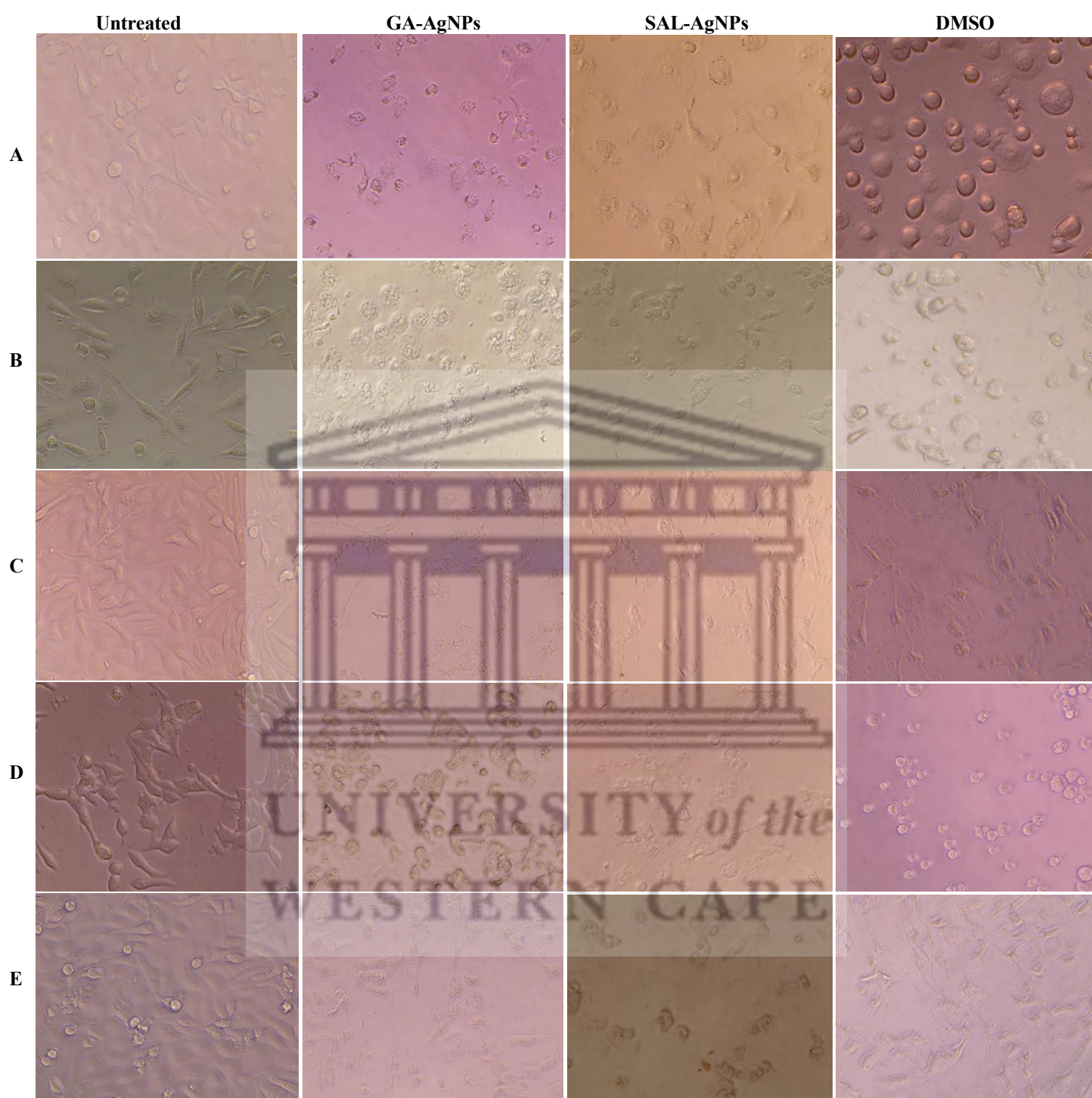


Figure 4.3: Effects of green AgNPs on cell morphology. KMST-6 (A), PC-3 (B), Caco-2 (C), MCF-7 (D), and A549 (E) treated after 24 hours with GA-AgNPs, SAL-AgNPs and 10% DMSO (Positive control).

4.2.2. Determination of the IC₅₀ of GA-AgNPs and SAL-AgNPs

The most widely used and informative measure of a drug's efficacy is its half-maximal inhibitory concentration (IC₅₀). It indicates how much drug is required to inhibit a biological process by half, providing a measure of antagonist drug potency in pharmacological research [41]. The initial screening was done at concentration range of 62.5–1000 µg/ml and proved to be highly toxic on all cell lines, and therefore reduced to ten-fold lower range i.e.; 6.25-100 µg/ml. The IC₅₀ of GA-AgNPs and SAL-AgNPs were further evaluated in the selected cells using MTT assay at the concentration range between 6.25-100 µg/ml. Two more cell lines: HaCaT (non-cancerous immortalized human keratinocytes, [42]) and A375 (human skin cancer cell line, [43]) were added.

The non-selective and dose-dependent cytotoxic effects of the two AgNPs on all cells are shown in Figure 4.4. GA-AgNPs was generally more toxic to the cells than SAL-AgNPs. KMST-6, HaCaT, A549, Caco-2, and MCF-7 cells were the most susceptible to the treatments, while the A375 and PC-3 cells showed some resistance at ≤12.5 µg/ml. When the SAL-AgNPs and GA-AgNPs were used to treat HaCaT cells, the toxic effects were immediate on the cells, the cell viability was reduced to <20% even on the cells exposed to 6.25 µg/ml and remained at a plateau across all concentrations. While significant effects of both SAL-AgNPs and GA-AgNPs on A375 and PC-3 cells were observed at 25-100 µg/ml, the cytotoxicity of SAL-AgNPs and GA-AgNPs treatments were dose dependent. The positive control, 10% DMSO, was cytotoxic across all cell lines exerting a cell viability of <40% in both non-cancer and cancer cell lines.

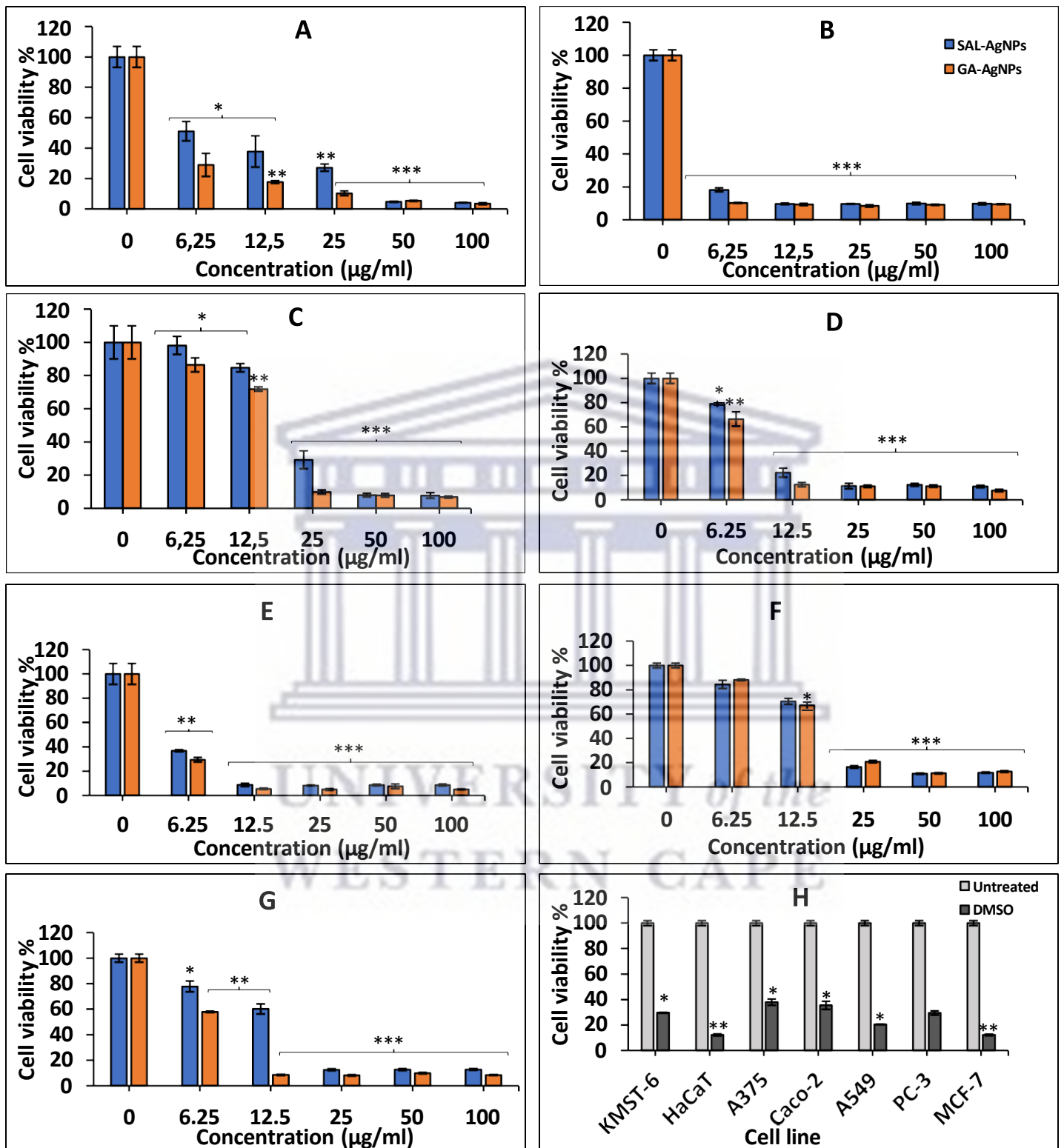


Figure 4.4: MTT cell viability assay for SAL-AgNPs (Left) and GA-AgNPs (Right). Cell lines used (A) KMST-6, (B) HaCaT, (C) A375, (D) Caco-2, (E) A549, (F) PC-3, (G) MCF-7 and (H) Positive control (DMSO 10%) for each cell line. Dose dependently treated respectively ranging from 6.25 µg/ml-100 µg/ml for 24 hours. Note: The level of significance is represented by $p < 0.05$, $p < 0.01$, $p < 0.001$.

Two additional cancer (A375) and non-cancer (HaCaT) cell lines were further studied to broaden the scope of the cytotoxicity study. These were included to demonstrate the effects of SAL-AgNPs and GA-AgNPs on a skin cancer (A375) cell line. Figure 4.5 shows that SAL-AgNPs and GA-AgNPs also induced similar morphological and cell density changes on A375 cells as highlighted in Figure 4.3. The morphological changes were observed when A375 was treated with 50-100 $\mu\text{g/ml}$ SAL-AgNPs and 25-100 $\mu\text{g/ml}$ GA-AgNPs. HaCaT treated with 6.25-100 $\mu\text{g/ml}$ SAL-AgNPs and 6.25-100 $\mu\text{g/ml}$ GA-AgNPs showed the same morphological and cell density changes. Similarly, the exact characteristics were observed when A375 and HaCaT were treated with 10% DMSO. Thus, when comparing untreated A375 and HaCaT cells to their respective treatments, the cells were also rounded and disfigured demonstrating features that are characteristic of cell death via the apoptosis pathway [44].



Figure 4.5: Cellular morphological changes after exposure to SAL-AgNPs and GA-AgNPs, as well as 10% DMSO positive control on (A) A375 and (B) HaCaT cells. Morphological changes of (A) A375 treated with 50-100 $\mu\text{g/ml}$ SAL-AgNPs and 25-100 $\mu\text{g/ml}$ GA-AgNPs and (B) HaCaT treated with 6.25-100 $\mu\text{g/ml}$ SAL-AgNPs and GA-AgNPs are shown.

The IC_{50} of GA-AgNPs and SAL-AgNPs on a number of cancer (MCF-7, PC-3, A375, A549, Caco-2) and non-cancer (KMST-6, HaCaT) cells are shown in Table 4.2. The two AgNPs had

relatively similar responses based on the IC₅₀ values, with GA-AgNPs being more toxic to the cells than SAL-AgNPs. The low IC₅₀ values mean that both GA-AgNPs and SAL-AgNPs are potent at low concentrations, therefore resulting in lower systemic toxicity when applied to the different cell lines. However, when comparing the IC₅₀ values of A375 and PC-3 to the rest of the cell lines, GA-AgNPs and SAL-AgNPs are less potent on the aforementioned cell lines. The lower potency in A375 and PC-3 could potentially be due to slightly more resistance or a defense mechanism. Non-cancer cell lines (KMST-6, HaCaT) demonstrated low IC₅₀ values and display the potency of GA-AgNPs and SAL-AgNPs. A notable difference in IC₅₀ values can be seen between GA-AgNPs and SAL-AgNPs in the MCF-7 cell line, thus deeming GA-AgNPs more potent (IC₅₀: 5.170 ± 0.59) than SAL-AgNPs (IC₅₀: 12.40 ± 1.01).

Table 4.2: The IC₅₀ of GA-AgNPs and SAL-AgNPs on various cell lines

Cell lines	IC ₅₀ (µg/ml) ±SD	
	GA-AgNPs	SAL-AgNPs
KMST-6	3.784 ± 1.21	7.528 ± 1.33
HaCaT	2.732 ± 0.45	3.077 ± 0.64
A375	13.95 ± 1.12	20.36 ± 1.31
Caco-2	6.213 ± 1.01	6.401 ± 0.98
A549	3.285 ± 0.34	3.875 ± 0.56
PC-3	15.68 ± 0.72	14.99 ± 0.81
MCF-7	5.170 ± 0.59	12.40 ± 1.01

Plant extract-synthesized AgNPs have emerged quickly to take on the battle with cancer, a number of studies have reported the potential anticancer activities of biogenic AgNPs. AgNPs synthesized with *Pinus Roxburghii* were shown to possess cytotoxic activity against prostate and lung cancer cells. The AgNPs induced intrinsic apoptosis pathways via mitochondrial depolarization, DNA damage, increased ROS, cell cycle arrest, and caspase-3 activation [45]. AgNPs synthesized using *Nepeta deflersiana* showed anticancer potential against human cervical cancer (HeLa) cells. The cytotoxicity of green AgNPs was concentration dependent, with treatments at 5- 100 µg/ml illustrating <35% cell viability and treatments with 1 and 2 µg/ml showing >80% cell viability [11]. It was also found that the AgNPs induced oxidative stress as ROS levels increased. This increase in ROS could eventually lead to damage to the mitochondrial membrane and disruptions in the cell cycle [11]. Exposure of A549 cells to AgNPs synthesized using *Gloriosa superba* L. tuber extract resulted in a dose dependent cytotoxicity. The AgNPs inhibited A549 cell growth at 50-100 µg/ml and had an IC₅₀ value of 46.54 µg/ml [46]. In another study, AgNPs synthesized using an aqueous leaf extract of *Artocarpus interger* showed anticancer activity on MCF-7 and Mg-63 (osteosarcoma) cells. The cell viability of MCF-7 cells when treated with 90 µg/ml was <55% and when treated with 130 µg/ml the cell viability was <30%. The cell viability of Mg-63 cells was <55% at 70 µg/ml and ≤20% at 130 µg/ml [47].

4.3. Real-time analysis of the effects of SAL-AgNPs and GA-AgNPs

Real-time effects of SAL-AgNPs and GA-AgNPs were studied on PC-3 and MCF-7 cells using xCELLigence Real-time Cell Analysis (RTCA) system.

In cell culture-based assays, the xCELLigence RTCA system can be used to study cell adhesion, proliferation, and apoptosis induced by treatments. This system was used in different types of breast cancer cells treated with AgNPs to investigate its pathway-network analysis [49]. Following xCELLigence RTCA analysis, the cell index of MCF-7, HCC70, and, HCC1954 cells was lower in cells treated with AgNPs for 24 hours [49]. The *in vitro* cytotoxicity of Green AgNPs synthesized from *Daucus carota* was evaluated on U87MG brain glioblastoma cells using the xCELLigence system. Following AgNPs treatment, the xCELLigence analysis revealed that the AgNPs had a dose dependent decrease on cell index of U87MG cells [16].

The effects of the GA and SAL AgNPs were monitored in PC-3 and MCF-7 cells from 0–24 hours as shown in Figure 4.6. The xCELLigence RTCA data confirmed the dose-dependent effects of the AgNPs in both PC-3 (Figure 4.6) and MCF-7 (Figure 4.7) cells, and that GA-AgNPs had superior effects compared to SAL-AgNPs (Figures 4.6 and 4.7); as was the case with the MTT assay (Figure 4.4). SAL-AgNPs and GA-AgNPs treatments showed a drastic decrease in cell viability at the concentrations ranging from 25-100 $\mu\text{g/ml}$ in relation to the untreated cells. There was a slight peak following treatment with 6.25 and 12.5 $\mu\text{g/ml}$, the peaks were much more profound from 25 $\mu\text{g/ml}$. This could be the effect of the cells reacting to the addition of the treatment, initially cell index took a dip that could possibly be due to the cells being in shock when exposed to the treatment. However, there was an immediate increase in cell index, which could be due to the cells showing somewhat of a resistance to the treatments which was short-lived as the cell index was reduced and remained at that state from the 30th hour (equivalent to 6 hours of treatment) until the end of the run (total of 24 hours treatment). The cell index at 6.25 and 12.5 $\mu\text{g/ml}$ were more or less similar, and illustrated a slight reduction when compared to the untreated cells. Despite not being as prominent as the cell index at higher concentrations, there was somewhat a reduction in cell index of cells treated with 6.25 and 12.5 $\mu\text{g/ml}$ compared to the untreated. The positive control (10% DMSO) had an immediate reduction of cell index that was maintained throughout the duration of the study. This could be an indication that the cells never recovered from the cytotoxic effects of the treatment.

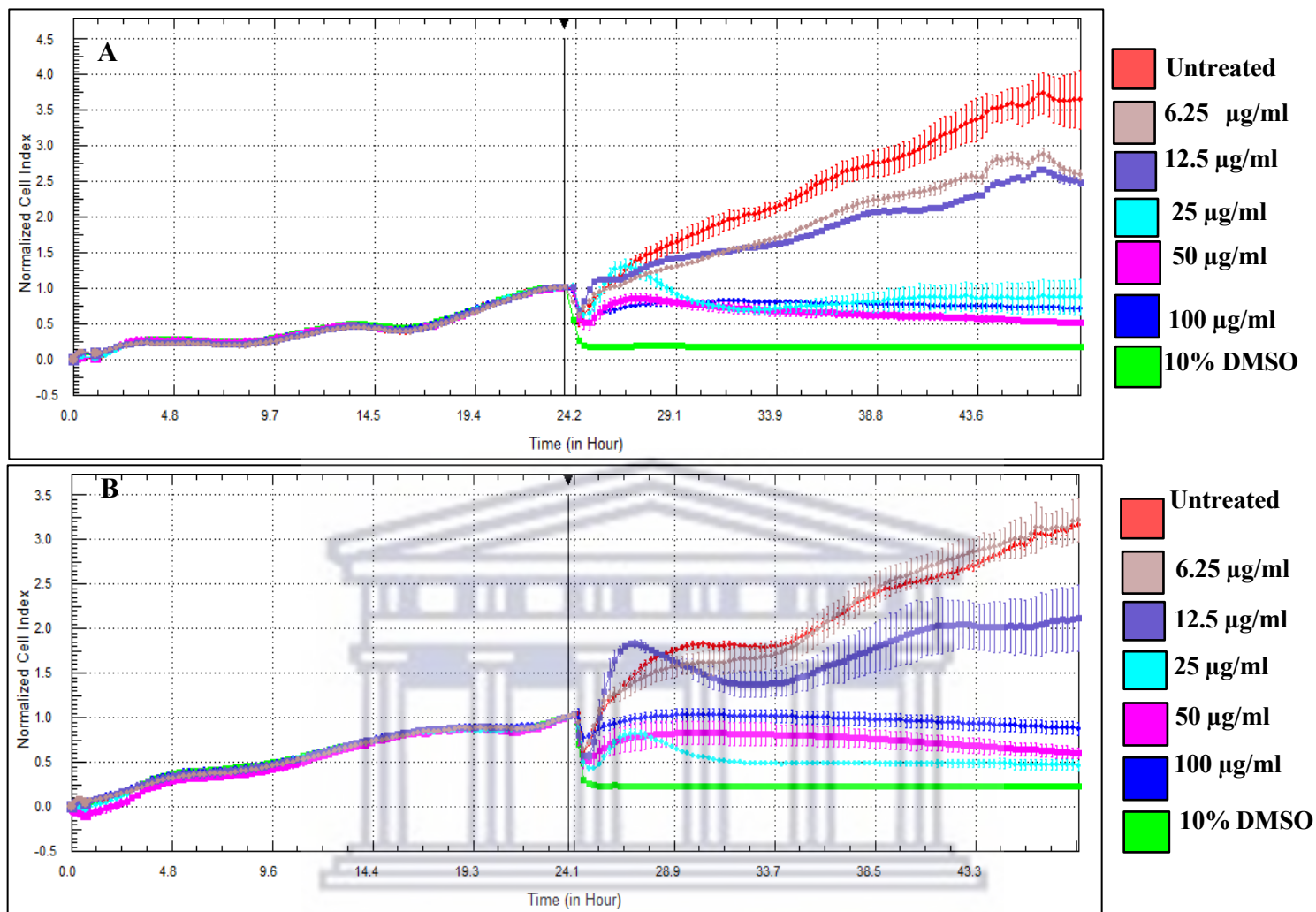


Figure 4.6: Realtime analysis of the effects of (A) SAL-AgNPs and (B) GA-AgNPs on PC-3 cells using xCELLigence RTCA. The cells were treated with their respective AgNPs at 6.25–100 $\mu\text{g/ml}$ and a positive control of 10% DMSO. The solid black vertical line pointed by the arrow represents the point where treatment started.

Similar trends were observed in both the PC-3 and MCF-7 cells treated with the two green AgNPs (Figures 4.6 and 4.7). However, the cell indices of MCF-7 cells treated with both AgNPs were significantly reduced from 25-100 $\mu\text{g/ml}$. Moreover, MCF-7 cells were shown to be more susceptible to the treatments compared to the PC-3 cells, i.e. the cell index were below 0.5 (MCF-7 cells) vs >0.5 for PC-3 cells. Based on this data, it was clear that the effects take effect as early as 4 hours of treatment and are sustainable until the 24th hour. In addition, SAL-AgNPs seemed to be less toxic than the GA-AgNPs, while similar responses were seen with GA-AgNPs at 12.5-100 $\mu\text{g/ml}$, for SAL-AgNPs it only starts from 25 $\mu\text{g/ml}$. These differences

confirmed the MTT results for MCF-7 cells treated with SAL-AgNPs and GA-AgNPs (Figure 4.4), as the cell viability recorded for MCF-7 cells treated with 12.5 $\mu\text{g/ml}$ SAL-AgNPs was $\sim 60\%$ and when treated with GA-AgNPs at the same concentration, the viability was $<10\%$. These findings confirmed that the two assays are complementary to each other, and further the xCELLigence RTCA system can identify the exact time in which the treatment takes effect and monitor these effects over time.

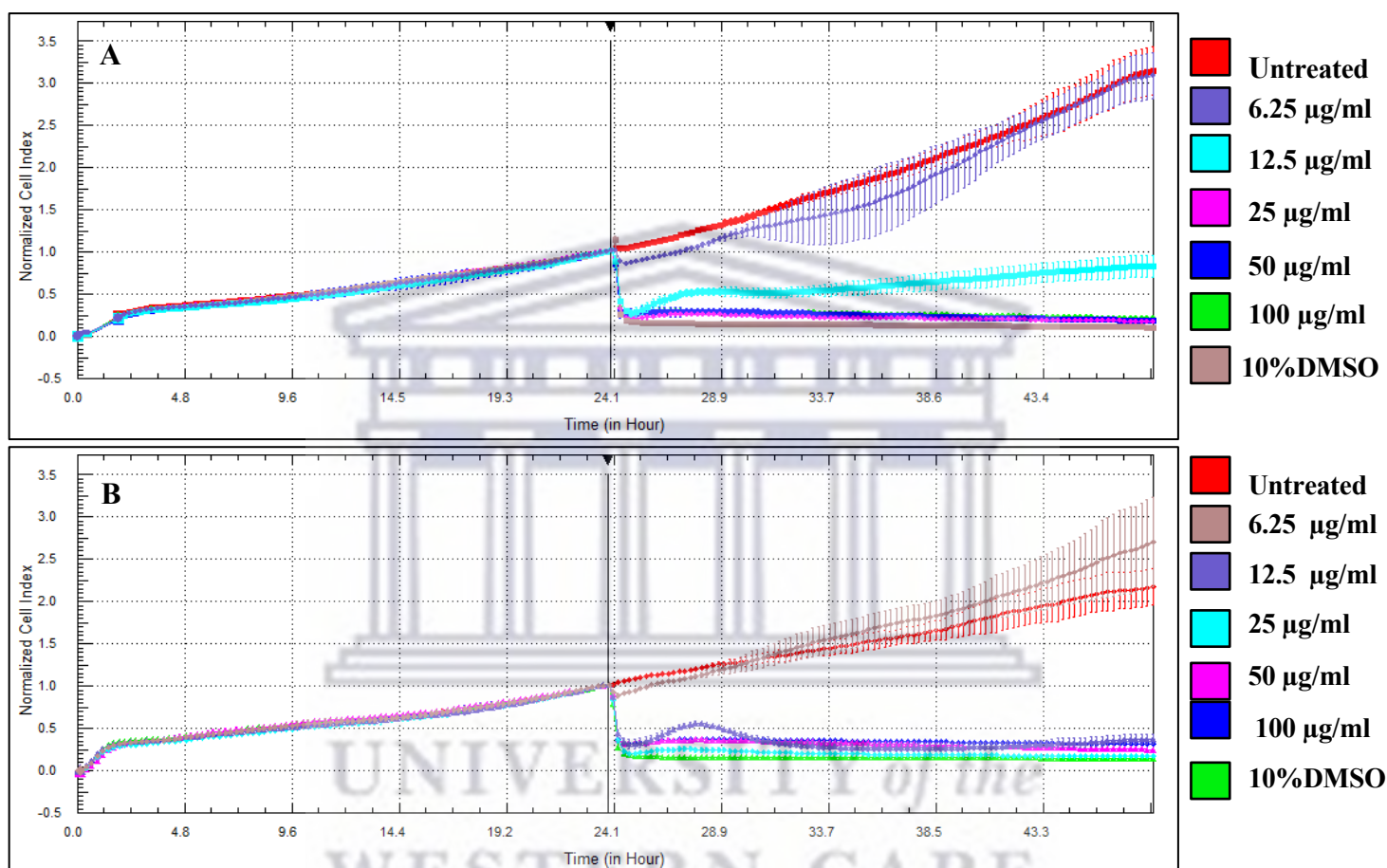


Figure 4.7: Realtime analysis of the effects of (A) SAL-AgNPs and (B) GA-AgNPs on MCF-7 cells using xCELLigence RTCA. The cells were treated with their respective AgNPs at 6.25–100 $\mu\text{g/ml}$ and a positive control of 10% DMSO. The solid black vertical line pointed by the arrow represents the point where treatment started

In Figure 4.8, the xCELLigence RTCA profile of PC-3 cells treated with GA-AgNPs was more closely examined and compared to the MTT assay. This was done in order to determine the concentration of GA-AgNPs for the gene expression analysis in PC-3 cells. Concentrations at 25-100 $\mu\text{g/ml}$ had cell viability that was below 20%, this concentration range would not be recommended for gene expression, as an important signaling functions could be missed. There

was a flatline in the cell index following treatment with concentration range between 25– 100 $\mu\text{g/ml}$ (Figures 4.8A and B), indicating little to no viable cells. Thus, if a concentration at this range was to be selected for gene expression, only death genes will be detected or expressed. Since the genes of interest are more of the anticancer effects of the GA-AgNPs, the concentrations between 6.25–12.5 $\mu\text{g/ml}$ were more suitable as they have a more progressive decline in cell index. Therefore, since 6.25 $\mu\text{g/ml}$ of GA-AgNPs seemed to be more or less similar to that of the untreated, there will be no significant differences in the gene expression between this concentration and the untreated. Hence, leaving the option of using 12.5 $\mu\text{g/ml}$ as the concentration to study the effect of GA-AgNPs on gene expression. Although a progressive decline is observed in cell index over the course of the 24 hours treatment with 12.5 $\mu\text{g/ml}$, at the end there are still enough viable cells to extract more information with regards to the genes responsible or genes involved in the death of the cells.

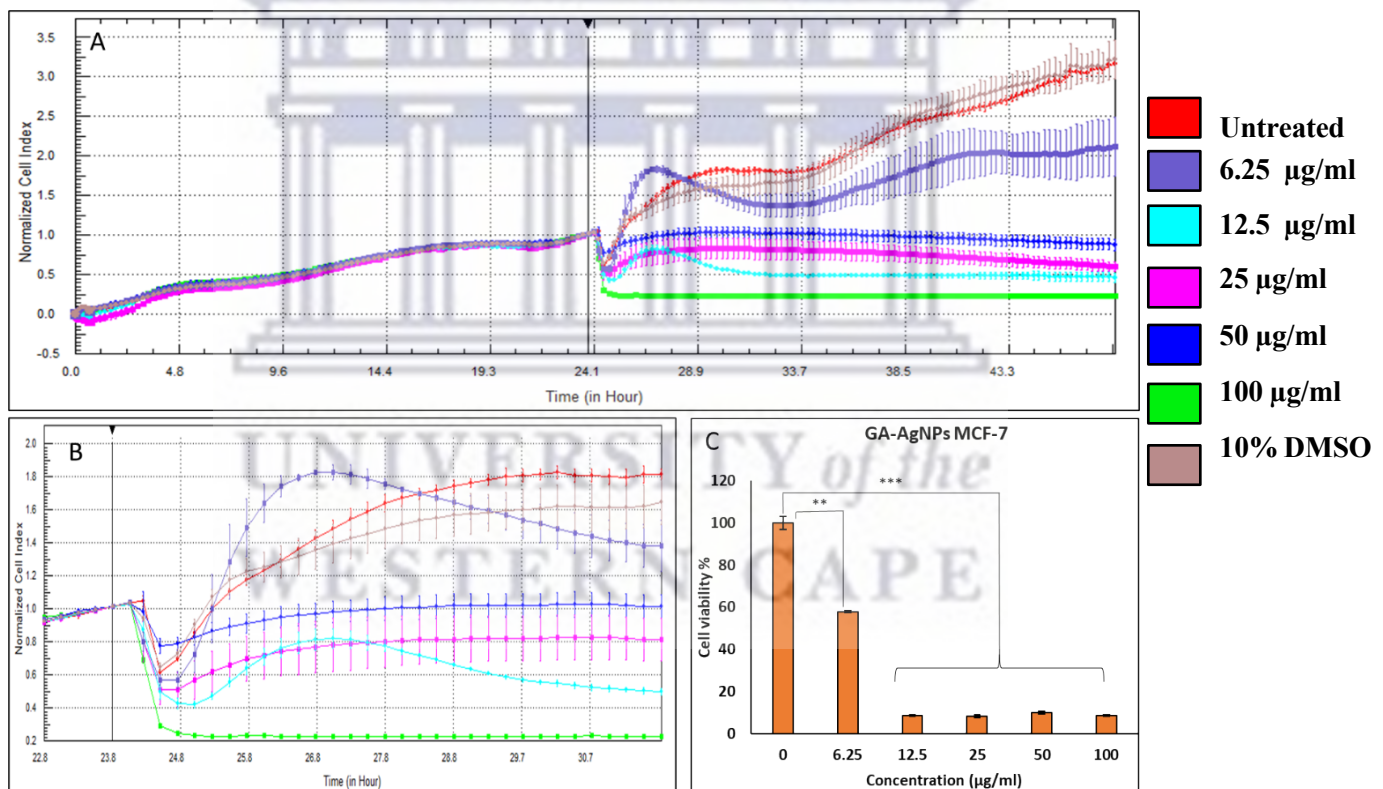


Figure 4.8: RTCA and MTT of GA-AgNPs on human cancer cell line PC-3 cells. (A) Represents the xCELLigence assay of PC-3 over 48 hours, the point where treatment commenced is shown by the black bar. (C) Represents the MTT assay of PC-3 over 24 hours treated with GA-AgNPs.

4.4. Molecular effects of GA-AgNPs on PC-3 cells

The most active green AgNPs (GA-AgNPs) were selected to investigate molecular effects or genes affected by the AgNPs. This is a costly exercise and therefore, only one cell line (PC-3 cells) was studied. MCF-7 was not chosen due to the cell index profile, the goal was to imitate the exact time length of treatment used in the MTT assay which was 24 hours. When comparing cell indexes of MCF-7 and PC-3 after treatment with GA-AgNPs, only concentrations 12.5-100 µg/ml showed potent cytotoxic effects and cell index is low after 24 hours. However, when PC-3 cells were treated with 12.5 µg/ml GA-AgNPs, there was a gradual decrease in their cell index making it a fit model to investigate gene expression. If a higher concentration, and shorter treatment time were chosen the regulation of the genes of interest will be missed.

4.4.1. RNA and cDNA Analysis using Agarose gel Electrophoresis

The integrity of the RNA and cDNA samples extracted from the PC-3 cells treated with 12.5 µg/ml of GA-AgNPs and untreated samples was analyzed using agarose gel electrophoresis. Agarose gel electrophoresis is a common technique for separating DNA and RNA, based on their size and charge. The flow or migration of the nucleic acids is solely determined by molecular weight, with smaller molecules moving faster than larger ones [18]. Agarose gel electrophoresis is the most efficient method for separating DNA fragments ranging in size from 100 base pair (bp) to 25 kilobase pair (kbp) [50]. Many applications of agarose have been made, including the analysis of gene mutations related to certain cancer types, molecular changes caused by chemicals and radiation, and plasmodium resistance to anti-malaria drugs [51].

In Figure 4.9, the RNA products were confirmed on a 1% agarose gel by the presence of 28S between 750 and 1000bp and 18S RNA at ~250 bp bands on the gel. The 28S and 18S bands are associated with mammalian RNA and used as markers when assessing the RNA integrity [52]. The 28S band seemed to be more intense in brightness compared to 18S. This difference in intensity could be due to the ratio of 28S to 18S that was reported to be 2:1 [53]. There was no contamination or degradation and as such, the integrity of the RNA was good and intact.

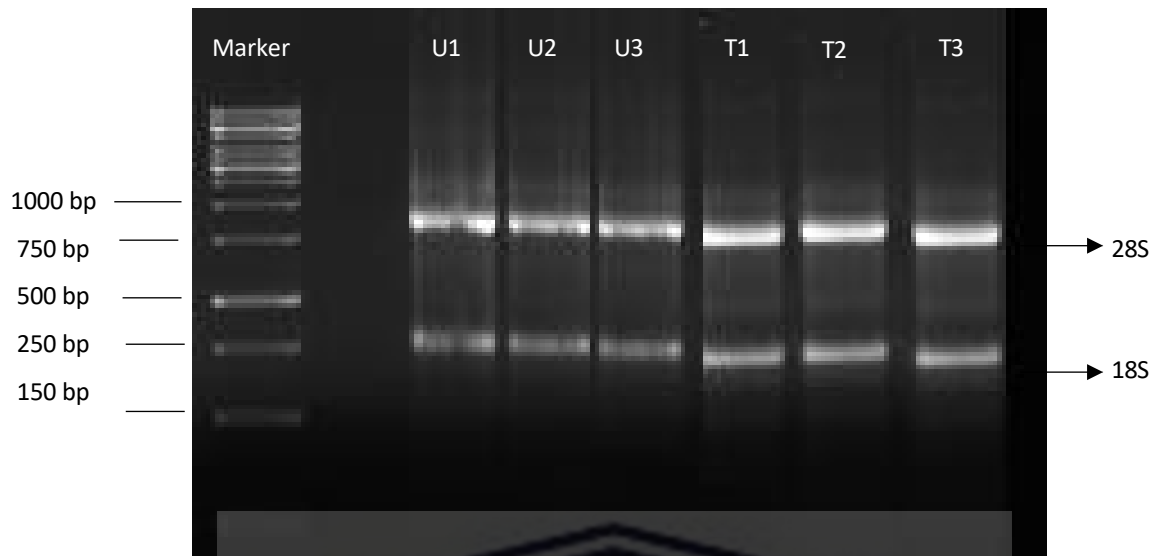


Figure 4.9: Agarose gel analysis of RNA extracted from PC-3 cells. Marker used was a 1 kbp ladder. Samples are labelled as follows: U1-U3 – samples from untreated PC-3 cells in a triplicate, whereas T1-T3 are samples from PC-3 cells treated with 12.5 µg/ml GA-AgNPs.

Similarly, agarose gel was used to confirm the cDNA product where conventional PCR was used to amplify GAPDH. GAPDH is a house-keeping gene, and its expression is not expected to change even in diseased conditions [19]. This step was to ascertain the synthesis of cDNA from the RNA samples before it was used in RT-qPCR for gene expression. There were bands or amplicons visible at <200 bp in all samples as shown in Figure 4.10, amplification of GAPDH confirmed the presence of cDNA in both untreated and treated PC-3 cells. The GAPDH amplicon size is ~180 bp [54].



Figure 4.10: Agarose gel analysis of cDNA of PC-3 cells. Marker used was a 1kbp ladder. Samples are labelled as follows: B - sample with no cDNA present; U1-U3 – cDNA extracted from untreated PC-3 cells; T1-T3 - cDNA extracted from PC-3 cells treated with 12.5 $\mu\text{g/ml}$ GA-AgNPs

4.5. Gene expression analysis using RT-qPCR

Reverse Transcription polymerase chain reaction (RT-qPCR) was used to assess the effect of GA-AgNPs in the expression of 86 genes involved in molecular toxicology pathways in PC-3 cells. RT-qPCR has significantly altered the field of gene expression measurement, as it collects data as the PCR process takes place, combining amplification and detection into a single step [55]. This is accomplished through the use of various fluorescent chemistries that correlate PCR product concentration to fluorescence intensity. The point in time (or PCR cycle) at which the target amplification was first detected defines a reaction. This value is commonly referred to as the cycle threshold (Ct), which is the time when fluorescence intensity exceeds background fluorescence. As a result, the more target DNA there is in the starting material, the faster a significant increase in fluorescent signal will appear, yielding a lower Ct.

RT-qPCR is a simple, low-cost technique used by molecular biologists to measure gene expression. The calculation of a target gene's relative expression by qPCR is based on the use of reference gene(s) as endogenous control(s). Reference or house-keeping genes should have consistent expression across all experimental conditions, or else transcriptional quantification will be unreliable. Historically, the genes used as references for qPCR or housekeeping genes

were those related to basic cell functions that were thought to be expressed at constant rates in all conditions [19].

The clustergram in Figure 4.11 confirmed that GA-AgNPs induced toxicity in the PC-3 cells, with most of the genes upregulated in their expression and sixteen of the genes downregulated. However, only genes with expression that was ≥ 1 fold difference to the untreated were differentially expressed.



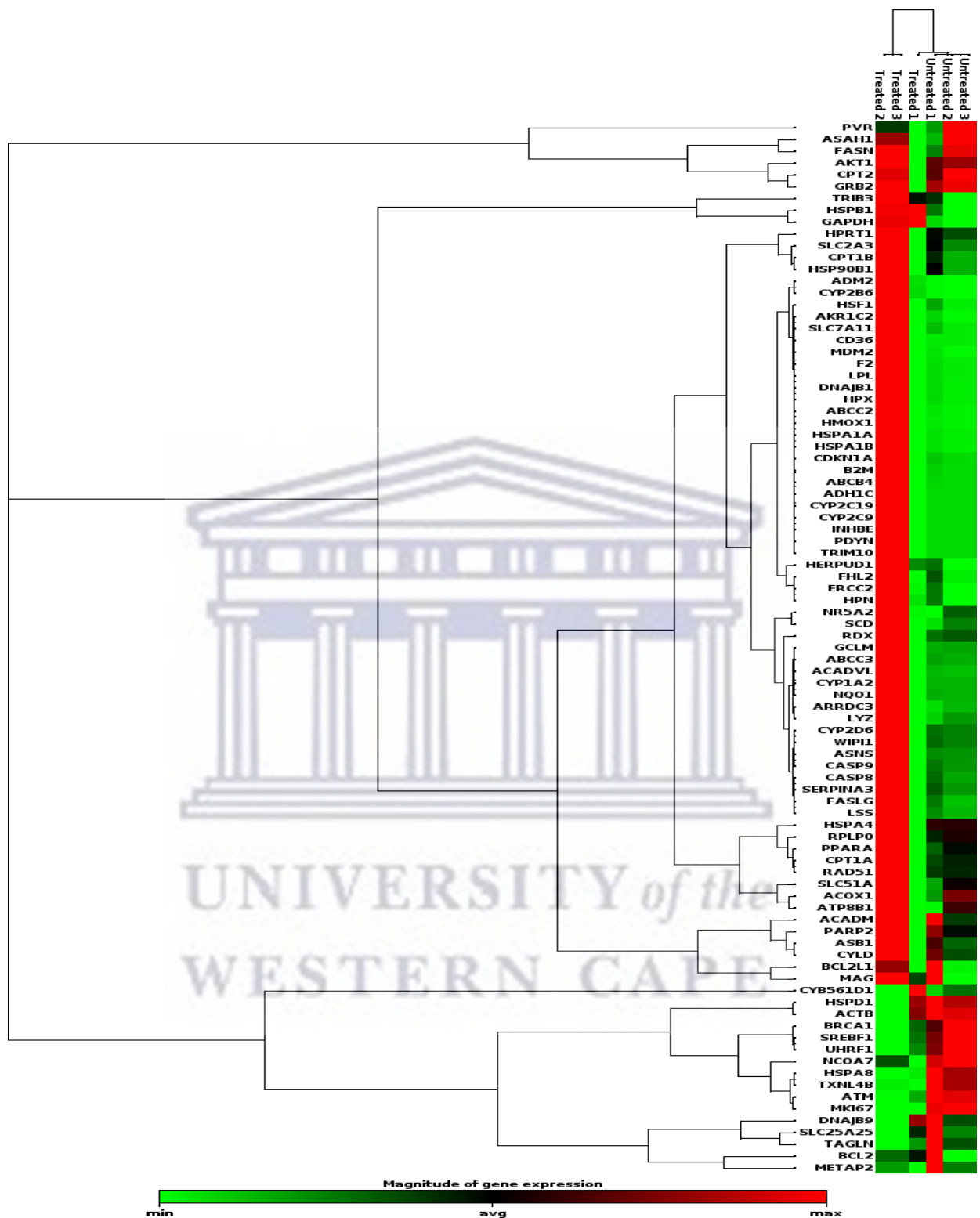


Figure 4.11: Clustergram showing gene expression in untreated versus GA-AgNPs-treated PC-3 cells. Treated 1 - 3 represent PC-3 exposed to 12.5 ug/ml GA-AgNPs and untreated 1 - 3 represent PC-3 untreated cells. Green blocks illustrated down regulation of genes whereas the red blocks indicated the upregulation of genes. Darker blocks are average or normal expression.

Table 4.3 below illustrates ten genes whose expressions were significantly affected by the GA-AgNPs treatment in PC-3 cells vs untreated. The expression of the genes showed fold change with a p value ≤ 0.05 . Majority of these genes (including *HSPA8* and *SREBF1*) were downregulated in relation to untreated controls, whereas two of these genes (*HSPB1* and *TRIB3*) are upregulated. In a previous study that used the Human Molecular Toxicology PathwayFinder RT2 Profiler PCR Array, three of the affected genes (*HSPA8*, *SREBF1* and *TRIB3*) were dysregulated in Caco-2 cells after treatment with citrate capped gold nanoparticles [56]. The functions of the genes highlighted in Table 4.3 might therefore shed some insights as to how the GA- AgNPs induce its anticancer activities in the PC-3 cells.

Table 4.3: Differentially expressed genes in the PC-3 cells treated with GA-AgNPs.

Gene name	Gene Code	Fold Change	Fold Regulation	p-value (<0.05)
Ataxia telangiectasia mutated	<i>ATM</i>	0.71	-1.40	0.000082
Breast cancer susceptibility gene 1	<i>BRCA1</i>	0.79	-1.27	0.006778
Heat shock cognate 71 kDa protein	<i>HSPA8</i>	0.85	-1.18	0.000127
Heat Shock Protein Family B (small) member 1	<i>HSPB1</i>	1.53	1.53	0.000569
Marker of Proliferation Ki-67	<i>MKI67</i>	0.87	-1.15	0.000000
Nuclear receptor coactivator 7	<i>NCOA7</i>	0.89	-1.12	0.003062
Sterol Regulatory Element Binding Transcription Factor 1	<i>SREBF1</i>	0.76	-1.31	0.003198
Tribbles pseudokinase 3	<i>TRIB3</i>	1.92	1.92	0.036962
Thioredoxin Like 4B	<i>TXNL4B</i>	0.81	-1.23	0.000110
Ubiquitin Like With PHD And Ring Finger Domains 1	<i>UHRF1</i>	0.85	-1.18	0.001804

Note: PC-3 cells were treated with 12.5 $\mu\text{g/ml}$ of GA-AgNPs for 24 hours, gene expression was evaluated using the human toxicology pathway finder array. A fold change of ≥ 1 represented dysregulation of a gene. All P-values < 0.05 are significant results.

Ataxia-telangiectasia mutated (ATM) gene

ATM gene plays a crucial role in mammalian DNA damage response, cancer progression and initiation, and redox signaling pathways [57]. The gene consists of 66 exons and is situated on chromosome 11 (11q22-23). While in an active monomeric form, the size of *ATM* is 370 kDa. *ATM* is also an important member of the PI3K-related protein kinase family [58], and *ATM* responds to DNA damage in mammalian cells via Mre11/Rad50/Nbs1 (MRN) complex. MRN complex is the site for *ATM* binding, once this binding occurs, *ATM* then goes through a conformational change from a resting homodimer to an active monomer form [57]. Once active, *ATM* phosphorylates numerous downstream targets that are essential for DNA damage repair, apoptosis, cell cycle arrest, and cell cycle checkpoints. As such, *ATM* can be considered a major tumor suppressor gene [59].

ATM's major tumor suppressing mechanisms are inducing apoptosis and cell cycle arrest via activating p53, SIRT1, CHK1, CHK2, DBC1, RAIDD and other downstream targets. Therefore, cancer cells can downregulate *ATM*, for instance, in breast cancer cells *ATM* expression is reduced due to miRNA-18a, and it can also be suppressed by the phosphatase WIP1 which directly dephosphorylates *ATM* and p53 [57]. However, this may not be the case in other tumor cells, such as Melanoma cancer cells, increase *ATM* expression by increasing MAGE-C2 levels, that associates with KAP1 and promotes its Ser84 phosphorylation, whereas PCa cells increased levels of *ATM* by binding to the androgen receptor on the *ATM* gene enhancer region. Similarly, in pancreatic cancer cells, *ATM* levels were increased by overexpression of transcription factor CUX1. These cancer cells that are capable of upregulating *ATM* levels may have developed mechanisms to evade *ATM*-induced cell cycle arrest and apoptosis [57].

In this study, *ATM* expression was down regulated in the GA-AgNPs-treated PC-3 cells, with a fold regulation of -1.40 and a fold change of 0.71 compared to the untreated. The increased levels of *ATM* in PC-3 cells might be involved in the proliferation of the PC-3 cancer cells, thus indicating that PC-3 may have developed mechanisms to continue proliferating by evading *ATM*-induced apoptosis. However, when the PC-3 cancer cells were exposed to GA-AgNPs it was down regulated (Table 4.3) *ATM* and caused cell death.

Breast cancer gene 1 (BRCA1)

BRCA1 was first linked to breast and ovarian cancers in the 1990s, however, recent studies have shown that *BRCA1* plays a role in other cancers too. Located on chromosome 17, and consisting of 1 863 amino acids composed of 4 exons, *BRCA1* possess numerous domains that are crucial for multiple functions [60].

BRCA1 along with *BRCA2* proteins have a critical function during the process of DNA double strand break repairs via regulation of homologous recombination (HR). Additionally, *BRCA1* regulates non-homologous end joining (NHEJ) repair pathway. When broken DNA ends are directly ligated without the need for a homologous template, NHEJ is one of the main DNA repair pathways. HR is a high-fidelity, error-free repair at the site of correction, but it takes longer to complete. NHEJ, on the other hand, is an error-prone DNA repair that frequently results in mutations at the site of damage [61]. There has been increasing evidence indicating that *BRCA1* regulates oxidative stress and this may be another mechanism in preventing carcinogenesis. However, the mechanisms of the regulation is poorly understood [62].

Table 4.3 showed that expression of *BRCA1* was down regulated in the PC-3 cells by GA-AgNPs. *BRCA1* illustrated a fold change 0.79, and a fold regulation of -1.27. Although most associated with female cancers, expression of *BRCA1* in PCa patients enrolled in the Health Professionals Follow-up Study (HPFS) between 40 and 75 years of age in 1986, a cohort of selected men was studied who suffered with PC-3. *BRCA1* gene expression *BRCA1* was reported in 60 of 589 tumors. The *BRCA1*-positive tumors showed a 2.16-fold higher Ki-67 proliferative indices, and higher tumor aneuploidy. Thus indicating that *BRCA1* expression is possible in other cancers and was associated with more aggressive tumors as *BRCA1*-negative tumors showed lower gleason scores and proliferation rate than that of *BRCA1*-positive tumors. The study was concluded that the more aggressive form of PC-3 have higher *BRCA1* expression [63]. *BRCA1* and *BRCA2* expression was reported in Ugandan men suffering from PCa. *BRCA1* as opposed to *BRCA2*, was expressed in men with higher gleason scores and more aggressive forms of PCa. There was even lower co-expression levels of *BRCA1* and *BRCA2*, and hypothesized that it would be rare that both *BRCA* genes would be co-expressed in PCa patients [64].

Heat Shock Protein member 8 (HSPA8) gene

Heat shock proteins (HSPs) are a large family of highly homologous chaperone proteins that are induced in response to temperature changes (hence their original name), but also to environmental, physical, and chemical stresses such as cold, ultraviolet irradiation, and wound healing. Their rapid expression reduces the severity of any damage caused by these stresses and speeds up cell recovery [65]. The *HSP70* family of chaperones, one of the most ubiquitous classes of chaperones, is composed of at least 13 members, including stress-induced proteins such as *HSPA1A* [*HSP70-1/HSP72*; 72 kDa], and members that are not stress-inducible, such as *HSPA5* (*GRP78/Bip/Mif-2*), *HSPA8* (*HCC70/HSP73/HSP71*; 73 kDa) and *HSPA9* (*mtHSP70/HSP75/GRP75/mortalin*; 75 kDa). *HSPA1A* and *HSPA8* are found in the cytosol, the nucleus, extracellular exosomes, and at the cell membrane, respectively [66].

The *HSPA8* chaperone is a member of the large *HSP70* family and functions as a protein folding catalyst, ensuring the re-folding of misfolded conformers, and as a controller, targeting proteins for degradation. These functions appear to be based on *HSPA8*'s ability to interact with hydrophobic segments in an ATP-controlled manner. *HSPA8* is important in the presentation of antigenic peptides to CD4⁺ T cells by MHC class II molecules. It also functions as an adenosine 5'-triphosphatase in the disassembly of clathrin-coated vesicles during the transport of membrane components in cells. It is essential for autophagy, particularly chaperone-mediated autophagy [67].

As indicated in Table 4.3, *HSPA8* gene showed a fold change of 0.85, and a fold regulation of -1.18. In a study done on acute myeloid leukemia cancer, the association between expression of *HSPA8* and clinical diagnosed phenotypes of acute myeloid leukemia (AML) was investigated. The AML cohort was compared to that of normal healthy blood cells cohort and revealed that there were expression levels of *HSPA8* in AML patients was higher. Upon further investigations, high *HSPA8* expression levels was found to be one of the highest risk factors associated with a shorter overall survival in univariate and multivariate Cox Proportional-Hazards regression (COX) analysis, acting as an independent prognostic factor of

Cytogenetically Normal Acute Myeloid Leukemia (CN-AML) survival. The study was then taken further and the relationship between high *HSPA8* expression and various oncogenic activities and signaling pathways, such as the *PI3K-Akt* and calcium signaling pathways was investigated. It was found that constitutive *PI3K* activation, in particular, was linked to decreased overall and disease-free survival in 60% of AML patients. *HSPA8* high expression in AML has been identified as a potential independent prognostic factor in CN-AML patients, and linked to cancer-related genomic changes, including oncogene and tumor suppressor [68].

Heat shock protein beta-1 (HSPB1) gene

Autophagy is reportedly regulated by several novel proteins, including *HSP beta-1 (HSPB1)*, also known as *HSP27*. *HSP27* and *HSP25* (in humans and rats) are members of the small *HSP* (*sHSP*) subfamily, which includes proteins with low molecular mass and conserved COOH-terminal domains (the -crystallin domain). *HSP27* and *HSP25* are widely expressed *sHSPs* that are activated in response to a wide range of unfavorable physiological and environmental conditions. These *sHSPs* protect cells from potentially lethal situations, primarily by participating in cell death pathways such as necrosis and apoptosis [69]. *HSPB1* is the best-studied member of the *HSPB* family and has a variety of functions, including apoptosis inhibition, proteotoxic stress reduction, and cytoskeleton dynamics regulation [70].

The effects of *HSPB1* expression was investigated along with microRNA miR-1 expression in PCa cells. *HSPB1* and miR-1 levels in PCa cell lines were genetically altered, supporting the evidence that *HSPB1* regulates miR-1 indicating for the first time that an *HSP* functions as a regulator of microRNA expression. These findings contributed to a better understanding of survival mechanisms in drug-resistant PCa cells. Aside from inhibiting apoptotic pathways, chemotherapy-induced *HSPB1* expression initiated miR-1 inhibition and, ultimately, the restoration of pro-oncogenic androgen receptor and *TGFBI* signals. As a result, promising new targets for alternative therapy approaches. In PCa therapy, *HSPB1* inhibition and miR-1 mimicking nucleic acid compounds may reduce *HSPB1*-miR-1-driven treatment resistance [71]. In this study, the expression of *HSPB1* was reduced by GA-AgNPs treatment (Table 4.3) in PC-3 cells with a fold regulation and a fold change of 1.53.

Proliferation marker protein Ki-67 (MKI67) gene

MKI67 is a cell proliferation-related protein that is encoded by the *MKI67* gene. *Ki-67/MKI67* exists in the cell cycle during the G1, S, G2, and mitosis phases [72]. The *MKI67* gene located on chromosome 10q25-ter mainly functions to encode 2 *MKI67* isoforms (345 and 395 kDa, respectively). *Ki-67* shows high expression within cancer cells and can be regarded as a prognostic prediction factor for cancer and has been extensively studied as a potential prognostic predictor of cancer proliferation. There is a lot of evidence that *MKI67* plays a role in cancer diagnosis [73].

MKI67 had a fold regulation of -1.15 and a fold change of 0.87 in the GA-AgNPs treated PC-3 cells (Table 4.3). *MKI67* downregulation could suggest that there is little to no proliferation in GA-AgNPs treated PC-3 cells. This could suggest that when PC-3 cells are exposed to GA-AgNPs, cell proliferation is lowered and *MKI67* gene expression is downregulated. In a study evaluating the gene expression of *MKI67* in 535 PCa patients undergoing radical prostatectomy, the tumor epithelial cells expressing *Ki-67*, *Ki-67*'s relationship with PCa as well as its prognostic value was investigated. *Ki-67* expression in tumor epithelium was significantly associated with biochemical failure. A high level of *Ki-67* was found to be an independent poor prognostic factor for biochemical failure-free survival [74].

Nuclear receptor coactivator 7 (NCOA7) gene

Human *NCOA7* was discovered more than 20 years ago as an estrogen receptor binding protein, and it was later shown to bind other nuclear receptors as well. Its role in the signaling properties of these receptors *in vivo*, however, is still unknown. *NCOA7* has recently been classified as a member of a small group of so-called (*Tre2/Bub2/Cdc16*, *Lysin Motif*) domain containing antioxidant proteins and its role in protection from oxidative stress *in vitro* has been confirmed, although the mechanism remains unknown [75]. Table 4.3 showed that PC-3 cells exposed to GA-AgNPs showed that *NCOA7* had a fold regulation of -1.12 and a fold change of 0.89. This

could suggest that *NCOA7* could be a marker of cancer as it would be highly expressed in active proliferating tumor cells.

NCOA7 has been reportedly seen as a potential biomarker for oral squamous cell carcinoma (OSCC) [76]. *NCOA7* expression was found to be up-regulated in OSCC tissues and correlate with a variety of clinicopathologic parameters, including lesion site, tumor differentiation status, and lymph node metastasis. Furthermore, overexpression of *NCOA7* was shown to promote OSCC cell proliferation in both *in vitro* and *in vivo* models. A mechanistic study was also conducted and demonstrated that *NCOA7* induces OSCC cell proliferation potentially by activating aryl hydrocarbon receptor (AHR) [76].

Sterol regulatory element-binding transcription factor 1 (SREBF1) gene

SREBPs are transcription factors that play an important role in the regulation of lipid homeostasis in all vertebrates. In mammals, there are three *SREBP1* isoforms: *SREBP1a/SREBF1-1*, *SREBP1b/SREBF1-2*, and *SREBP1c/SREBF1-3*, as well as the closely related *SREBP2/SREBF2*. *SREBP1a* and 1c are encoded by a single gene with alternative transcription start sites, whereas *SREBP2* is encoded by a separate gene [77]. *SREBF1* is primarily responsible for regulating the expression of factors required for fatty acid synthesis, whereas *SREBF2* is in charge of cholesterol homeostasis. *SREBF1* has potent antitumor functions in a variety of cancers, including prostate, breast, and liver cancers. Fatostatin and betulin, two *SREBF* inhibitors, significantly reduce tumor cell growth and viability. *SREBF1* levels and activities are tightly regulated by endogenous sterol levels through negative feedback regulation. The *PI3K/Akt/mTOR* signaling pathway also stabilizes and activates *SREBF1* protein in cancer cells. However, the cancer-specific epigenomic regulation of *SREBF1* is still unknown [78].

In this investigation, when the PC-3 cells were treated with GA-AgNPs, *SREBF1* had a reported fold regulation of -1.31 and fold change of 0.76. This could possibly indicate that high expression of *SREBF1* is related to aggressive proliferation of tumor cells, and thus, GA-

AgNPs lowers the expression of *SREBF1* (Table 4.3) and could be an indication of a cell death mechanism.

An investigation of *SREBF1* expression was done in colorectal cancer (HT29) cells which also evaluated the *MMP7* and *NF-κB* pathway activation. The *SREBF1* expression levels were manipulated in colorectal cancer cells through transfection of plasmids containing the *SREBF1* gene or by shRNA. Expression of *SREBF1* with *MMP7* and *p65* was detected, with *NF-κB* inhibitor *SN50* used to test the relationship of *SREBF1*, *NF-κB* pathway and *MMP7* [79]. The researchers discovered that *SREBP1* expression was significantly higher in colon adenocarcinoma than in noncancerous tissues, particularly at the invasive tumor front, including tumor budding. *SREBP1* overexpression in HT29 cells promoted angiogenesis, increased reactive oxygen species (ROS) levels, phosphorylation of *NF-B-p65*, and increased *MMP7* expression. The effect of *SREBP1* on expression of *MMP7* was lost following treatment with the *NF-κB* inhibitor *SN50* [79].

Tribbles homolog 3 (TRIB3) gene

TRIB3 is one of three human orthologues of the *Drosophila* protein tribbles, which regulates cell proliferation and migration during development. Cell cycle progression, proliferation, differentiation, stress response, cell signaling, metabolism, inflammation, immunity, and development are all regulated by mammalian tribbles proteins [80]. The *TRIB3* protein is also involved in signal pathways such as the *MAPK*, *PI3K*, *NF-B*, and *TGF-beta* pathways [81].

When PC-3 cells were exposed to the GA-AgNPs treatment, the *TRIB3* gene had a fold regulation of 1.92 and a fold change of 1.92. From this, it could possibly indicate that the *TRIB3* is involved in an apoptotic pathway as cell viability and cell index is decreased in treated PC-3 cells. Thus, upregulation of *TRIB3* (Table 4.3) is associated with increased apoptosis in treated PC-3 cells.

The role of *TRIB3* expression levels was also investigated on endometrial cancer cells (EC) and *AKT* pathway signaling. *TRIB3* Transfecting EC cells (ISK and AN3CA cells) resulted in overexpression and knockdown of *TRIB3* on EC [82]. The group of researchers found that the expression level of *TRIB3* was higher in EC than normal endometrium tissues, and its overexpression promoted apoptosis and suppressed proliferation of EC cells. Furthermore, *TRIB3* inhibited EC cell migration and invasion while decreasing *MMP-2* and *MMP-9* levels. *TRIB3* inhibition, on the other hand, increased *MMP-2* and *MMP-9* expression, as well as EC cell proliferation and migration, while suppressing apoptosis. Similarly, overexpression of *TRIB3* decreased while knockdown increased the level of *p-AKT* [82]. The study concluded that *TRIB3* inhibited EC cell proliferation and migration while promoting apoptosis, most likely by regulating the *AKT* signaling pathway [82].

Thioredoxin Like 4B (TXNL4B) gene

TXNL4B are thought to be involved in mRNA splicing via spliceosomes. It is found in the cytosol and nucleoplasm. However not much is known about the *TXNL4B* and its role in cancer. However, in this study *TXNL4B* has shown a fold regulation of -1.23 and a fold change of 0.81 (Table 4.3).

Ubiquitin like with PHD and ring finger domains 1 (UHRF1) gene

UHRF1 is required in both normal and cancer cells for mediating mitotic inheritance of DNA methylation by targeting DNA Methyltransferase 1 (*DNMT1*) to replication forks. Furthermore, *UHRF1* regulates de novo DNA methylation by recruiting de novo *DNMTs* (*DNMT3A* and *DNMT3B*) to chromatin, allowing these enzymes to establish new DNA methylation sites [83]. *UHRF1* can participate in DNA methylation modification and posttranslational histone modification via specific structural domains, thereby regulating gene expression and contributing to tumor occurrence and development [84]. Recent evidence suggests that *UHRF1* is oncogenic in human cancers. *UHRF1* is an *E2F1* target that is required for the cell cycle's G1/S transition. Furthermore, it is found to be overexpressed in a variety of tumor types, including breast, lung, liver, pancreatic, bladder, prostate, and colorectal cancers [85].

In this study, *UHRF1* gene was down regulated in the PC-3 cells (Table 4.3). *UHRF1* gene illustrated a fold regulation of -1.18 and a fold change of 0.85. This down regulation of *UHRF1* is indicative of the type of cell death pathway responsible for PC-3 cell death.

The inhibitory effect of Dihydroartemisinin (DHA), a novel anticancer agent, on the expression of *UHRF1* in PC-3 cells has been reported. Both *UHRF1* and DNA methyltransferase 1 (*DNMT1*) mRNA expressions, and UHRF1, DNMT1, and p16 protein expressions were studied. In PC-3 cells, DHA decreased the expression of *UHRF1* and *DNMT1*, while increasing the expression of p16. In PC-3 cells, DHA-treated groups had lower levels of *p16* promoter methylation. The results showed that DHA also significantly increased apoptosis and G1/S cell-cycle arrest in PC-3 cells. The findings suggested that *UHRF1/DNMT1* downregulation is involved in a variety of cellular events, including G1 cell arrest, *p16* demethylation, and apoptosis [86].

In another recent study the expression and recurrence of *UHRF1* was investigated in PCa after radical prostatectomy. *UHRF1* expression was knocked down and links between *UHRF1* expression and clinical features of PCa were investigated. The findings revealed that *UHRF1* was overexpressed in nearly all PCa cell lines. *UHRF1* knockdown inhibited cell proliferation and migration and induced apoptosis in the cells. *UHRF1* expression levels were linked to some clinical characteristics of PCa and found to be an independent prognostic factor for biochemical recurrence-free survival. *UHRF1* was identified as an oncogene in PCa and appears to be capable of predicting the risk of biochemical recurrence in PCa patients following radical prostatectomy, suggesting that it could be a potential therapeutic target for PCa [87].

4.6. STRING Analysis of DEGs

The STRING database's goal is to collect, score, and integrate all publicly available sources of protein-protein interaction data, as well as to supplement these with computational predictions. Its ultimate goal is to create a comprehensive and objective global network that includes both direct (physical) and indirect (functional) interactions [20]. Thus using STRING, the Protein-protein interactions (PPI) between Differentially Expressed Genes (DEGs) was investigated.

The STRING analysis in Figure 4.12 shows 4 PPIs between *MKI67* and *UHRF1*; *UHRF1* and *BRCA1*; *BRCA1* and *ATM*; *HSPA8* and *HSPB1*. However, the PPI between *HSPA8* and *HSPB1* are unrelated. Other genes such as *TRIB3*, *SREBF1*, *TXNL4B* and *NCOA7* were also unrelated to any PPI and were outside the proposed protein networks. The PPI enrichment p-value was 0.0443, thus suggesting that the PPI network has significantly more interactions than expected. This means that the proteins interact with each other more than a random set of proteins with the same size and degree distribution drawn from the genome. Such enrichment indicates that the proteins as a group are at least partially connected through their biological functions.

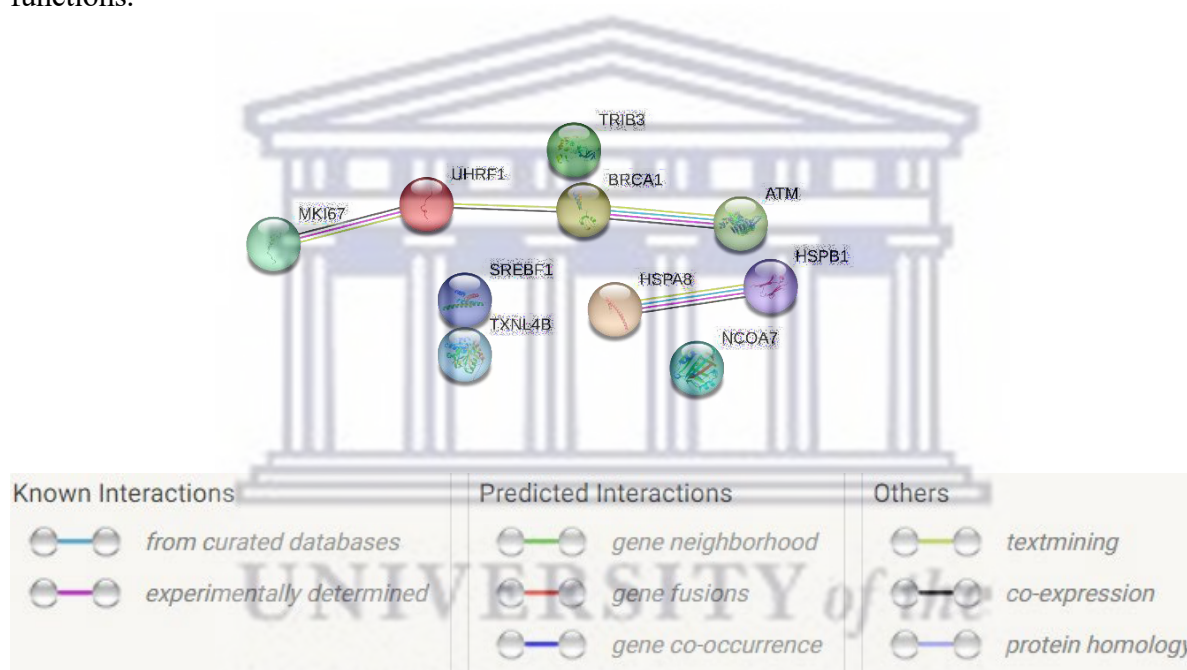


Figure 4.12: STRING Analysis showing PPIs of DEGs in PC-3 cells treated with 12.5 µg/ml GA-AgNPs.

The number of connections are indicated by lines, and no connections are gene bubbles whose biological functions are not connected to the other DEGs.

4.7 Conclusion

Plant extract-synthesized AgNPs namely; Gum Arabic (GA-AgNPs), *Cotyledon Orbiculata* (CO-AgNPs), *Carpobrotus Edulis* (Cefe-AgNPs), *Salvia Africana-lutea* (SAL-AgNPs), and Red Wine (RW-AgNPs) were under study within the laboratory and obtained for the investigation of their anti-cancer and molecular effects on human cancer (MCF-7, PC-3, A375, A549, Caco-2) and non-cancer (HaCaT, and KMST-6) cell lines. Following the MTT assay RW-AgNPs, CO-AgNPs and Cefe-AgNPs were shown to be biocompatible and non-toxic at concentrations up to 1 mg/ml on non-cancer (KMST-6) cell line; although they lacked

anticancer activities on cancer (MCF-7, PC-3, A549, Caco-2) cell lines. These NPs previously demonstrated wound healing and antimicrobial effects and might potentially be safe when used by humans. On the contrary, the GA-AgNPs and SAL-AgNPs illustrated non-selective cytotoxicity on the previously mentioned cell lines. The cytotoxic effect of GA-AgNPs and SAL-AgNPs was further investigated on all cell lines including two additional cancer (A375) and non-cancer (HaCaT) cell lines. The treatments of GA-AgNPs and SAL-AgNPs were streamlined in a dose-dependent manner up to 100 µg/ml, following the MTT assay of the treatments on all cell lines, it was found that GA-AgNPs was more toxic and potent compared to SAL-AgNPs hence. Due to a limited amount of laboratory funds, and equipment a selection was performed based on the streamlined MTT assay of GA-AgNPs and SAL-AgNPs on all cell lines, for further studies using xCELLigence Real-time cell analysis (RTCA). Thus, based on figure 4.4, majority of the graph profiles are flatlined when the cells are exposed to the treatments. MCF-7 and PC-3 showed promising profiles with regards to the dose-dependent decrease in cell viability. Furthermore, MCF-7 and PC-3 are ranked amongst the most common cancer cells and are promising targets for anti-cancer treatments. Following RTCA, GA-AgNPs and SAL-AgNPs depicted cytotoxic effects on MFC-7 and PC-3 cell lines. However, the RTCA graph profiles are fairly similar for both cell lines with the respective treatments, interestingly the profile observed when PC-3 cells were treated with 12.5 GA-AgNPs µg/ml shows a decline in cell index after a few hours of treatment and is a promising target for further gene expression studies. Further investigations of the molecular effects of GA-AgNPs in PC-3 cells were done using RT-qPCR to evaluate the genes involved in their cytotoxicity effects. *TRIB3* is a gene suggested to be involved in apoptosis and was upregulated in PC-3 cells when treated with GA-AgNPs, thereby, potentially inducing apoptosis. GA-AgNPs also reduced *UHRF1* gene, a gene that is usually overexpressed in PC-3 cells and involved in proliferation and progression of tumor cells. Other genes such as *BRCA1* and *ATM* showed the similar trend of down regulation upon treatment of PC-3 cells, and since *BRCA1* and *ATM* are known to be over expressed in other cancer cells or possibly originate from different tissues, their downregulation in PC-3 cells can indicate the potential of these AgNPs in treatment of metastatic cancers. In conclusion, GA-AgNPs potentially induces apoptotic cell death in PC-3 cells. Further studies are therefore warranted to explore further the mechanisms and potential anticancer activity of the GA-AgNPs *in vivo*. In addition, strategies to help improve their biocompatibility and reduce their non-selectivity are advised before they can be considered for clinical application.

References

1. Tran, K.B.; Lang, J.J.; Compton, K.; Xu, R.; Acheson, A.R.; Henrikson, H.J.; Kocarnik, J.M.; Penberthy, L.; Aali, A.; Abbas, Q.; et al. The Global Burden of Cancer Attributable to Risk Factors, 2010-19: A Systematic Analysis for the Global Burden of Disease Study 2019. *Lancet* **2022**, *400*, 563–591, doi:10.1016/S0140-6736(22)01438-6.
2. Pan American Health Organization, World Cancer Day 2023: Close the care gap. Available online: <https://www.paho.org/en/campaigns/world-cancer-day-2023-close-care-gap#:~:text=Globally%2C%20there%20were%20an%20estimated,10%20million%20deaths%20from%20cancer>. (Accessed on 26 July 2023).
3. Brennan, P.; Davey-Smith, G. Identifying Novel Causes of Cancers to Enhance Cancer Prevention: New Strategies Are Needed. *JNCI: Journal of the National Cancer Institute* **2022**, *114*, 353–360, doi:10.1093/JNCI/DJAB204.
4. Charmsaz, S.; Collins, D.M.; Perry, A.S.; Prencipe, M. Novel Strategies for Cancer Treatment: Highlights from the 55th IACR Annual Conference. *Cancers (Basel)* **2019**, *11*, doi:10.3390/CANCERS11081125.
5. Lettieri-Barbato, D.; Aquilano, K. Pushing the Limits of Cancer Therapy: The Nutrient Game. *Front Oncol* **2018**, *8*, 148, doi:10.3389/FONC.2018.00148/BIBTEX.
6. Gavas, S.; Quazi, S.; Karpiński, T.M. Nanoparticles for Cancer Therapy: Current Progress and Challenges. *Nanoscale Res Lett* **2021**, *16*, 173, doi:10.1186/S11671-021-03628-6.
7. Yao, Y.; Zhou, Y.; Liu, L.; Xu, Y.; Chen, Q.; Wang, Y.; Wu, S.; Deng, Y.; Zhang, J.; Shao, A. Nanoparticle-Based Drug Delivery in Cancer Therapy and Its Role in Overcoming Drug Resistance. *Front Mol Biosci* **2020**, *7*, 193, doi:10.3389/FMOLB.2020.00193/BIBTEX.
8. Abass Sofi, M.; Sunitha, S.; Ashaq Sofi, M.; Khadheer Pasha, S.K.; Choi, D. An Overview of Antimicrobial and Anticancer Potential of Silver Nanoparticles. *J King Saud Univ Sci* **2022**, *34*, 101791, doi:10.1016/J.JKSUS.2021.101791.
9. Vishwanath, R.; Negi, B. Conventional and Green Methods of Synthesis of Silver Nanoparticles and Their Antimicrobial Properties. *Current Research in Green and*



UNIVERSITY *of the*
WESTERN CAPE

10. Alharbi, N.S.; Alsubhi, N.S. Green Synthesis and Anticancer Activity of Silver Nanoparticles Prepared Using Fruit Extract of *Azadirachta Indica*. *J Radiat Res Appl Sci* **2022**, *15*, 335–345, doi:10.1016/J.JRRAS.2022.08.009.
11. Al-Sheddi, E.S.; Farshori, N.N.; Al-Oqail, M.M.; Al-Massarani, S.M.; Saquib, Q.; Wahab, R.; Musarrat, J.; Al-Khedhairi, A.A.; Siddiqui, M.A. Anticancer Potential of Green Synthesized Silver Nanoparticles Using Extract of *Nepeta Deflersiana* against Human Cervical Cancer Cells (HeLA). *Bioinorg Chem Appl* **2018**, doi:10.1155/2018/9390784.
12. Xu, Z.; Feng, Q.; Wang, M.; Zhao, H.; Lin, Y.; Zhou, S. Green Biosynthesized Silver Nanoparticles With Aqueous Extracts of *Ginkgo Biloba* Induce Apoptosis via Mitochondrial Pathway in Cervical Cancer Cells. *Front Oncol* **2020**, *10*, 2282, doi:10.3389/FONC.2020.575415/BIBTEX.
13. Fadaka, A.O.; Meyer, S.; Ahmed, O.; Geerts, G.; Madiehe, M.A.; Meyer, M.; Sibuyi, N.R.S. Broad Spectrum Anti-Bacterial Activity and Non-Selective Toxicity of Gum Arabic Silver Nanoparticles. *Int J Mol Sci* **2022**, *23*, doi:10.3390/IJMS23031799.
14. Dube, P.; Meyer, S.; Madiehe, A.; Meyer, M. Antibacterial Activity of Biogenic Silver and Gold Nanoparticles Synthesized from *Salvia Africana-Lutea* and *Sutherlandia Frutescens*. *Nanotechnology* **2020**, *31*, doi:10.1088/1361-6528/ABB6A8.
15. Tyavambiza, C.; Elbagory, A.M.; Madiehe, A.M.; Meyer, M.; Meyer, S. The Antimicrobial and Anti-Inflammatory Effects of Silver Nanoparticles Synthesised from *Cotyledon Orbiculata* Aqueous Extract. *Nanomaterials* **2021**, *11*, 1343, doi:10.3390/NANO11051343.
16. Ejidike, I.P.; Clayton, H.S. Green Synthesis of Silver Nanoparticles Mediated by *Daucus Carota L.*: Antiradical, Antimicrobial Potentials, in Vitro Cytotoxicity against Brain Glioblastoma Cells. <http://mc.manuscriptcentral.com/tgcl> **2022**, *15*, 297–310, doi:10.1080/17518253.2022.2054290.
17. Tyavambiza, C.; Meyer, M.; Wusu, A.D.; Madiehe, A.M.; Meyer, S. The Antioxidant and In Vitro Wound Healing Activity of *Cotyledon Orbiculata* Aqueous Extract and the Synthesized Biogenic Silver Nanoparticles. *Int J Mol Sci* **2022**, *23*, doi:10.3390/IJMS232416094.

18. Yılmaz, M.; Ozic, C.; Gok, İ.; Yılmaz, M.; Ozic, C.; Gok, İ. Principles of Nucleic Acid Separation by Agarose Gel Electrophoresis. *Gel Electrophoresis - Principles and Basics* **2012**, doi:10.5772/38654.
19. Freitas, F.C.P.; Depintor, T.S.; Agostini, L.T.; Luna-Lucena, D.; Nunes, F.M.F.; Bitondi, M.M.G.; Simões, Z.L.P.; Lourenço, A.P. Evaluation of Reference Genes for Gene Expression Analysis by Real-Time Quantitative PCR (QPCR) in Three Stingless Bee Species (Hymenoptera: Apidae: Meliponini). *Scientific Reports* **2019** *9:1* **2019**, *9*, 1–13, doi:10.1038/s41598-019-53544-0.
20. Szklarczyk, D.; Gable, A.L.; Lyon, D.; Junge, A.; Wyder, S.; Huerta-Cepas, J.; Simonovic, M.; Doncheva, N.T.; Morris, J.H.; Bork, P.; et al. STRING V11: Protein–Protein Association Networks with Increased Coverage, Supporting Functional Discovery in Genome-Wide Experimental Datasets. *Nucleic Acids Res* **2019**, *47*, D607, doi:10.1093/NAR/GKY1131.
21. Szklarczyk, D.; Gable, A.L.; Nastou, K.C.; Lyon, D.; Kirsch, R.; Pyysalo, S.; Doncheva, N.T.; Legeay, M.; Fang, T.; Bork, P.; et al. The STRING Database in 2021: Customizable Protein–Protein Networks, and Functional Characterization of User-Uploaded Gene/Measurement Sets. *Nucleic Acids Res* **2021**, *49*, D605–D612, doi:10.1093/NAR/GKAA1074.
22. Ahmad, S.; Munir, S.; Zeb, N.; Ullah, A.; Khan, B.; Ali, J.; Bilal, M.; Omer, M.; Alamzeb, M.; Salman, S.M.; et al. Green Nanotechnology: A Review on Green Synthesis of Silver Nanoparticles — an Ecofriendly Approach. *Int J Nanomedicine* **2019**, *14*, 5087, doi:10.2147/IJN.S200254.
23. Simon, S.; Sibuyi, N.R.S.; Fadaka, A.O.; Meyer, S.; Josephs, J.; Onani, M.O.; Meyer, M.; Madiehe, A.M. Biomedical Applications of Plant Extract-Synthesized Silver Nanoparticles. *Biomedicines* **2022**, *10*.
24. Prasad, N.; Thombare, N.; Sharma, S.C.; Kumar, S. Gum Arabic – A Versatile Natural Gum: A Review on Production, Processing, Properties and Applications. *Ind Crops Prod* **2022**, *187*, 115304, doi:10.1016/J.INDCROP.2022.115304.
25. Kamatou, G.P.P.; Makunga, N.P.; Ramogola, W.P.N.; Viljoen, A.M. South African *Salvia* Species: A Review of Biological Activities and Phytochemistry. *J Ethnopharmacol* **2008**, *119*, 664–672, doi:10.1016/J.JEP.2008.06.030.

26. Snopek, L.; Mlcek, J.; Sochorova, L.; Baron, M.; Hlavacova, I.; Jurikova, T.; Kizek, R.; Sedlackova, E.; Sochor, J. Contribution of Red Wine Consumption to Human Health Protection. *Molecules : A Journal of Synthetic Chemistry and Natural Product Chemistry* **2018**, *23*, doi:10.3390/MOLECULES23071684.
27. Akinyede, K.A.; Ekpo, O.E.; Oguntibeju, O.O. Ethnopharmacology, Therapeutic Properties and Nutritional Potentials of *Carpobrotus Edulis*: A Comprehensive Review. *Scientia Pharmaceutica* **2020**, *Vol. 88, Page 39* **2020**, *88*, *39*, doi:10.3390/SCIPHARM88030039.
28. Singh, A.; Gaud, B.; Jaybhaye, S. Optimization of Synthesis Parameters of Silver Nanoparticles and Its Antimicrobial Activity. *Mater Sci Energy Technol* **2020**, *3*, 232–236, doi:10.1016/J.MSET.2019.08.004.
29. Dawadi, S.; Katuwal, S.; Gupta, A.; Lamichhane, U.; Thapa, R.; Jaisi, S.; Lamichhane, G.; Bhattarai, D.P.; Parajuli, N. Current Research on Silver Nanoparticles: Synthesis, Characterization, and Applications. *J Nanomater* **2021**, doi:10.1155/2021/6687290.
30. Rizwana, H.; Alwhibi, M.S.; Aldarson, H.A.; Awad, M.A.; Soliman, D.A.; Bhat, R.S. Green Synthesis, Characterization, and Antimicrobial Activity of Silver Nanoparticles Prepared Using *Trigonella Foenum-Graecum* L. Leaves Grown in Saudi Arabia. *Green Processing and Synthesis* **2021**, *10*, 421–429, doi:10.1515/gps-2021-0043.
31. Rosman, N.S.R.; Harun, N.A.; Idris, I.; Ismail, W.I.W. Eco-Friendly Silver Nanoparticles (AgNPs) Fabricated by Green Synthesis Using the Crude Extract of Marine Polychaete, *Marphysa Moribidii*: Biosynthesis, Characterisation, and Antibacterial Applications. *Heliyon* **2020**, *6*, e05462, doi:10.1016/J.HELIYON.2020.E05462.
32. Yeshchenko, O.A.; Dmitruk, I.M.; Alexeenko, A.A.; Kotko, A. V.; Verdal, J.; Pinchuk, A.O. Size and Temperature Effects on the Surface Plasmon Resonance in Silver Nanoparticles. *Plasmonics* **2012**, *7*, 685–694, doi:10.1007/S11468-012-9359-Z.
33. Saad, H.; Rahman, M.K.A.; Yassin, I.; Muad, A.M. Characterization of Ethanol Concentrations at Ultraviolet Wavelength Region. *Journal of Fundamental and Applied Sciences* **2018**, *9*, 384, doi:10.4314/jfas.v9i4s.22.

34. Clayton, K.N.; Salameh, J.W.; Wereley, S.T.; Kinzer-Ursem, T.L. Physical Characterization of Nanoparticle Size and Surface Modification Using Scattering Diffusometry. *Biomicrofluidics* **2016**, *10*, doi:10.1063/1.4962992.
35. Ghasemi, M.; Turnbull, T.; Sebastian, S.; Kempson, I. The Mtt Assay: Utility, Limitations, Pitfalls, and Interpretation in Bulk and Single-Cell Analysis. *Int J Mol Sci* **2021**, *22*, doi:10.3390/IJMS222312827/S1.
36. Badmus, J.A.; Ekpo, O.E.; Hussein, A.A.; Meyer, M.; Hiss, D.C. Cytotoxic and Cell Cycle Arrest Properties of Two Steroidal Alkaloids Isolated from *Holarrhena Floribunda* (G. Don) T. Durand & Schinz Leaves. *BMC Complement Altern Med* **2019**, *19*, 1–9, doi:10.1186/S12906-019-2521-9/FIGURES/4.
37. Canga, I.; Vita, P.; Oliveira, A.I.; Castro, M.Á.; Pinho, C. In Vitro Cytotoxic Activity of African Plants: A Review. *Molecules* **2022**, *27*.
38. Ahmed, A.O.K.; Sibuyi, N.; Fadaka, A.O.; Maboza, E.; Olivier, A.; Madiehe, A.M.; Meyer, M.; Geerts, G. Prospects of Using Gum Arabic Silver Nanoparticles in Toothpaste to Prevent Dental Caries. *Pharmaceutics* **2023**, *15*, Page 871 **2023**, *15*, 871, doi:10.3390/PHARMACEUTICS15030871.
39. Fadaka, A.O.; Sibuyi, N.R.S.; Madiehe, A.M.; Meyer, M. Nanotechnology-Based Delivery Systems for Antimicrobial Peptides. *Pharmaceutics* **2021**, *13*, doi:10.3390/PHARMACEUTICS13111795.
40. Ullah, I.; Khalil, A.T.; Ali, M.; Iqbal, J.; Ali, W.; Alarifi, S.; Shinwari, Z.K. Green-Synthesized Silver Nanoparticles Induced Apoptotic Cell Death in MCF-7 Breast Cancer Cells by Generating Reactive Oxygen Species and Activating Caspase 3 and 9 Enzyme Activities. *Oxid Med Cell Longev* **2020**, *2020*, doi:10.1155/2020/1215395.
41. Aykul, S.; Martinez-Hackert, E. Determination of Half-Maximal Inhibitory Concentration Using Biosensor-Based Protein Interaction Analysis. *Anal Biochem* **2016**, *508*, 97–103, doi:10.1016/J.AB.2016.06.025.
42. Macário, I.P.E.; Oliveira, H.; Menezes, A.C.; Ventura, S.P.M.; Pereira, J.L.; Gonçalves, A.M.M.; Coutinho, J.A.P.; Gonçalves, F.J.M. Cytotoxicity Profiling of Deep Eutectic Solvents to Human Skin Cells. *Sci Rep* **2019**, *9*, doi:10.1038/s41598-019-39910-y.

43. Zhang, L.; Yan, B.; Meng, S.; Zhou, L.; Xu, Y.; Du, W.; Shan, L. Theaflavin Induces Apoptosis of A375 Human Melanoma Cells and Inhibits Tumor Growth in Xenograft Zebrafishes Through P53- and JNK-Related Mechanism. *Front Pharmacol* **2020**, *11*, 1317, doi:10.3389/FPHAR.2020.01317/BIBTEX.
44. Hu, X.M.; Li, Z.X.; Lin, R.H.; Shan, J.Q.; Yu, Q.W.; Wang, R.X.; Liao, L.S.; Yan, W.T.; Wang, Z.; Shang, L.; et al. Guidelines for Regulated Cell Death Assays: A Systematic Summary, A Categorical Comparison, A Prospective. *Front Cell Dev Biol* **2021**, *9*, 368, doi:10.3389/FCELL.2021.634690/BIBTEX.
45. Kumari, R.; Saini, A.K.; Kumar, A.; Saini, R. V. Apoptosis Induction in Lung and Prostate Cancer Cells through Silver Nanoparticles Synthesized from Pinus Roxburghii Bioactive Fraction. *J Biol Inorg Chem* **2020**, *25*, 23–37, doi:10.1007/S00775-019-01729-3.
46. Murugesan, A.K.; Pannerselvam, B.; Javee, A.; Rajenderan, M.; Thiyagarajan, D. Facile Green Synthesis and Characterization of Gloriosa Superba L. Tuber Extract-Capped Silver Nanoparticles (GST-AgNPs) and Its Potential Antibacterial and Anticancer Activities against A549 Human Cancer Cells. *Environ Nanotechnol Monit Manag* **2021**, *15*, 100460, doi:10.1016/J.ENMM.2021.100460.
47. Majeed, S.; Bakhtiar, N.F.B.; Danish, M.; Mohamad Ibrahim, M.N.; Hashim, R. Green Approach for the Biosynthesis of Silver Nanoparticles and Its Antibacterial and Antitumor Effect against Osteoblast MG-63 and Breast MCF-7 Cancer Cell Lines. *Sustain Chem Pharm* **2019**, *12*, 100138, doi:10.1016/J.SCP.2019.100138.
48. Cerignoli, F.; Abassi, Y.A.; Lamarche, B.J.; Guenther, G.; Ana, D.S.; Guimet, D.; Zhang, W.; Zhang, J.; Xi, B. In Vitro Immunotherapy Potency Assays Using Real-Time Cell Analysis. *PLoS One* **2018**, *13*, e0193498, doi:10.1371/JOURNAL.PONE.0193498.
49. Rodríguez-Razón, C.M.; Yañez-Sánchez, I.; Ramos-Santillan, V.O.; Velásquez-Ordóñez, C.; Gutiérrez-Rubio, S.A.; García-García, M.R.; López-Roa, R.I.; Sánchez-Hernández, P.E.; Daneri-Navarro, A.; García-Iglesias, T. Adhesion, Proliferation, and Apoptosis in Different Molecular Portraits of Breast Cancer Treated with Silver Nanoparticles and Its Pathway-Network Analysis. *Int J Nanomedicine* **2018**, *13*, 1081–1095, doi:10.2147/IJN.S152237.

50. Lee, P.Y.; Costumbrado, J.; Hsu, C.Y.; Kim, Y.H. Agarose Gel Electrophoresis for the Separation of DNA Fragments. *J Vis Exp* **2012**, 3923, doi:10.3791/3923.
51. Syaifudin, M. Gel Electrophoresis: The Applications and Its Improvement with Nuclear Technology. In Proceedings of the AIP Conference Proceedings; American Institute of Physics Inc., **2021**, 2331.
52. Burman, L.G.; Mauro, V.P. Analysis of RRNA Processing and Translation in Mammalian Cells Using a Synthetic 18S RRNA Expression System. *Nucleic Acids Res* **2012**, *40*, 8085, doi:10.1093/NAR/GKS530.
53. Skrypina, N.A.; Timofeeva, A. V.; Khaspekov, G.L.; Savochkina, L.P.; Beabealashvili, R.S. Total RNA Suitable for Molecular Biology Analysis. *J Biotechnol* **2003**, *105*, 1–9, doi:10.1016/S0168-1656(03)00140-8.
54. Nazari, F.; Parham, A.; Maleki, A.F. GAPDH, β -Actin and B2-Microglobulin, as Three Common Reference Genes, Are Not Reliable for Gene Expression Studies in Equine Adipose- and Marrow-Derived Mesenchymal Stem Cells. *J Anim Sci Technol* **2015**, *57*, doi:10.1186/S40781-015-0050-8.
55. Wong, M.L.; Medrano, J.F. Real-Time PCR for mRNA Quantitation. *Biotechniques* **2005**, *39*, 75–85, doi:10.2144/05391RV01/ASSET/IMAGES/LARGE/TABLE2.JPEG.
56. Wusu, A.D.; Sibuyi, N.R.S.; Moabelo, K.L.; Goboza, M.; Madiehe, A.; Meyer, M. Citrate-Capped Gold Nanoparticles with a Diameter of 14 Nm Alter the Expression of Genes Associated with Stress Response, Cytoprotection and Lipid Metabolism in CaCo-2 Cells. *Nanotechnology* **2021**, *33*, 105101, doi:10.1088/1361-6528/AC3C7C.
57. Phan, L.M.; Rezaeian, A.H. ATM: Main Features, Signaling Pathways, and Its Diverse Roles in DNA Damage Response, Tumor Suppression, and Cancer Development. *Genes (Basel)* **2021**, *12*, doi:10.3390/GENES12060845.
58. Kaur, H.; Salles, D.C.; Murali, S.; Hicks, J.L.; Nguyen, M.; Pritchard, C.C.; de Marzo, A.M.; Lanchbury, J.S.; Trock, B.J.; Isaacs, W.B.; et al. Genomic and Clinical-Pathologic Characterization of ATM-Deficient Prostate Cancer. *Clin Cancer Res* **2020**, *26*, 4869, doi:10.1158/1078-0432.CCR-20-0764.
59. Lee, J.H.; Mand, M.R.; Kao, C.H.; Zhou, Y.; Ryu, S.W.; Richards, A.L.; Coon, J.J.; Paull, T.T. ATM Directs DNA Damage Responses and Proteostasis via Genetically

- Separable Pathways. *Sci Signal* **2018**, *11*, doi:10.1126/SCISIGNAL.AAN5598/SUPPL_FILE/AAN5598_TABLES_S1_AND_S2.ZIP.
60. Liu, Y.; Lu, L.Y. BRCA1 and Homologous Recombination: Implications from Mouse Embryonic Development. *Cell Biosci* **2020**, *10*, 1–10, doi:10.1186/S13578-020-00412-4/TABLES/2.
61. Gorodetska, I.; Kozeretska, I.; Dubrovskaya, A. BRCA Genes: The Role in Genome Stability, Cancer Stemness and Therapy Resistance. *J Cancer* **2019**, *10*, 2109, doi:10.7150/JCA.30410.
62. Yi, Y.W.; Kang, H.J.; Bae, I. BRCA1 and Oxidative Stress. *Cancers (Basel)* **2014**, *6*, 771, doi:10.3390/CANCERS6020771.
63. Stopsack, K.H.; Gerke, T.; Zareba, P.; Pettersson, A.; Chowdhury, D.; Ebot, E.M.; Flavin, R.; Finn, S.; Kantoff, P.W.; Stampfer, M.J.; et al. Tumor Protein Expression of the DNA Repair Gene BRCA1 and Lethal Prostate Cancer. *Carcinogenesis* **2020**, *41*, 904–908, doi:10.1093/CARCIN/BGAA061.
64. Amsi, P.T.; Yahaya, J.J.; Kalungi, S.; Odida, M. Immunohistochemical Expression of BRCA1 and BRCA2 in a Cohort of Ugandan Men with Prostate Cancer: An Analytical Cross-Sectional Study. *African Journal of Urology* **2020**, *26*, 1–9, doi:10.1186/S12301-020-00079-W/TABLES/3.
65. Stricher, F.; Macri, C.; Ruff, M.; Muller, S. HSPA8/HSC70 Chaperone Protein: Structure, Function, and Chemical Targeting. *Autophagy* **2013**, *9*, 1937–1954, doi:10.4161/AUTO.26448.
66. Bonam, S.R.; Ruff, M.; Muller, S. HSPA8/HSC70 in Immune Disorders: A Molecular Rheostat That Adjusts Chaperone-Mediated Autophagy Substrates. *Cells* **2019**, *8*, doi:10.3390/CELLS8080849.
67. Dores-Silva, P.R.; Cauvi, D.M.; Coto, A.L.S.; Silva, N.S.M.; Borges, J.C.; De Maio, A. Human Heat Shock Cognate Protein (HSC70/HSPA8) Interacts with Negatively Charged Phospholipids by a Different Mechanism than Other HSP70s and Brings HSP90 into Membranes. *Cell Stress Chaperones* **2021**, *26*, 671–684, doi:10.1007/S12192-021-01210-8/FIGURES/10.

68. Li, J.; Ge, Z. High HSPA8 Expression Predicts Adverse Outcomes of Acute Myeloid Leukemia. *BMC Cancer* **2021**, *21*, 1–11, doi:10.1186/S12885-021-08193-W/FIGURES/6.
69. Matsumoto, T.; Urushido, M.; Ide, H.; Ishihara, M.; Hamada-Ode, K.; Shimamura, Y.; Ogata, K.; Inoue, K.; Taniguchi, Y.; Taguchi, T.; et al. Small Heat Shock Protein Beta-1 (HSPB1) Is Upregulated and Regulates Autophagy and Apoptosis of Renal Tubular Cells in Acute Kidney Injury. *PLoS One* **2015**, *10*, e0126229, doi:10.1371/JOURNAL.PONE.0126229.
70. Kennedy, D.; Jäger, R.; Mosser, D.D.; Samali, A. Regulation of Apoptosis by Heat Shock Proteins. *IUBMB Life* **2014**, *66*, 327–338, doi:10.1002/IUB.1274.
71. Stope, M.B.; Stender, C.; Schubert, T.; Peters, S.; Weiss, M.; Ziegler, P.; Zimmermann, U.; Walther, R.; Burchardt, M. Heat-Shock Protein HSPB1 Attenuates MicroRNA MiR-1 Expression Thereby Restoring Oncogenic Pathways in Prostate Cancer Cells. *Anticancer Res* **2014**, *34*.
72. Xiong, D.D.; Zeng, C.M.; Jiang, L.; Luo, D.Z.; Chen, G. Ki-67/MKI67 as a Predictive Biomarker for Clinical Outcome in Gastric Cancer Patients: An Updated Meta-Analysis and Systematic Review Involving 53 Studies and 7078 Patients. *J Cancer* **2019**, *10*, 5339, doi:10.7150/JCA.30074.
73. Wu, S. yi; Liao, P.; Yan, L. yu; Zhao, Q. yi; Xie, Z. yu; Dong, J.; Sun, H. tao Correlation of MKI67 with Prognosis, Immune Infiltration, and T Cell Exhaustion in Hepatocellular Carcinoma. *BMC Gastroenterol* **2021**, *21*, 1–19, doi:10.1186/S12876-021-01984-2/FIGURES/7.
74. Richardsen, E.; Andersen, S.; Al-Saad, S.; Rakaee, M.; Nordby, Y.; Pedersen, M.I.; Ness, N.; Grindstad, T.; Movik, I.; Dønnem, T.; et al. Evaluation of the Proliferation Marker Ki-67 in a Large Prostatectomy Cohort. *PLoS One* **2017**, *12*, e0186852, doi:10.1371/JOURNAL.PONE.0186852.
75. Merkulova, M.; Păunescu, T.G.; Nair, A. V.; Wang, C.Y.; Capen, D.E.; Oliver, P.L.; Breton, S.; Brown, D. Targeted Deletion of the Ncoa7 Gene Results in Incomplete Distal Renal Tubular Acidosis in Mice. *Am J Physiol Renal Physiol* **2018**, *315*, F173–F185, doi:10.1152/AJPRENAL.00407.2017/ASSET/IMAGES/LARGE/ZH20031884730009.JPEG.

76. Xie, X.; Jiang, Y.; Yuan, Y.; Wang, P.; Li, X.; Chen, F.; Sun, C.; Zhao, H.; Zeng, X.; Jiang, L.; et al. MALDI Imaging Reveals NCOA7 as a Potential Biomarker in Oral Squamous Cell Carcinoma Arising from Oral Submucous Fibrosis. *Oncotarget* **2016**, *7*, 59987, doi:10.18632/ONCOTARGET.11046.
77. Ruiz, C.F.; Montal, E.D.; Haley, J.A.; Bott, A.J.; Haley, J.D. SREBP1 Regulates Mitochondrial Metabolism in Oncogenic KRAS Expressing NSCLC. *FASEB J* **2020**, *34*, 10574–10589, doi:10.1096/FJ.202000052R.
78. Li, L.Y.; Yang, Q.; Jiang, Y.Y.; Yang, W.; Jiang, Y.; Li, X.; Hazawa, M.; Zhou, B.; Huang, G.W.; Xu, X.E.; et al. Interplay and Cooperation between SREBF1 and Master Transcription Factors Regulate Lipid Metabolism and Tumor-Promoting Pathways in Squamous Cancer. *Nature Communications* **2021**, *12*:1 **2021**, *12*, 1–17, doi:10.1038/s41467-021-24656-x.
79. Gao, Y.; Nan, X.; Shi, X.; Mu, X.; Liu, B.; Zhu, H.; Yao, B.; Liu, X.; Yang, T.; Hu, Y.; et al. SREBP1 Promotes the Invasion of Colorectal Cancer Accompanied Upregulation of MMP7 Expression and NF-KB Pathway Activation. *BMC Cancer* **2019**, *19*, 1–8, doi:10.1186/s12885-019-5904-X/FIGURES/4.
80. Orea-Soufi, A.; Castillo-Lluva, S.; Salvador-Tormo, N.; Martín-Cabrera, P.; Recuero, S.; Gabicagoeascoa, E.; Moreno-valladares, M.; Mendiburu-Eliçabe, M.; Blanco-Gómez, A.; Ramos-Pittol, J.M.; et al. The Pseudokinase TRIB3 Negatively Regulates the HER2 Receptor Pathway and Is a Biomarker of Good Prognosis in Luminal Breast Cancer. *Cancers (Basel)* **2021**, *13*, 5307, doi:10.3390/CANCERS13215307/S1.
81. Yang, J.; Lin, J.; An, J.; Zhao, Y.; Jing, S.; Yu, M.; Zhu, Y.; Yao, Y. TRIB3 Promotes the Malignant Progression of Bladder Cancer: An Integrated Analysis of Bioinformatics and in Vitro Experiments. *Front Genet* **2021**, *12*, 406, doi:10.3389/FGENE.2021.649208/BIBTEX.
82. Qu, J.; Liu, B.; Li, B.; Du, G.; Li, Y.; Wang, J.; He, L.; Wan, X. TRIB3 Suppresses Proliferation and Invasion and Promotes Apoptosis of Endometrial Cancer Cells by Regulating the AKT Signaling Pathway. *Onco Targets Ther* **2019**, *12*, 2235, doi:10.2147/OTT.S189001.
83. Kong, X.; Chen, J.; Xie, W.; Brown, S.M.; Cai, Y.; Wu, K.; Fan, D.; Nie, Y.; Yegnasubramanian, S.; Tiedemann, R.L.; et al. Defining UHRF1 Domains That Support

- Maintenance of Human Colon Cancer DNA Methylation and Oncogenic Properties. *Cancer Cell* **2019**, *35*, 633, doi:10.1016/J.CCELL.2019.03.003.
84. Pan, X.; Li, C.; Cai, Y.; Wu, S. Comprehensive Pan-Cancer Analysis Reveals the Role of UHRF1-Mediated DNA Methylation and Immune Infiltration in Renal Cell Carcinoma. *J Oncol* **2022**, *2022*, doi:10.1155/2022/3842547.
85. Niinuma, T.; Kitajima, H.; Kai, M.; Yamamoto, E.; Yoroazu, A.; Ishiguro, K.; Sasaki, H.; Sudo, G.; Toyota, M.; Hatahira, T.; et al. UHRF1 Depletion and HDAC Inhibition Reactivate Epigenetically Silenced Genes in Colorectal Cancer Cells. *Clin Epigenetics* **2019**, *11*, 1–13, doi:10.1186/S13148-019-0668-3/FIGURES/7.
86. Du, S.; Xu, G.; Zou, W.; Xiang, T.; Luo, Z. Effect of Dihydroartemisinin on UHRF1 Gene Expression in Human Prostate Cancer PC-3 Cells. *Anticancer Drugs* **2017**, *28*, 384–391, doi:10.1097/CAD.0000000000000469.
87. Wan, X.; Yang, S.; Huang, W.; Wu, D.; Chen, H.; Wu, M.; Li, J.; Li, T.; Li, Y. UHRF1 Overexpression Is Involved in Cell Proliferation and Biochemical Recurrence in Prostate Cancer after Radical Prostatectomy. *Journal of Experimental and Clinical Cancer Research* **2016**, *35*, 1–14, doi:10.1186/S13046-016-0308-0/TABLES/3.

